The Philosophical Magazine

FIRST PUBLISHED IN 1798

A Journal of Theoretical Experimental and Applied Physics

UNIVERSITY OF HAWAII
LIBRARY
FEB 12 '60

Vol. 4 **October 1959** **No. 46**
Eighth Series

£1 5s. 0d., plus postage
Annual Subscription £13 10s. 0d., payable in advance

Printed and Published by
TAYLOR & FRANCIS LTD
RED LION COURT, FLEET STREET, LONDON, E.C.4

THE PHILOSOPHICAL MAGAZINE

Editor

Professor N. F. Mott, M.A., D.Sc., F.R.S.

Editorial Board

Sir Lawrence Bragg, O.B.E., M.C., M.A., D.Sc., F.R.S.
Sir George Thomson, M.A., D.Sc., F.R.S.
Professor A. M. Tyndall, C.B.E., D.Sc., F.R.S.

Authors wishing to submit papers for publication in the Journal should send manuscripts directly to the Publishers.

Manuscripts should be typed in *double* spacing on one side of quarto (8 × 10 in.) paper, and authors are urged to aim at absolute clarity of meaning and an attractive presentation of their texts.

References should be listed at the end in alphabetical order of authors and should be cited in the text in terms of author's name and date. Diagrams should normally be in Indian ink on white card, with lettering in soft pencil, the captions being typed on a separate sheet.

A leaflet giving detailed instructions to authors on the preparation of papers is available on request from the Publishers.

Authors are entitled to receive 25 offprints of a paper in the Journal free of charge, and additional offprints can be obtained from the Publishers.

The *Philosophical Magazine* and its companion journal, *Advances in Physics*, will accept papers for publication in experimental and theoretical physics. The *Philosophical Magazine* publishes contributions describing new results, letters to the editor and book reviews. *Advances in Physics* publishes articles surveying the present state of knowledge in any branch of the science in which recent progress has been made. The editors welcome contributions from overseas as well as from the United Kingdom, and papers may be published in English, French and German.

INTERNATIONAL JOURNAL

OPTICA ACTA

European Journal of Optics — **Journal Européen d'Optique** — **Europäische Zeitschrift für Optik**

English Editor: C. G. Wynne, 13 Elwill Way, Beckenham, Kent, U.K.

Rédacteur Français: A. Maréchal, 3 Boulevard Pasteur, Paris, France

Deutscher Herausgeber: G. Franke, Laufdorfer Weg 2, Wetzlar, Germany

Editorial Board

J. M. Otero y Navascues, *Madrid;* R. W. Ditchburn, *Reading;* A. Arnulf, *Paris;* A. Biot, *Gand;* J. Cabannes, *Paris;* P. Fleury, *Paris;* F. Gabler, *Vienna;* G. Hansen, *Oberkochen;* E. Ingelstam, *Stockholm;* H. Korte, *Braunschweig;* W. S. Stiles, *London;* G. Toraldo di Francia, *Florence;* A. C. S. van Heel, *Delft.*

Contents of April, 1959

Correction Approchée de l'Effet de Lobe en Radioastronomie. Par J. Arsac, Observatoire de Meudon

Colour Perception with the Peripheral Retina. By J. D. Moreland and A. Cruz, Technical Optics Section, Imperial College, London

A Fourier Analyser for Optical Frequency Response Determinations. By J. M. Naish, Royal Aircraft Establishment, Hampshire England

Photo-sensitive Reactions in Foveae of Normal and Cone-monochromatic Observers. By R. A. Weale, Visual Research Division, Ophthalmological Research Unit, (Medical Research Council), Institute of Ophthalmology, Judd Street, London, W.C.1

Contrast Transfer in the Grating Spectrograph. By A. Lohmann, Institute of Optical Research, Stockholm 70, Sweden

Doppelbrechungs-interferenzfarben sehr dünner Plättchen. Von S. Rösch, Wetzlar

Price per part £1 (1375 fr.), (DM 11.75), ($2.80), plus postage

Subscription price per volume (4 parts) £3 15s. (5155 fr.), (DM 44), ($10.50), post free, payable in advance

Printed and Published by

TAYLOR & FRANCIS LTD

RED LION COURT, FLEET STREET, LONDON, E.C.4

Physics in Medicine and Biology

**A Taylor & Francis Journal published in association
with The Hospital Physicists' Association**

Editor: J. E. Roberts, D.Sc.
Consultant Editor: Professor N. F. Mott, F.R.S.

Editorial Board

N. W. Bellwood, *London*; R. Bonet-Maury, *Paris*; J. Dainty, *Edinburgh*; H. E. Johns, *Toronto*; W. A. Langmead, *Dumfriesshire*; D. A. McDonald, *London*; J. S. Mitchell, *Cambridge*; G. J. Neary, *Harwell*; B. Rajewsky, *Frankfurt*; J. Rotblat, *London*; S. Rowlands, *London*; H. P. Schwan, *Philadelphia*; R. Sievert, *Stockholm*; F. W. Spiers, *Leeds*; J. F. Tait, *Massachusetts*; A. J. H. Vendrik, *Nijmegen.*

Contents of July, 1959

The Basic Design Data of a Guarded-field Thimble Ionization Chamber: A Theoretical Investigation. By Barry Barber, M.A., A.Inst.P., Physics Department, London Hospital Research Laboratories, Ashfield Street, London, E.1

A Theoretical Approach to the Radiation Dose-rate Distribution from Combined X- or γ-ray Beams with special reference to Wedge-filtered Beams. By R. Sear, B.Sc., A.Inst.P., Physics Department, The London Hospital Research Laboratories, London, E.1

Miniature Ionization Chambers for Measurements in Body Cavities. By S. Benner, Ph.D., M.D., I. Ragnhult, M.Sc., and G. Gebert, Radiophysics Institute, University of Gothenburg, Sahlgrenska Sjukhuset, Gothenburg C, Sweden

A Simple Circuit for Simultaneous Dose-rate and Dose Measurements. By Sven Benner, Ph.D., M.D., Radiophysics Institute, University of Gothenburg, Sahlgrenska Sjukhuset, Gothenburg C, Sweden

A Note on the Calibration of X-ray Dosemeters. By John Tooze and Boyce Worthley, Anti-Cancer Committee, University of Adelaide, South Australia

The Stopping-power Correction for Graphite Cavity-chambers used with 2 mV X-rays. By G. P. Barnard, D.Sc., Ph.D., M.I.E.E., F.Inst.P. and A. R. S. Marsh, The National Physical Laboratory, Teddington, Middlesex

An Experimental Evaluation of Microspectrophotometry. By K. W. Keohane, B.Sc., Ph.D., and W. K. Metcalf, M.D., B.S., Department of Anatomy, The University, Bristol, 8

An Experimental Determination of the Propagation of Fluid Oscillations in a Tube with a Visco-elastic Wall; together with an Analysis of the Characteristics Required in an Electrical Analogue. By M. G. Taylor, M.D., Ph.D., Physiology Department, Medical College of St. Bartholomew's Hospital, London

Subscription price per volume £3 10s. post free, payable in advance
4 parts per volume—£1 per part plus postage

Printed and Published by

TAYLOR & FRANCIS, LTD

RED LION COURT, FLEET STREET, LONDON, E.C.4

Orders originating in U.S.A. and Canada should be sent to the
Academic Press Inc., 111 Fifth Avenue, New York 3, N.Y., U.S.A.

A new International Journal

Molecular Physics

Editor: **H. C. LONGUET-HIGGINS, F.R.S.**
Associate Editor: **J. H. VAN DER WAALS**

Editorial Board:

J. Bjerrum, *Copenhagen*; G. Careri, *Padua*; C. A. Coulson, *Oxford*; F. H. C. Crick, *Cambridge*; P. J. W. Debye, *Cornell*; D. Hadži, *Ljubljana*; O. Hassel, *Oslo*; W. Heitler, *Zürich*; J. O. Hirschfelder, *Wisconsin*; D. F. Hornig, *Princeton*; J. A. A. Ketelaar, *Amsterdam*; J. G. Kirkwood, *Yale*; R. Kronig, *Delft*; J. W. Linnett, *Oxford*; A. Liquori, *Rome*; Dame Kathleen Lonsdale, *London*; P-O. Löwdin, *Uppsala*; M. Magat, *Paris*; R. S. Mulliken, *Chicago*; A. Münster, *Frankfurt*; L. J. Oosterhoff, *Leiden*; L. E. Orgel, *Cambridge*; J. A. Pople, *Teddington*; I. Prigogine, *Brussels*; R. E. Richards, *Oxford*; J. S. Rowlinson, *Manchester*; G. S. Rushbrooke, *Newcastle upon Tyne*; L. E. Sutton, *Oxford*; H. W. Thompson, *Oxford*; B. Vodar, *Bellevue, Paris.*

Contents of July, 1959

Long-range Interaction of Two 1s-hydrogen Atoms Expressed in Terms of Natural Spin-orbitals. By J. O. Hirschfelder, Theoretical Chemistry Laboratory, Chemistry Department, University of Wisconsin, Madison, Wisconsin and P. O. Löwdin, Quantum Chemistry Group, University of Uppsala, Uppsala, Sweden

Efficiencies of Third Bodies in the Reaction $H+O_2+M=HO_2+M$. By P. G. Dickens and J. W. Linnett, Inorganic Chemistry Laboratory, Oxford

Diffusion Coefficients of Gases from the Rate of Approach to the Steady State in Thermal Diffusion. By S. C. Saxena and E. A. Mason, Institute for Molecular Physics, University of Maryland, College Park

The Pairing of Electronic States in Alternant Hydrocarbons. By A. D. McLachlan, Department of Theoretical Chemistry, University Chemical Laboratory, Lensfield Road, Cambridge, England

The Electron Spin Resonance Spectrum of a γ-irradiated Single Crystal of Glycine. By D. K. Ghosh and D. H. Whiffen, Chemistry Department, University of Birmingham

Thallium Nuclear Resonance Spectra, Part II. By R. Freeman, R. P. H. Gasser and R. E. Richards, Physical Chemistry Laboratory, South Parks Road, Oxford

Electron Transfer Spectra of Hexahalide Complexes. By C. K. Jørgensen, Chemistry Department A, Technical University of Denmark, Copenhagen

Price per part £1 5s. 0d. plus postage
Subscription per volume (4 issues) £4 15s. 0d. post free, payable in advance

Printed and Published by
TAYLOR & FRANCIS LTD
RED LION COURT, FLEET STREET, LONDON, E.C.4

Orders originating in U.S.A. and Canada should be sent to the
Academic Press Inc., 111 Fifth Avenue, New York 3, N.Y., U.S.A.

A new International Journal

ERGONOMICS

HUMAN FACTORS IN WORK, MACHINE CONTROL AND EQUIPMENT DESIGN

General Editor
A. T. WELFORD
University of Cambridge, Psychological Laboratory, Downing Place, Cambridge

Associate Editor (Anatomy and Physiology)
W. F. FLOYD

Assistant Editor
Miss H. M. CLAY

Editorial Board

H. Bastenier, *Belgium*; R. B. Bromiley, *Canada* ; R. Bonnardel, Bernard Metz, *France*; E. A. Müller, *Germany*; M. G. Bennett, W. E. Hick, Sir Charles Lovatt Evans, L. G. Norman, *Great Britain*; F. H. Bonjer, *Netherlands*; S. P. M. Forssman, *Sweden*; E. Grandjean, *Switzerland*; H. S. Belding, P. M. Fitts, *U.S.A.*

Contents of May, 1959

Some Problems of Scientific Thinking. By Sir Frederic Bartlett, St. John's College, Cambridge

Accident-proneness in Motor-vehicle Drivers. By D. Russell Davis and Patricia A. Coiley, Medical Psychology Laboratory, University of Cambridge

A Note on Panel Layout for Numbers of Identical Items. By B. Shackel, Psychological Research Laboratory, E.M.I. Electronics Ltd., Hayes, Middlesex, England

The Effects of Aptitude, Fitness, Physical Working Capacity, Skill and Motivation on the Amount and Quality of Work. By F. H. Bonjer, Department of Occupational Health, Netherlands Institute for Preventive Medicine, Leiden, Holland

Circulatory Responses to Change from Recumbent to Erect Posture as an Index of Heat Stress. By J. R. Brown, G. P. Crowden and P. F. Taylor, Department of Applied Physiology, London School of Hygiene and Tropical Medicine

The Estimation of the Transfer Function of a Human Operator by a Correlation Method of Analysis. By J. G. Henderson, Electrical Engineering Department, University of Birmingham

The Judgment of Velocity and Prediction of Motion. By D. J. Gerhard, Department of Scientific and Industrial Research, London

E.P.A. Project No. 335. " Fitting the Job to the Worker "

Price £1 5s. 0d. per part plus postage
Subscription price per volume £4 15s. 0d. post free, payable in advance

Printed and Published by
TAYLOR & FRANCIS LTD
RED LION COURT, FLEET STREET, LONDON, E.C.4

Orders originating in U.S.A. and Canada should be sent to the
Academic Press Inc., 111 Fifth Avenue, New York 3, N.Y., U.S.A.

Journal of Electronics and Control

A Philosophical Magazine Associated Journal

Editor:
J. Thomson, M.A., D.Sc., M.I.E.E., F.Inst.P.
Consultant Editor:
Professor N. F. Mott, F.R.S.
Editorial Board:
Professor P. Aigrain (France)
Professor H. B. G. Casimir (Holland)
J. F. Coales (U.K.)
Professor K. G. Emeleus (U.K.)
D. W. Fry (U.K.)
Dr. W. Klein (Germany)
Dr. R. Kompfner (U.S.A.)

Contents of July, 1959

Electronics Section

Fast Wave Couplers for Longitudinal Beam Parametric Amplifiers. By A. Ashkin, W. H. Louisell and C. F. Quate, Bell Telephone Laboratories, Incorporated, Murray Hill, New Jersey

Tuning and the Equivalent Circuit of Multi-resonator Magnetrons. By T. S. Chen, Electron Tube Division, Radio Corporation of America, Harrison, New Jersey

The Thermoelectric Figure of Merit and its Relation to Thermoelectric Generators. By R. P. Chasmar and R. Stratton, Research Department, Metropolitan-Vickers Electrical Co. Ltd.

The Figure of Merit of a Thermoelectric Generator. By R. Stratton, Research Department, Metropolitan-Vickers Electrical Co. Ltd., Trafford Park, Manchester

The Definition of Noise Factor when applied to Systems Containing Negative Resistance Elements. By B. L. Humphreys, Mullard Research Laboratories, Salfords, Surrey

Control Section

Approximation Errors in Diode Function-generators. By N. Ream, Battersea College of Technology, Battersea Park Road, London, S.W.11

Price per part £1 5s. plus postage
Price per volume £7 post free, payable in advance
6 monthly issues per volume

Printed and Published by

TAYLOR & FRANCIS LTD
RED LION COURT, FLEET STREET, LONDON, E.C.4

Orders originating in U.S.A. and Canada should be sent to the
Academic Press Inc., 111 Fifth Avenue, New York 3, N.Y., U.S.A.

INTERNATIONAL JOURNAL OF RADIATION BIOLOGY
and related studies in Physics, Chemistry and Medicine

Editor
W. M. DALE, M.D., D.SC.
Dept. of Biochemistry, Christie Hospital & Holt Radium Institute, Withington, Manchester, 20
Assistant Editor
JOHN WAKEFIELD, B.A., F.Z.S.

Editorial Board
Charlotte Auerbach, *U.K.;* J. H. Baxendale, *U.K.;* D. W. van Bekkum, *Holland;* E. H. Betz, *Belgium;* H. A. S. van den Brenk, *Australia;* A. A. Buzzatti-Traverso, *Italy;* J. Coursaget, *France;* F. Devik, *Norway;* M. Haissinsky, *France;* A. Hollaender, *U.S.A.;* B. F. Kaufmann, *U.S.A.;* G. Klein, *Sweden;* H. Langendorff, *Germany;* M. Magat, *France;* M. Nakaidzumi, *Japan;* E. Paterson, *U.K.;* H. Ulrich, *Switzerland;* M. Westergaard, *Denmark.*

Contents of July, 1959

The Relative Biological Efficiency of Single Doses of Fast Neutrons and Gamma-rays on *Vicia faba* Roots and the Effect of Oxygen. Part I. Reduction of Root Growth. By G. J. Neary, S. M. Tonkinson and F. S. Williamson, Medical Research Council Radiobiological Research Unit, Harwell, Didcot, Berks

The Relative Biological Efficiency of Single Doses of Fast Neutrons and Gamma-rays on *Vicia faba* Roots and the Effect of Oxygen. Part II. Chromosome Damage: the Production of Micronuclei. By H. J. Evans, G. J. Neary and F. S. Williamson, Medical Research Council Radiobiological Research Unit, Harwell, Didcot, Berks

The Relative Biological Efficiency of Single Doses of Fast Neutrons and Gamma-rays on *Vicia faba* Roots and the Effect of Oxygen. Part III. Mitotic Delay. By G. J. Neary, H. J. Evans, S. M. Tonkinson and F. S. Williamson, Medical Research Council Radiobiological Research Unit, Harwell, Didcot, Berks

The Effects of X-radiation on the Processes Leading to DNA-synthesis in Regenerating Rat Liver. By J. J. Jaffe, L. G. Lajtha, June Lascelles, Margery G. Ord and L. A. Stocken, Department of Biochemistry and the Churchill Hospital, University of Oxford

Modification of Radiation-induced Intestinal Injury in Rats by Chilling after Irradiation. By W. D. Gude, A. C. Upton and T. T. Odell, Jr., Biology Division, Oak Ridge National Laboratory, Oak Ridge, Tennessee

The Modification of Acute Mortality in Mice by Variation of the Dose-rate and the Overall Time of Irradiation. By M. J. Corp and F. E. Neal, M.R.C. Radiobiological Research Unit, A.E.R.E., Harwell, Berks

Comparison of Protective Effects of Hind-leg Shielding and Isologous Bone-marrow Injection in X-irradiated Rats. By J. M. Loiselle, L. F. Lamerton and Kay Adams, Physics Department, Institute of Cancer Research, Royal Cancer Hospital, Fulham Road, London, S.W.3

Radiation-induced Tissue Breakdown. IV. The Source of Degraded Amino Acids in Irradiated Rats. By Georg Gerber, Gisela Gerber, K. I. Altman and L. H. Hempelmann, Division, of Experimental Radiology, School of Medicine and Dentistry, University of Rochester, Rochester, New York

The Effect of Triethylene-melamine on the Fertility of Female Mice. By B. M. Cattanach, Institute of Animal Genetics, University of Edinburgh

Modification of X-ray Damage to the Lens by Partial Shielding. By Antoinette Pirie and S. M. Drance, Nuffield Laboratory of Ophthalmology, University of Oxford

Enzymatic Activity Related to DNA-synthesis in Regenerating Liver of Irradiated Rats. By S. Okada and L. H. Hempelmann, From the Division of Experimental Radiology, University of Rochester School of Medicine and Dentistry, Rochester 20, N.Y.

Price per part £1 0s. 0d. plus postage
Subscription per volume (4 issues) £3 15s. 0d. post free, payable in advance
Printed and Published by
TAYLOR & FRANCIS LTD
RED LION COURT, FLEET STREET, LONDON, E.C.4
Orders originating in U.S.A. and Canada should be sent to the
Academic Press Inc., 111 Fifth Avenue, New York 3, N.Y., U.S.A.

Announcing the new publication

CONTEMPORARY PHYSICS

A Journal of Interpretation and Review

Editor:
G. R. Noakes, M.A., F.Inst.P.

Editorial Board:
Consultant Editors: Sir Lawrence Bragg, O.B.E., M.C., M.A., D.Sc., F.R.S.
Sir George Thomson, M.A., D.Sc., F.R.S.

Advisory Editors: Professor L. F. Bates, Ph.D., D.Sc., F.R.S.
Dr. K. A. G. Mendelssohn, F.R.S.
Dr. F. A. Vick, O.B.E.

Contents of October, 1959

Molecular Beams. By O. R. Frisch, Cavendish Laboratory, Cambridge

The Structure of the Atomic Nucleus. By R. J. Blin-Stoyle, Fellow of Wadham College and Senior Research Officer in Theoretical Physics, University of Oxford

Alexander von Humboldt and the Organization of International Collaboration in Geophysical Research. By L. Kellner, Imperial College of Science and Technology, London

The Selection and Design of Experiments for Alternating Current Teaching. By H. V. Beck, Cavendish Laboratory, Cambridge

Skidding Friction. The Effect of Hysteresis Losses in Tyre Tread Rubber. By Barbara E. Sabey, Road Research Laboratory, Department of Scientific and Industrial Research

Light Sources using Radioisotopes. By E. J. Wilson and J. D. H. Hughes, Isotope Division, Harwell

Price per part 5s. 0d. (75 cents) plus postage

Subscription price per volume of 6 parts £1 7s. 0d. ($4.00), post free, payable in advance

Printed and Published by

TAYLOR & FRANCIS LTD

RED LION COURT, FLEET STREET, LONDON, E.C.4

Advances in Physics

A Quarterly Supplement of the Philosophical Magazine

Editor:
B. H. Flowers, M.A., D.Sc.

Consultant Editor:
Professor N. F. Mott, M.A., D.Sc., F.R.S.

Editorial Board:
Sir Lawrence Bragg, O.B.E., M.C., M.A., D.Sc., F.R.S.
Sir George Thomson, M.A., D.Sc., F.R.S.
Professor A. M. Tyndall, C.B.E., D.Sc., F.R.S.

Contents of July, 1959

Classical Theory of the Equilibrium Liquid Pair Distribution. By G. H. A. Cole, Physics Division, Clarke, Chapman & Co., Ltd., Gateshead, 8, Durham

The Saturation Magnetostriction of Ferromagnetics. By R. R. Birss, Imperial College, London

Soft Magnetic Materials. By E. W. Lee, Department of Physics, University of Nottingham and A. C. Lynch, Post Office Research Station, Dollis Hill, London, N.W.2

Price per part £1 plus postage

Price per annum £3 15s. post free

Printed and Published by

TAYLOR & FRANCIS LTD

RED LION COURT, FLEET STREET, LONDON, E.C.4

The Strength of Glass Fibres†

By D. G. HOLLOWAY
Physics Department, University College of North Staffordshire

[Received June 8, 1959]

ABSTRACT

Evidence from some simple experiments suggesting a source of important stress raising flaws in the surface of glass fibres is described. It is believed that these flaws are the major ones concerning strength, present in fibres drawn at low temperatures.

§ 1. INTRODUCTION

IT has been reported recently that the breaking strengths of glass fibres prepared by drawing samples from molten glass at very high temperature are much higher and more consistent than those reported by earlier workers and show no variation with diameter (Otto 1955, Thomas 1958). We have discovered an important source of flaws which occur in the surface of fibres drawn from rod at low temperatures and this has led to a possible understanding of the significance of this marked difference in the properties of the fibres. The experimental evidence is described in this note.

§ 2. DEFECTS IN THE SURFACE OF FIBRES

In the course of some other work on the strength of glass, lengths of fibre were drawn from a section of rod heated to comparatively low temperatures. The centre of a length of rod of 4–5 mm diameter was surrounded by a simple electrically heated oven and the current to the windings was increased until this centre section of the rod attained the temperature at which it flowed under the weight of the lower section. Fibres produced by this method as normally operated are about one metre in length, of diameter 150–300 microns and have strengths, when subject to strain over macroscopic areas of surface, of 100–150 kg/mm^2. That is similar to that reported in the older literature (Stanworth 1950) but significantly lower than for fibres drawn from much hotter glass. The influence of drawing conditions on the strength of fibres drawn in this way was investigated with a more refined oven the temperature of which was controlled to ± 2°C. It was remarked that when the oven was held at low temperatures so that attenuation of the rod took place very slowly over a period of half an hour or more, very weak fibres were produced, and that these had obvious defects in the surface (fig. 1, Pl. 135). Very careful microscopic examination of fibres drawn at the higher temperatures then revealed very small 'point' defects on the surface. The apparent size of the defects was dependent on the temperature at which the oven was operated while the number of defects could be appreciably reduced by thorough cleaning of the initial rod. Defects of a similar kind were found on fibres drawn from rods of Pyrex brand chemical resistant glass. E-glass† and a soda-lime–silica glass, when produced by heating in the oven or by hand drawing after heating in a flame. A series of experiments has been carried out to determine the nature and importance of these visible defects. Some of these experiments and the results obtained are described in the following sections.

---

† Communicated by the Author.

§ 3. The Influence of the Defects on the Breaking Strength

It was early and simply established that there was a qualitative correlation between the macroscopic strength of a fibre and the size of the defects present in its surface. Examination of the fracture edges of a series of specimens with relatively large defects revealed in the large majority of cases the presence of a defect at the edge (fig. 2, Pl. 135). The appearance of the cross section of the fibre at the fracture surface confirmed that fracture had started at or very close to the visible defect, even when the defect lay to one side of the line of maximum surface stress on the tensile side of a specimen fractured in bending. The photomicrograph in fig. 3 (Pl. 135) shows a typical fracture surface with the usual flat 'mirror' region around the origin of fracture and the surrounding progressively rougher hackle (Smekal 1936). Where the specimens contained very small defects it has not been possible with normal optical examination to locate the flaw at the fracture edge although in every case specimens broke in a region known from the initial microscopic examination to contain defects. The larger defects have a striation associated with them and the location of a defect at a fracture edge is most simply effected by detection of this striation. It is the absence of this which makes detection of smaller flaws particularly difficult even on the normal surface and probably accounts for the failure to detect small defects at the fracture edges of the stronger fibres.

There is no doubt in view of these observations that fracture of a specimen can originate at one of these visible flaws, so that further experiments were designed to establish the strength of the normal surface between the flaws. This was carried out by subjecting specimens to a high stress gradient in bending so that high maximum stresses might be attainable over a local region, provided this did not contain a severe flaw. Pieces of fibre approximately six centimetres long were placed on strips of microscope slide and waxed to the centre of the slide. Specimens were then transferred to the stage of an optical microscope and the upper surface of the fibre examined to determine the position of surface flaws relative to the edge of the slide. Subsequently the samples were placed in a jig and a load applied to the fibre so as to bend it across the edge of the slide on which it was mounted. With the point of application of the load close to the edge of the slide (3 mm) quite high stress gradients were achieved. The load was applied through a steel knife edge by means of a micrometer screw gauge which also served to measure the deflection of the fibre. Approximate values for the stresses at points on the upper surface of the fibre were computed from this measured deflection. The other parameters required, the diameter of the fibre, the distances of the edge of the supporting slide from the fixed portion of the fibre and from the fracture edge were measured with either a stage or an eyepiece micrometer on an optical microscope. Table 1 shows two series typical of the results for Pyrex fibres: in the second row the maximum surface stress is given and in the third the computed stress at the position of fracture. Since fracture occurs at a flaw it is of course the severity and the proximity of this to the region of maximum stress which limits the maximum stress attained with individual samples. The maximum stress is therefore a lower limit in each case to that which the local surface could support. The largest values in the first column indicate the stresses that the normal surface will withstand without fracture, i.e. about 400 kg mm^2. Similar results have been obtained with E-glass and soda-lime–silica glass fibres.

---

† The E-glass rod was obtained from Pilkington Brothers Ltd. and is an alumino-borosilicate glass with less than 1% alkali content, Littleton softening point approximately 845°c.

Table 1. Local Strength of Pyrex Fibres

Diameter of fibre (microns)	Stresses (kg/mm^2) on tensile surface	
	Maximum	At position of fracture
210	400	—
210	370	60
240	350	210
270	340	280
270	380	220
300	335	200
490	204	104
350	350	200
350	220	90
360	300	190
340	160	160
540	330	24
590	210	90
630	220	100
720	300	150

Fibres in the first group were drawn at a higher temperature than those in the second.

From these experiments it was inferred that the defects weaken the fibre in tension only, since their presence on the compression side did not preclude the possibility of reaching high maximum stresses. Moreover, the fact that fibres can withstand markedly higher stresses between visible flaws argues forcibly for the hypothesis that these are the major 'stress raisers' in these fibres. Additional evidence is provided by the results obtained with a series of specimens from a length of E-glass fibre which had a very much higher density of defects on one side. For specimens with this side of the fibre in tension the density of defects was such that there was in each case a defect very close to the point of maximum stress so that fracture occurred from this defect at quite low stresses. By contrast, for specimens arranged so that the defect side was in compression very high maximum stresses could be achieved and fracture occurred on the tensile side at relatively large distances from the point of maximum stress. Table 2 displays these results.

Table 2. Local Strength of E-Glass Fibres

Defect side in tension		Defect side in compression	
Maximum	At position of fracture	Maximum	At position of fracture
55	55	420	200
10	10	200	200
40	40	330	10
72	72	160	80

Tensile surface stresses (kg/mm²).

There is, then, good evidence that the major flaws in these fibres are intimately correlated with the visible defects.

§ 4. Nature of the Visible Defects

The dependence of the number of flaws on the cleanliness of the original rod and their size on the temperature at which the fibre was drawn suggest that they might be local devitrification crystals, nucleated perhaps by dirt particles on the surface. However, the rather poor definition of the flaws, apparent in fig. 1, which seems at least in part to be due to the nature of the defect, argues against this since one might expect devitrification crystals to be fairly well defined in shape, or even dendritic. Moreover, the temperature of the oven under the conditions which produce the larger defects is appreciably less than that at which the growth rate for devitrification crystals is a maximum. For example in the case of Pyrex maximum growth rate occurs at about 950°c (Cox and Kirby 1947) whereas large defects are still apparent on fibres produced at 850°c and are still increasing in size with decreasing temperature. Finally, and perhaps most significant, when a rod is reheated after having been allowed to undergo a very short draw at the end of the first heating the defects show no sign of growth. An alternative hypothesis is that the defects are local regions of different composition which result from the dissolution of small particles especially for example salt and silicacious dust which contaminated the original rod.

In order to determine whether such contamination would have any effect on the strength, a further series of tests was undertaken in which rods of Pyrex, E-glass and soda-lime-silica glass were deliberately and extensively contaminated with either sodium hydroxide or silica powder (prepared from fused silica tubing) prior to insertion in the drawing oven. With the exception of Pyrex and soda glass contaminated with sodium hydroxide, the effect of this deliberate contamination was to reduce catastrophically the strength of the resulting fibres (table 3). Microscopic examination of the surface revealed very large defects together with large numbers of smaller ones similar to those on the fibre illustrated in fig. 1. Contamination of the original rods with the salts from tap water, known to contain appreciable amounts of sodium and calcium salts, produces similar effects although in this case the larger defects have a granular appearance.

Table 3. Strengths of Fibres Drawn from Contaminated Rods

	Washed in distilled water	NaOH	SiO_2
Pyrex	100	101	27
E-glass	112	18	45
Soda glass	94	70	55

Tensile surface stresses (kg/mm^2). Standard deviations are about ±20%.

It is possible to produce simply E-glass or soda-lime–silica glass fibres which have high strengths comparable to those obtained by Thomas, by heating a section of the rod in an oxygen–coal-gas flame until it is very fluid and then removing and drawing out the hot glass into a fibre when the section of rod has cooled to a lower temperature. In terms of the hypothesis suggested above, this high temperature treatment prior to drawing has the effect of ensuring complete dissolution and thorough mixing with the rest of the glass of the impurities initially present on the surface of the rod and so avoiding the formation of small local regions of very different composition. High strength fibres can be produced in the same way from rods of E-glass and soda-lime–silica glass which have been extensively contaminated with either sodium hydroxide, silica powder or the salts from tap water. Again, if the major flaws in fibres drawn at low temperatures result from the dissolution of contaminate particles it should be possible to obtain high strength specimens by drawing from scrupulously clean rod under dust free conditions. We are currently building apparatus with which to examine this possibility. Meanwhile, further simple experiments suggest that this will prove to be possible. Rods of soda-lime–silica glass were subjected to a succession of cleaning processes including washing in a hot solution of detergent, in nitric acid, in alcohol and in a steam reflux until samples were obtained which when allowed to dry in air showed uniform drainage of the distilled water from the final wash without any tendency for the water to gather into small droplets. Fibres which were drawn at low temperatures from these rods broke at strains of 3% or greater. The remaining portions of the same rods were deliberately handled and then rolled on a laboratory bench so that they became lightly contaminated with dust particles. Fibres produced from these samples under the same low temperature conditions failed at about $\frac{1}{2}$% strain.

§ 5. SUMMARY

It is clear even from these simple experiments that chemical contamination of a glass surface which is subsequently heated to the working range of temperatures can reduce seriously the strength of the specimen. The local defects observed on the surface of fibres and at which fracture has been shown to occur are thought to arise in this way through the dissolution of material from contaminating particles into the glass to form small regions of different composition. Permanent stresses will arise in and around these local regions as the glass cools from the working temperature. It is not known yet whether these would be adequate to account for the lower applied stress required to induce local fracture, although in the case of the very large flaws which result from deliberate contamination some examples of actual cracking have been observed and in a few examples cracks running into the surrounding glass have been seen. That high stresses are withstood by areas of surface without visible flaws argues for the hypothesis that these are the major defects responsible for the low strength of these fibres. The frequency and size of flaws can be minimized by thoroughly cleaning the glass rod before drawing and apparently eliminated in the case of the 'softer' glasses by subjecting the glass to a very high temperature treatment immediately before drawing.

ACKNOWLEDGMENTS

The author would like to thank Messrs. D. Smith and P. A. P. Hastilow who carried out some of the measurements referred to in this note, and Mr. P. E. Jellyman of Messrs. Pilkington Bros. Ltd. Research Laboratories who kindly supplied the samples of E-glass in rod form. Financial support for this work has been received from the British Ceramic Research Association and is gratefully acknowledged.

REFERENCES

COX, S. M., and KIRBY, P. L., 1947, *Nature, Lond.*, **159,** 162.
OTTO, W. H., 1955, *J. Amer. ceram. Soc.*, **38,** 122.
SMEKAL, A., 1936, *J. Soc. Glass Tech.*, **20,** 432.
STANWORTH, J. E., 1950, *Physical Properties of Glass*, Chap. 4 (Oxford).
THOMAS, W. F., 1958, *Nature, Lond.*, **181,** 1006.

Ageing Effects in Bimetallic Films†

By C. Weaver and R. M. Hill‡
Department of Natural Philosophy,
The Royal College of Science and Technology, Glasgow

[Received June 22, 1959]

Abstract

Measurements of adhesion have been made on films of silver, gold, copper and aluminium with underlayers of chromium. The films have all been deposited on glass microscope slides by vacuum evaporation and the adhesion has been measured by drawing a smoothly rounded point across the surface whilst increasing the load on the point until a clear, well-defined channel was produced. It has been shown that in the case of bimetallic films, abnormally high figures may be obtained due to the formation of an intermediate layer by diffusion or intermetallic reaction. The results show a dependence upon the thickness of the chromium underlayer and time as well as upon the metal of the upper layer. Explanations are based upon a structural model for chromium films which assumes an aggregated structure formed of oxide-coated particles below 400 Å thickness and a continuous metallic structure above this thickness. It is shown that intermediate layer formation occurs only when the thickness of chromium exceeds 400 Å and where some degree of miscibility of the two metals exists. The rate of ageing depends upon the extent of miscibility.

§ 1. Introduction

The advantages of using a thin chromium underlayer, when preparing front surface mirrors by vacuum deposition of aluminium, have long been realized (Strong 1935, Holland 1956). A layer of chromium deposited on the glass substrate immediately before evaporation of the aluminium not only acts as a buffer, preventing attack of the aluminium by the alkali in the glass, but also improves the adhesion and general durability of the aluminium. This effect has been investigated by Heavens (1950) and by Weaver and Hill (1958) who attributed the increased adhesion partly to the better adhesion of chromium to glass as compared with aluminium, and partly to the effects of an intermetallic reaction at the interface between the chromium and the aluminium. The nature and effects of the intermetallic reaction were clarified further by observing the behaviour of aluminium films deposited on underlayers of nickel, cobalt and chromel (Weaver and Hill 1959). These metals effectively replaced the chromium and the ageing effects which occurred in each case were in accordance with the intermetallic compound formation shown in the binary phase diagrams. No evidence was found to support the theory of orientated overgrowth which had been suggested by Heavens (1950) in the case of aluminium on chromium.

---

† Communicated by the Authors.

‡ Now with Commonwealth Scientific and Industrial Research Organisation, Metrology Division, Sydney, N.S.W., Australia.

The present work covers the effect of chromium underlayers upon the adhesion of silver, gold, copper and aluminium. It is an attempt to extend our knowledge of phenomena in two-layer films by considering metals which are either completely non-miscible or only partially miscible as well as aluminium which forms both compounds and solutions with chromium. The binary phase diagrams (Hansen 1958) for chromium on the one hand and silver, gold, copper on the other show that for silver-chromium and copper-chromium the miscibility is limited even in the liquid state. In the case of silver, no solid solutions or compounds are known. Copper dissolves chromium slightly to form a solid solution having a maximum concentration of 0·6%. There may also be a slight solubility of copper in chromium but this is not definitely established and must in any case be very small. There are no other solid solutions or compounds. Gold and chromium are miscible in the liquid state and terminal solid solutions are formed over limited ranges at each end. The limits are, however, wider than for copper.

The choice of metals was guided to some extent by the earlier work of Heavens (1950) and Heavens and Collins (1952) who proposed a theory of oriented overgrowth. They did not, however, take any account of ageing effects such as are presented here.

§ 2. EXPERIMENTAL

The metal films were deposited on microscope slides. A rotating jig was used inside the vacuum chamber and operated through a Wilson seal so that the slides could be brought into position above each heater in turn. Separate heaters screened from each other were used for the chromium and the metal of the upper layer, and suitable masks were used in front of the slides so that the chromium, which was deposited first, covered two-thirds of the length of the slide measuring from one end: while the upper layer covered two-thirds of the slide length measured from the other end. The centre of the slide was thus covered by a two-layer film while the two ends carried single films of the separate metals. The microscope slides were cleaned by vigorous scrubbing with Teepol solution to remove dirt and grease and then rinsed under running water and finally dried on a linen cloth and polished with lens tissue immediately before placing them in the vacuum chamber. The full surface of the slide was exposed to a glow discharge for about 15 min during the pumping cycle and the evaporations were carried out at a pressure of about $2–5 \times 10^{-5}$ mm Hg as measured by an ionization gauge in the vacuum chamber. A manually operated shutter was used to cover the heaters so that they could be brought up to the operating temperature before swinging the shutter aside and allowing deposition to start.

The chromium films were deposited at a rate of about 10 Å/sec and the thickness of each was monitored during deposition and finally measured *in vacuo* by determining the optical transmission for white light. A calibration curve of film thickness against transmission was obtained by weighing a number of specimen slides, covered with chromium only, on a micro-balance immediately after deposition. The thickness was calculated from the bulk density so that an effective weight thickness was obtained. The upper layers of silver, gold, copper and aluminium were evaporated to be just opaque, corresponding to thicknesses of several hundred angstroms.

Measurements of adhesion were made immediately after removal of the slides from the vacuum chamber, the three sections on each slide giving values for the chromium alone, the two-layer film and for the upper layer of silver, gold, copper or aluminium when in direct contact with glass. Some of the specimens were then aged at room temperature for about two weeks while others were aged in hot-air ovens at 120°C for about three days. Measurements of adhesion were repeated at suitable time intervals during ageing. The measurements were made by drawing a smoothly rounded chrome-steel point across the films and finding the minimum load required on the point in each case to remove the film leaving a clear channel. This method was described by Heavens (1950) and has been analysed by Benjamin and Weaver (1959) for the case of single films. They showed that the shearing force at the film/substrate interface could be calculated from the critical load and the tip radius of the point.

It has also been shown by Weaver and Hill (1958, 1959) that in the case of two-layer films, such measurements are no longer purely dependent on adhesion. Where intermetallic reactions occurred between the metals of the two layers, abnormal adhesion figures were obtained. The results indicated that the formation of a hard intermediate layer of an intermetallic compound tended to spread the applied load on the point over a wider area so that a greater load was required to produce the required shearing force at the film/substrate interface and ensure removal of the film from the substrate. The excess loads thus gave an indication of hardening in an intermediate layer and valuable information could be obtained from ageing effects.

All measurements of this nature will, however, be referred to here as adhesion measurements even though this may not always be strictly correct.

§ 3. Results

3.1. *Silver–Chromium*

It has been shown previously (Weaver and Hill 1958, 1959) that in the case of two-layer films the measured adhesion depends upon both time and the thickness of the underlayer. The results obtained for films of silver upon chromium immediately after preparation are shown in fig. 1. Silver films alone on glass have a low adhesion which rises slightly on ageing. For the two-layer films there was a marked dependence upon the thickness of the chromium underlayer resulting in a step at a chromium film thickness of about 400 Å. This is in general agreement with the earlier observations of Heavens (1950) except that, as in the case of aluminium–chromium, our adhesions for thin films are not negligible and there is a smoother transition around 400 Å. In a number of cases it was noticed that, even though a clearly defined channel was produced by the chrome-steel point, some

Fig. 1

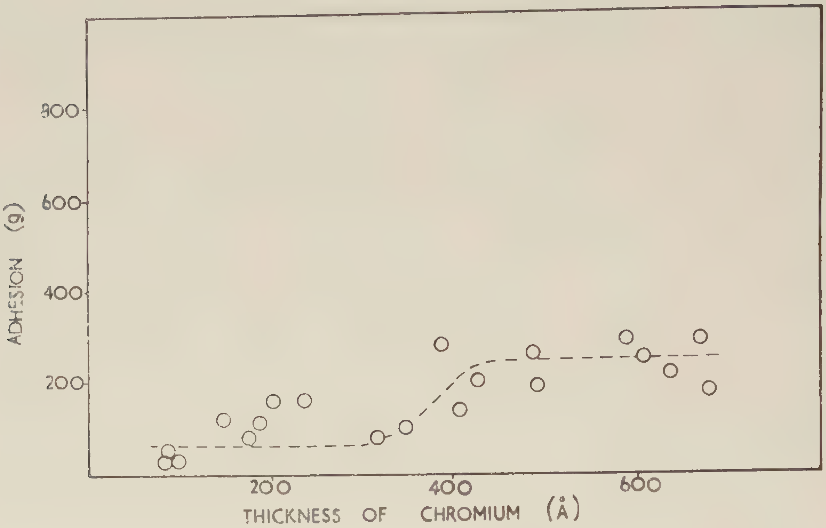

Initial adhesion of silver–chromium two-layer films on glass.

Fig. 2

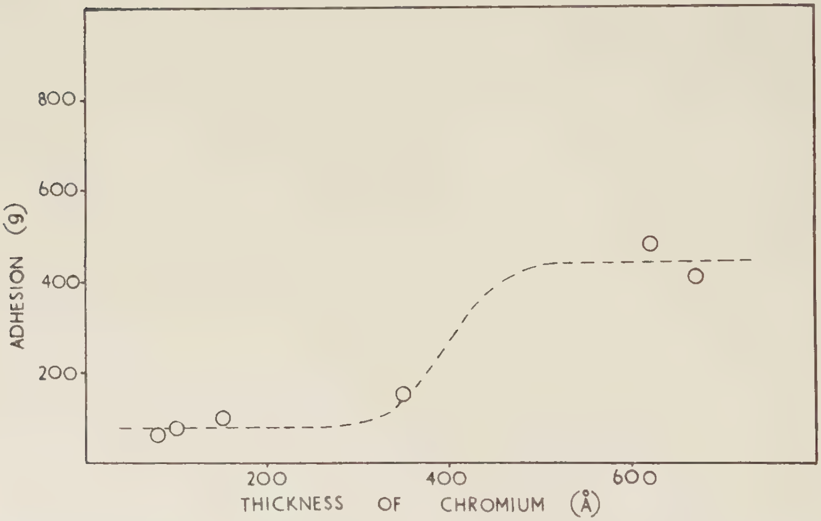

Final adhesion of silver–chromium two-layer films aged at room temperature.

chromium remained on the glass. This effect was confined to the thinner chromium films and was often difficult to detect when the chromium was very thin and almost transparent. The low adhesion values obtained with chromium films below 400 Å could, however, be attributed almost entirely to this stripping effect. For thicknesses of chromium exceeding 400 Å the measured adhesion was of the same order as the chromium alone and no signs of peeling of the silver were observed.

The adhesions after ageing for two weeks at room temperature are shown in fig. 2. The only significant change was that the adhesions had risen somewhat where the thickness of chromium exceeded 400 Å. This could be due simply to the ageing of the chromium underlayer. The adhesion of the chromium itself increases with ageing and the adhesion of the double-layer film is not appreciably different. Films aged at 120° gave, after about three days, the final adhesion results shown in fig. 3. The only significant point was that the adhesion of films having a thin chromium underlayer increased somewhat when aged at this higher temperature. For thicker chromium underlayers the adhesion of the two-layer film corresponded to the adhesion of the chromium itself.

Fig. 3

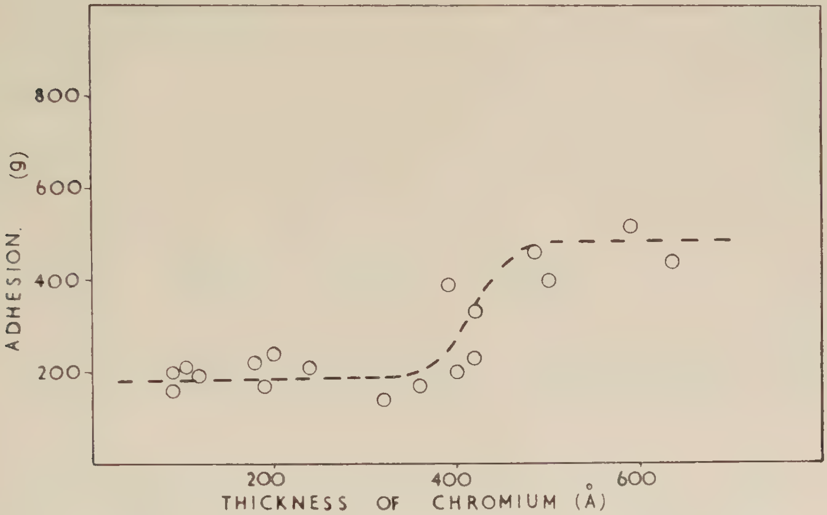

Final adhesion of silver–chromium two-layer films aged at 120°C.

3.2. *Gold–Chromium*

Measurements of initial adhesion of gold–chromium two layer films gave the results shown in fig. 4. Gold films themselves on glass have a poor adhesion, requiring a load of about 2 g to remove them and there is no change with time. In the same way as for silver, the adhesion of double-layer films of gold upon chromium showed a dependence upon the thickness of chromium with a step at about 400 Å. Stripping of the gold off the chromium was again observed for small thicknesses of chromium and this accounted for the low adhesion figures. These results and the presence of a step at 400 A are again in general agreement with earlier observations (Heavens and Collins 1952). For thicker chromium underlayers, no stripping occurred and the measured adhesion was noticeably greater than in the case of silver and certainly greater than the basic adhesion of the chromium underlayer.

Fig. 4

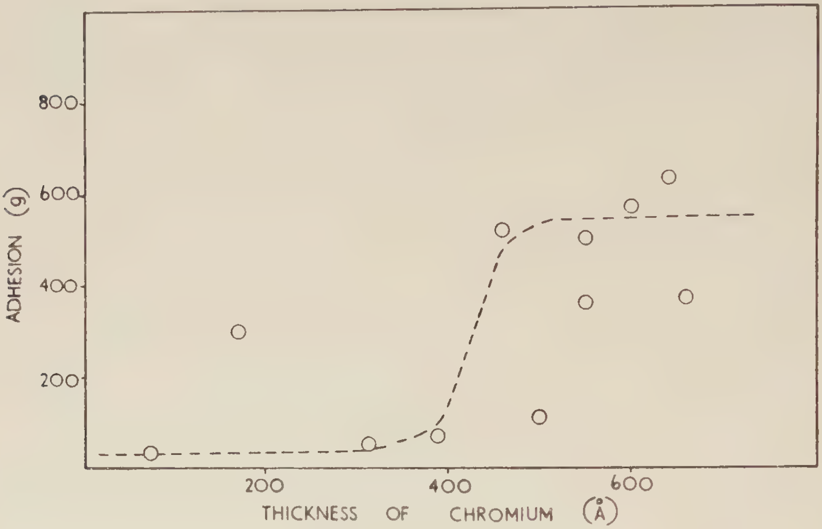

Initial adhesion of gold–chromium two-layer films on glass.

Fig. 5

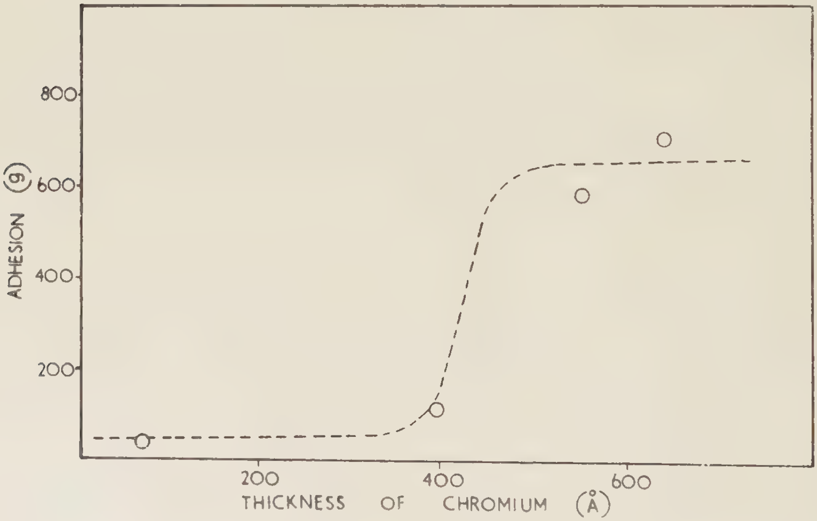

Final adhesion of gold–chromium two-layer films aged at room temperature.

The adhesion figures given in fig. 5, obtained after ageing films at room temperature, showed little difference from the initial figures apart from an increased adhesion for thick chromium underlayers. Stripping of the gold off the chromium still occurred where the chromium films were below 400 Å thick. As in the case of silver, ageing at 120°c produced an increased adhesion for films with thin chromium underlayers. This is shown in fig. 6. No stripping of the gold was observed. It can also be seen that where the thickness of chromium exceeded 400 Å, there was no significant increase in adhesion.

Fig. 6

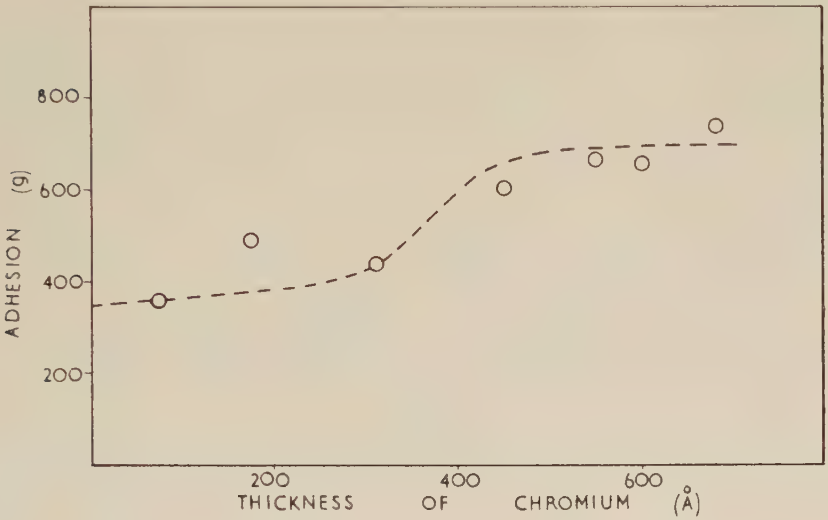

Final adhesion of gold–chromium two-layer films aged at 120°c.

3.3. *Copper–Chromium*

Two-layer films of copper on chromium were investigated by Heavens and Collins (1952) but no figures were given. They claimed that the increase in adhesion was independent of the thickness of the chromium underlayer but this has not been confirmed by our results. Initial adhesion measurements gave the results shown in fig. 7. In spite of a certain amount of scatter the general trend still indicated a step in the region of 400 Å with higher adhesions for thick chromium underlayers. There was, however, a very pronounced increase in adhesion where the chromium underlayer was less than 400 Å, particularly as compared with silver and gold. Copper films alone on glass have a higher adhesion than silver or gold but the critical load required to remove the films is still only of the order of 30 g, rising to this value very rapidly and showing little change thereafter. There was therefore a marked increase in adhesion over the whole range of chromium film thickness but the step around 400 Å still remained. No stripping of copper off the chromium could be seen in any specimens.

Ageing at room temperature gave final results of the same order of magnitude as may be seen in fig. 8. Ageing at 120° resulted, however, in a decreased adhesion where the chromium underlayer was below 400 Å thick.

Fig. 7

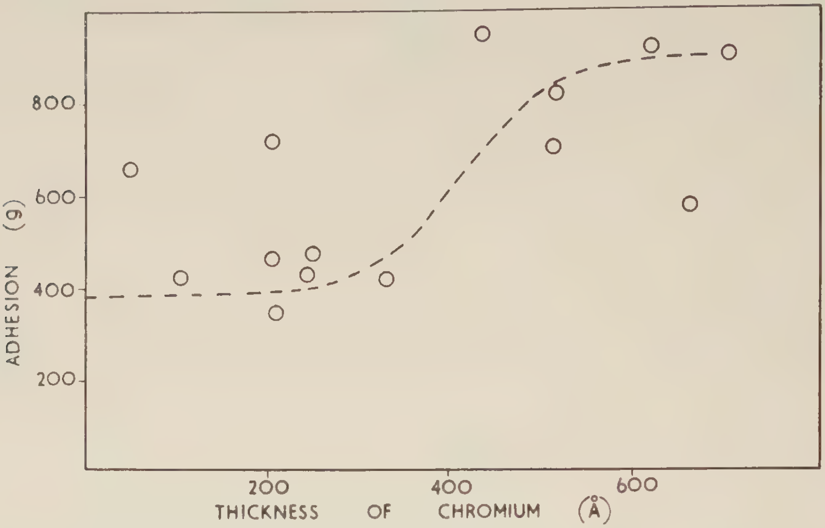

Initial adhesion of copper–chromium two-layer films on glass.

Fig. 8

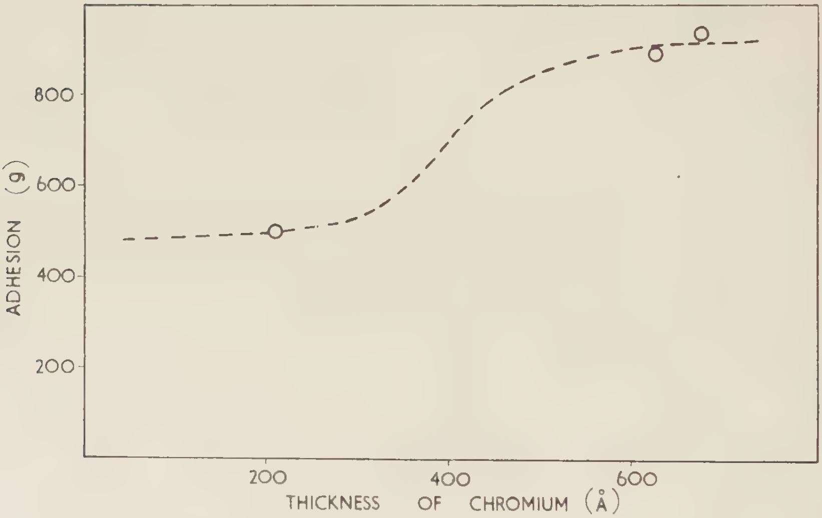

Final adhesion of copper–chromium two-layer films aged at room temperature.

The final figures were comparable with the adhesions of silver and gold specimens which had the same thickness of chromium and had been subjected to the same ageing treatment, but were below the original, initial values for copper–chromium films. These results are shown in fig. 9 and it may be seen that the ageing had little effect when the chromium underlayer was thicker.

Fig. 9

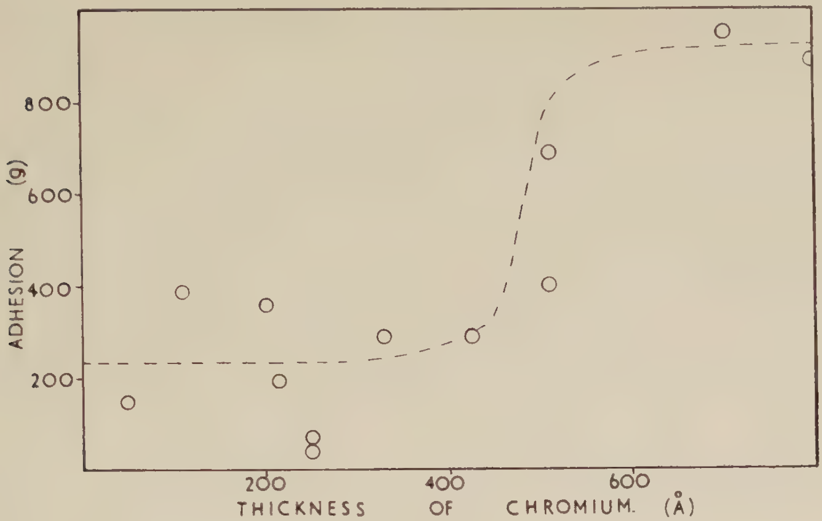

Final adhesion of copper–chromium two-layer films aged at 120°c.

3.4. *Aluminium–Chromium*

Ageing curves for aluminium on chromium have been given previously (Weaver and Hill 1958) and its behaviour has been discussed. Further results are given in figs. 10, 11, 12, which show initial adhesion values and

Fig. 10

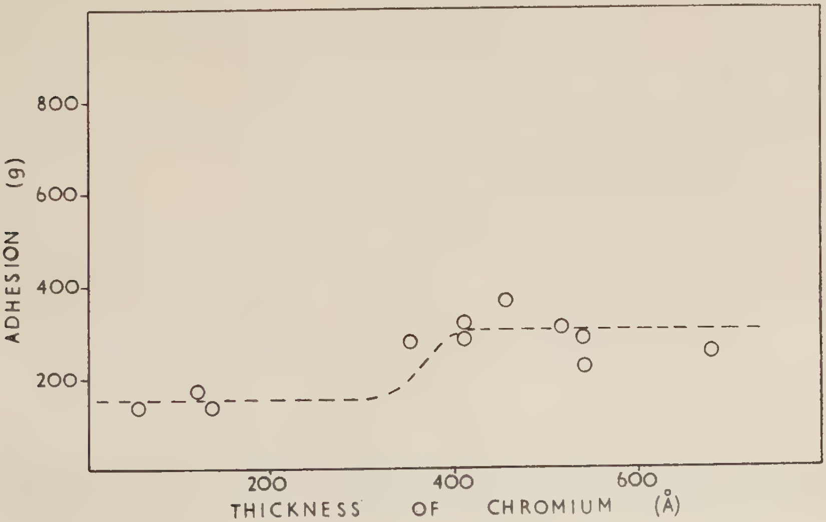

Initial adhesion of aluminium–chromium two-layer films on glass.

Fig. 11

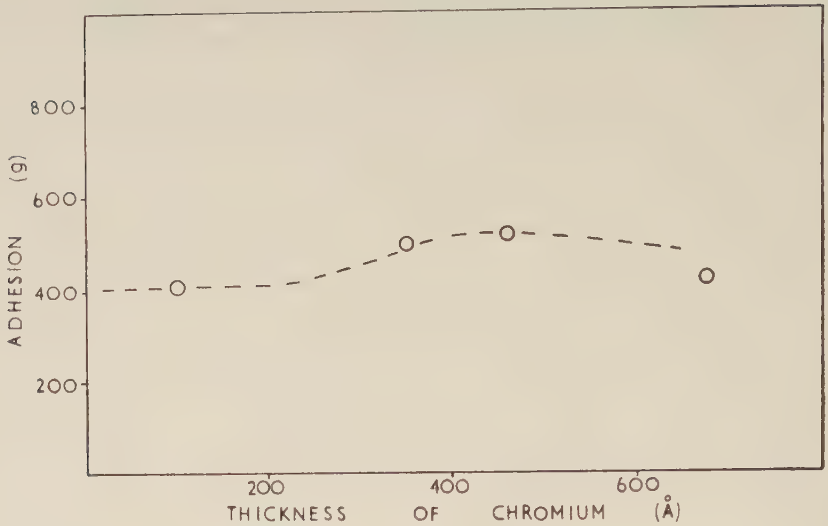

Final adhesion of aluminium–chromium two-layer films aged at room temperature.

Fig. 12

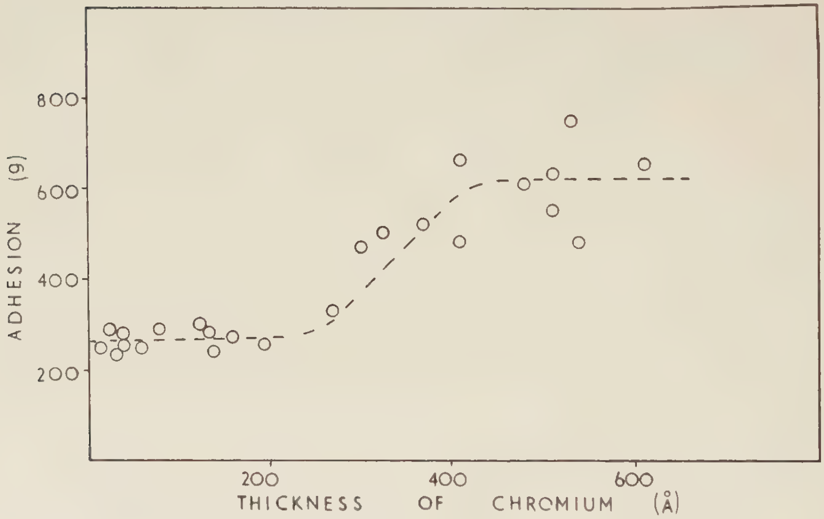

Final adhesion of aluminium–chromium two-layer films aged at 120°c.

the results of ageing at room temperature and 120°c respectively. In this form the results show clearly the effects of the thickness of the chromium underlayer in the same way as for the preceding three metals. No stripping of the aluminium off the chromium was noticed under any conditions and the curves for aluminium generally tended to show resemblances to the results for copper but with somewhat lower adhesion figures in most cases.

§ 4. Discussion

4.1. *General*

The most obvious feature of the results which have been presented is the step which occurs in all the curves at a chromium film thickness of about 400 Å. This feature is peculiar to chromium and did not occur with underlayers of nickel, cobalt or even chromel (Weaver and Hill 1959). The explanation must therefore lie in the structure of the chromium films. The optical properties of evaporated chromium films (Hill and Weaver 1958) have already indicated that the films are non-homogeneous. Analysis of the experimental data suggested that chromium films were formed of particles or aggregates which could be regarded as oblate spheroids with the minor axis perpendicular to the substrate, and that each particle was surrounded by a very thin film of oxide formed during deposition. In the growth of a chromium film from the vapour, the first layer forms as minute spheroids and successive layers are formed of particles which become progressively larger and more oblate as the film thickness increases, tending eventually to the form of platelets. As the platelets become larger and extend laterally the film structure approaches the bulk metal and for films exceeding 500 Å in thickness the optical constants of the upper layers are almost identical with those of bulk metal (Hill and Weaver 1958 a). The results presented here suggest that this transition from an aggregated to a continuous structure takes place around 400 Å film thickness and that a true metal–metal contact at the interface of a two-layer film is only obtained when the thickness of chromium exceeds 400 Å. For thinner films the aggregated structure and the existence of an oxide barrier layer must be taken into account. It is therefore convenient in considering the results to classify according to the thickness of the chromium underlayer and to deal with thin films and thick films separately.

The factors which have to be taken into account are:

(1) The nature of the phase diagrams and degree of miscibility.

(2) The structures of the different metals; chromium is b.c.c. whereas the other metals are all f.c.c.

(3) The atomic diameters; silver, gold and aluminium have values of 2·88 Å, 2·878 Å and 2·85 Å respectively and are therefore almost identical while copper and chromium have values of 2·55 Å and 2·57 Å respectively (Hume-Rothery 1954).

(4) Oxide formation.

(5) The evidence for overgrowth (Heavens 1950, Heavens and Collins 1952).

4.2. *Initial adhesion*

4.2.1. *Thin films*

For both silver and gold the adhesion as shown in figs. 1 and 4 was poor and this was apparently due to peeling or stripping of the top film off the chromium underlayer. The method of measurement produced a clean, well-defined channel but this was due to lack of adhesion between the silver or gold and the underlying film. The residual chromium could not be detected in very thin films which were almost transparent but was observed with thicker chromium films which were still less than 400 Å thick. The lack of adhesion must be due to the oxide layer round the chromium particles since thicker chromium films gave comparatively good adhesion.

Copper and aluminium both showed fairly good adhesion and no stripping of the metal off the chromium could be detected. This could not be due to inter-diffusion and formation of a layer of compound or solid solution at the interface since gold forms solid solutions with chromium over a more extended range than copper and yet has a poor adhesion to chromium, of the same order as silver which does not form solid solutions at all. It is significant that both copper and aluminium adhere directly to glass much better than either silver or gold. Benjamin and Weaver (1959) have shown that this is due to an oxide bonding, or formation of an intermediate layer of metal oxide which is bonded to the glass on one side and to metal on the other and gives a gradual structural transition. The oxide surrounding the chromium particles in thin films would present a surface of a non-metallic nature to the incident metal atoms of the upper layer and we would suggest that the bonding of the top layer of metal onto this oxide is analogous to the bonding of metal to glass. This would explain the high adhesions of the oxide-forming metals, copper and aluminium, as compared with gold and silver. It has also been observed that copper on glass forms its oxide bond almost immediately and thereafter shows constant adhesion, whereas aluminium deposited on glass at normal evaporation pressures does not form a complete oxide bond immediately and the adhesion rises with time. Comparison of the initial parts of the curves in figs. 8 and 11 with the corresponding figs. 7 and 10 show that the same sort of thing is happening here upon ageing at room temperature. The analogy is, however, not perfect since it suggests that the lower adhesion figures for aluminium as compared with copper are due to differences in bonding to the chromium and this in turn implies a stripping of the top layer of metal from the chromium below. The absence of such stripping indicates that the bonding between the two metals in the two-layer film was adequate in both cases. The initial adhesion figures for a copper chromium film were almost the same as the figures for chromium alone, suggesting that the bonding of the copper to the chromium allowed full advantage to be taken of the basic adhesion of the chromium. The initial figures for an aluminium–chromium film, however, tended to be lower than the corresponding figures for the chromium alone. It would appear that the deposition of the aluminium on top of the chromium caused an initial decrease of the basic bonding of the chromium to the glass and we would attribute this to the high energy of the incident atoms, together with the high energy of formation of aluminium oxide, and attendant lattice expansion, introducing a strain into the thin chromium underlayer. This could cause a rearrangement of the internal structure and loosen somewhat the bonding to the glass substrate in a manner somewhat similar to the effects of strong compound formation as observed with aluminium–nickel and aluminium–cobalt films (Weaver and Hill 1959).

4.2.2. *Thick films*

Good adhesion of the upper layer to the chromium was obtained in all cases and no stripping of the top layer could be detected. The structural model which we have assumed for chromium films suggests that direct metal–metal contact would be obtained between the upper layer and the chromium for thicknesses of chromium exceeding 400 Å. Under these conditions the initial adhesion cannot be due to normal diffusion of the chromium into the upper layer of metal even though diffusion of the chromium atom is favoured firstly by the size and, secondly, by the melting points of the terminal solutions (Le Claire 1949, Mehl 1936). The rapidity with which the bonding is established would suggest that it is due either to the direct contact of metal to metal or to grain boundary diffusion. Silver and gold are very similar in properties and of almost identical size. Furthermore, the difference in polarizabilities is only small (van Vleck 1932). Consequently, substantial differences in the van der Waals forces between these metals and chromium are impossible, and differences in metallic bonding are unlikely; nevertheless a substantial difference does exist between the adhesion measurements. On the other hand grain boundary diffusion of the upper metal into the chromium is likely, firstly, because of the microcrystalline structure of thin films and, secondly because of the excess energy of the incident atoms which could supply the necessary activation energy. The higher adhesion of gold and copper as compared with silver could then be due (1) to the higher temperatures required for evaporation of these metals, and (2) to the solid solubility in these cases as contrasted with silver which shows no solid solubility. Aluminium also has regions of solid solubility and compound formation, but the gettering action which has often been observed with aluminium together with the high oxidation energy suggests that an oxide film barrier could be formed in this case where it is unlikely in the others, and thus retard diffusion. These views are confirmed to some extent by the relative magnitudes of the adhesion measurements. For silver and aluminium the adhesions of the two-layer films are of the same order as single films of chromium. The adhesion of the upper layer to the chromium is sufficient to prevent peeling and the adhesion of the chromium to the glass is obtained. The figures for gold and copper are, however, considerably higher and reference to the previous work upon aluminium with underlayers of nickel, cobalt and chromel (Weaver and Hill 1959) suggests the formation of a harder, strained intermediate layer at the metal–metal interface. This could be due to the formation of a layer of solid solution, of somewhat different lattice spacing, causing a resultant strain.

4.3. *Ageing at Room Temperature*

4.3.1. *Thin films*

Ageing at room temperature produced no significant changes in the adhesion of silver and gold films deposited upon thin chromium underlayers. Stripping of the top metal off the chromium still occurred. Copper films likewise showed little change but here the initial adhesion was good and any small increases could be attributed entirely to ageing of the chromium underlayer. Only aluminium showed marked increases in adhesion and the difference as compared with copper could be due in part to the continued formation of oxide at the aluminium-chromium interface, assuming, as explained in §4.2.1, a similarity to the behaviour of these metals on glass substrates. This must, however, be accompanied by an increase in the basic adhesion of the chromium underlayer to the glass substrate since the two-layer films have an initial adhesion which is lower than the adhesion of chromium films themselves, and the increase in adhesion on ageing is otherwise greater than we would expect on the basis of formation of an intermediate hard layer between the aluminium and chromium. Our earlier results for aluminium–chromium (Weaver and Hill 1958), obtained without using a shutter over the chromium heater and therefore showing poor adhesion of the chromium films, indicated an increase of about 150–250 g in the measured adhesion during ageing whereas our present results show an increase of the order of 300 g and it is the difference between these figures which we would assign to the ageing of the chromium itself.

The earlier electron diffraction results on thin films of aluminium and chromium also showed the formation of a solid solution and possibly compounds of the two metals, accompanying the oxidation of the aluminium. This indicates, in this case at least, a diffusion of metal through the oxide barrier during ageing. The enhanced adhesion figures certainly indicate a hard intermediate layer between the aluminium and chromium but the nature of this layer would appear somewhat complex, including oxides of both metals as well as the metallic solid solution and possibly compounds.

4.3.2. *Thick films*

In general, for this range of chromium thicknesses, the two-layer films showed increases in adhesion during ageing at room temperature. In the case of silver this corresponded simply to the ageing of the chromium underlayer. There was no evidence of further diffusion. A typical ageing curve shown in fig. 13 suggests that the initial grain boundary diffusion of silver into chromium causes strain and some loosening of the basic adhesion of the chromium followed by a recovery due presumably to slight structural readjustments at the glass–chromium interface. The final adhesion figures for the two-layer films are very close to the figures for chromium alone.

Fig. 13

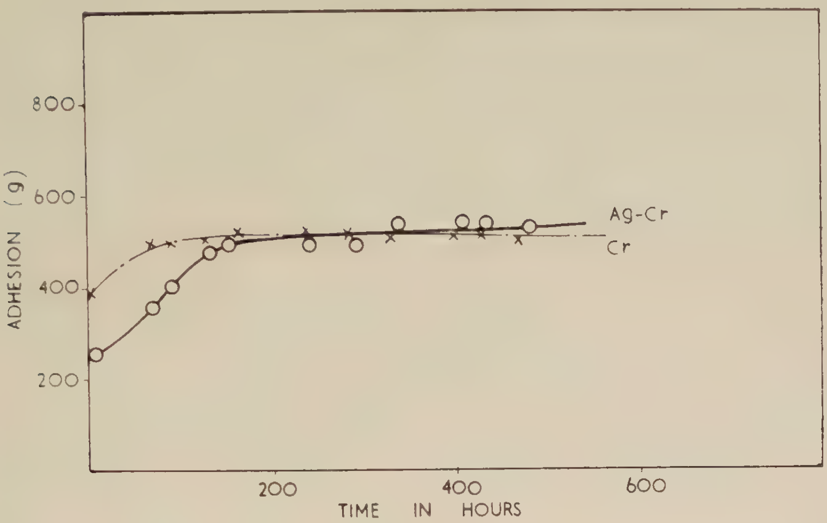

Ageing curve for silver–chromium two-layer film at room temperature. Thickness of chromium = 625 Å.

Fig. 14

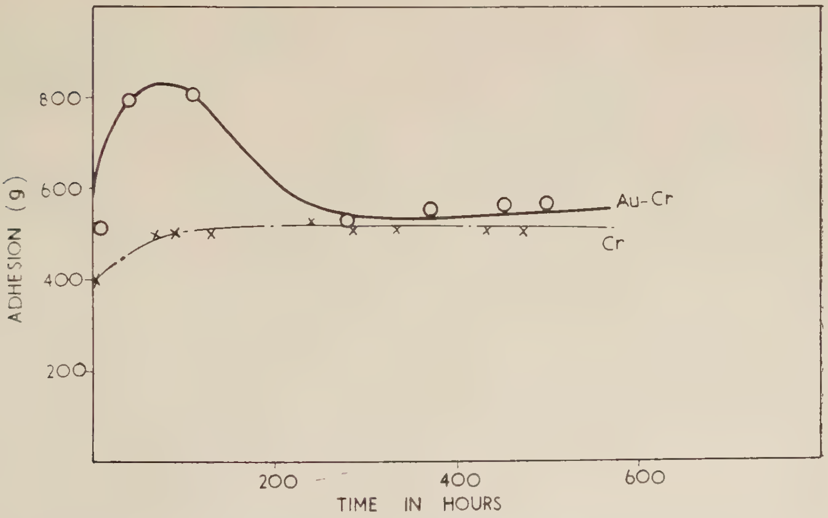

Ageing curve for gold–chromium two-layer film at room temperature. Thickness of chromium = 550 Å.

The ageing curves for gold–chromium and copper–chromium two-layer films shown in figs. 14 and 15 both show an initial peak followed by a decrease, suggesting the formation and precipitation of the solid solutions indicated by the phase diagrams, thus giving effects which are much less pronounced than those observed with aluminium underlaid by nickel or cobalt (Weaver and Hill 1959). The limited range of the solid solutions appears to cause rapid formation and precipitation. It would also mean that there would only be small differences in lattice spacings between the metals and the solid solutions and so no pronounced age-hardening effects are to be expected. Silver does not form solid solutions and does not show any peak in the ageing curves. Aluminium forms an extended range of compounds and solid solutions resulting in both excessive adhesion figures and ageing curves showing age-hardening.

Fig. 15

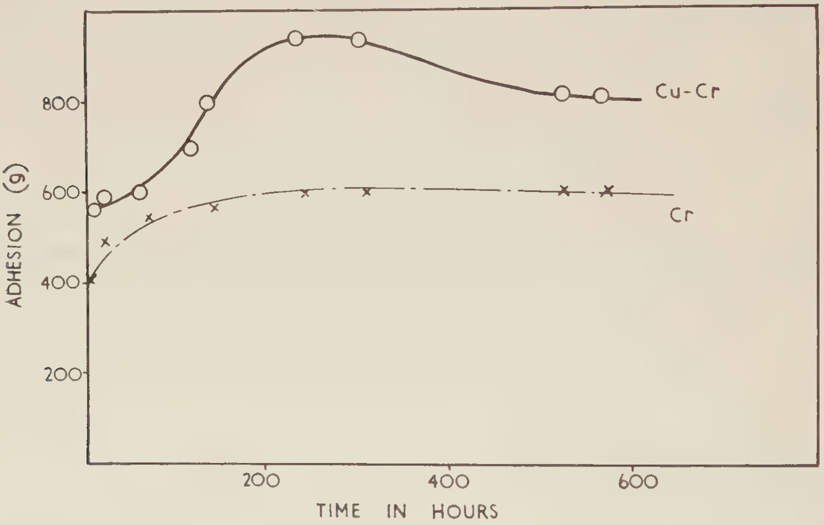

Ageing curve for copper-chromium two-layer film at room temperature. Thickness of chromium = 500 Å.

4.4. *Ageing at 120°C*

4.4.1 *Thin films*

Ageing at 120°c causes silver–chromium and gold–chromium two-layer films to acquire an adhesion which is not produced by ageing at room temperature. The upper metals no longer strip off the chromium underlayer after ageing. This increased bonding between the two metal layers cannot be due to an oxide bond since these are noble metals, and the existence of an oxide skin over the particles of chromium together with the lack of solid solutions between silver and chromium precludes the possibility of normal diffusion. It would therefore appear that the adhesion of the upper metal to the chromium underlayer is due to a form of grain boundary diffusion or penetration of the metal between the chromium aggregates which implies a surface diffusion of the noble metal over the oxide surface. A higher temperature would be needed for penetration of the oxide and in any case the lack of solid solutions in the case of silver would prevent diffusion through the barrier.

It is highly significant that in all cases the final adhesion is lower than the basic adhesion of chromium alone after the same treatment and yet no stripping of the upper metal could be detected in any instance. This suggests in the case of silver and gold at least, that the increase of adhesion between the noble metal and the chromium was accompanied by a reduction of the adhesion between the chromium and the glass. It would appear that the penetration of the metal between the particles of chromium creates a strain which is only accommodated by a partial breaking of the bonds between the chromium and the glass and some readjustment of the aggregated structure.

If this argument is admissible in the case of gold and silver, then the decrease in adhesion observed with copper is automatically explained as a decrease in the basic adhesion of the chromium underlayers, for there is no reason to suppose that copper would not diffuse over the oxide surface in the same manner. High adhesions were observed initially and even after ageing at room temperature because the strong bonding of the copper to the chromium allowed full advantage to be taken of the high basic adhesion of the chromium and no loosening of the chromium bonding was produced. The lower adhesion of aluminium–chromium films, as compared with films aged at room temperature, can be explained in the same way.

4.4.2. *Thick films*

In the case of silver–chromium films, ageing at 120°c produces results which differ little from those obtained at room temperature. The increases in adhesion produced by ageing correspond to ageing of the chromium underlayer. There is no evidence of any diffusion apart from the early grain-boundary diffusion discussed in §4.2.2. This is in accordance with the absence of solid solutions or compounds.

For both gold and copper the adhesion remains more or less constant but considerably greater than the adhesion of chromium itself. This suggests the formation of a hard intermediate layer between the upper metal and the chromium, tending to spread the applied load over a greater area so that a greater load is required to develop the same shearing forces at the chromium–glass interface. The absence of this effect with silver which is non-miscible with chromium, together with the fact that both gold-chromium and copper-chromium give high adhesion figures, suggests strongly that this layer is due to formation of solid solutions rather than oxide formation. Both gold and copper form terminal solid solutions over ranges which are severely limited. As explained in §4.3.2 and shown in figs. 14, 15, the ageing curves have peaks which suggest an early formation and precipitation of solid solution, the speed of formation being apparently due to the restricted concentration range. The high initial adhesion figures in both cases lead us to conclude that the solid solutions are almost completely formed before the adhesion measurements can be made and that only minor changes occur thereafter.

The adhesion figures for aluminium after ageing were also higher than the figures for chromium alone, but the high adhesion was only developed after ageing. This would seem to be accounted for by the wide range of solid solutions and compounds as compared with gold and copper. The development of a strained and therefore harder intermediate zone takes longer, although this could in part be due to a possible oxide barrier layer retarding diffusion as suggested in § 4.2.2.

§ 5. Conclusions

Acceptance of the model which has been proposed previously for chromium films on the basis of their optical properties leads to valid explanations of the adhesion figures. The general nature of the present results indicates that the transition from an aggregated to a continuous structure takes place at a film thickness around 400 Å. For thinner films of chromium the adhesion of the upper metal to the chromium is strongly affected by the oxide coating round the chromium aggregates and effective intermetallic adhesion is only obtained when the upper metal is oxygen-active and can form an 'oxide bond'. At higher temperatures, grain-boundary diffusion into these thin films of chromium can occur and produces a deterioration of the basic adhesion of the chromium to the glass substrate.

From the behaviour of silver deposited on thicker films of chromium it would appear that some grain-boundary diffusion of the upper metal into the lower is possible even where no solid state miscibility exists, but a direct metal–metal contact is essential for a high adhesion to be obtained and the measurements obtained cannot, in any case, be appreciably greater than the basic adhesion of the chromium underlayer.

Adhesion figures greater than the basic adhesion of the chromium underlayer are obtained where an intermediate layer is formed between the two metals of a two-layer film. As explained earlier, such layers appear to cause strain and a degree of hardness which tends to distribute the applied load over a greater area so that the critical loads required are correspondingly greater. Some degree of solid-state miscibility appears to be essential for such intermediate layers to be formed and the formation and stabilization is more rapid where the range of solid solutions is small. A wide range of solid solutions and compounds as in the case of aluminium seems to lead to slower ageing. The earlier results on aluminium films with underlayers of nickel and cobalt indicate that preferential compound formation can cause the ageing to go a stage further, sometimes with disastrous results. Where the compound formation can be controlled as with chromel underlayers excellent results can be obtained, giving highly durable films.

The existence of oxide at the interface between the two metal films does not appear to affect results, except as an oxide on the lower metal preventing inter-diffusion. With thick chromium underlayers, the increased adhesion of gold which does not oxidize is comparable with the adhesions of copper and aluminium which do oxidize. Furthermore, copper films on thin chromium underlayers appear to be bonded by an intermediate layer of oxide but there is no increase of adhesion measurements above the figures for chromium itself, and with aluminium there is actually a decrease of adhesion. This leads us to conclude that the presence of oxide has no direct effect on adhesion measurements. The increased adhesion figures which have been obtained can be attributed entirely to formation of solid solutions or compounds and the consequent hardening effects.

The evidence for oriented overgrowth appears to have been extremely limited and the suggestion that a randomly oriented layer of chromium could induce random orientation of the top layer is somewhat difficult to accept. The difference in structures between chromium (b.c.c.) and the other metals (f.c.c.) is against overgrowth and no further evidence in favour of this theory has been found.

ACKNOWLEDGMENTS

Finally, one of us (R.M.H.) wishes to thank the Caird Trust for the provision of a post-graduate research grant.

REFERENCES

BENJAMIN, P., and WEAVER, C., 1959, *Proc. roy. Soc.* A, **252, 418.**

HANSEN, M., 1958, *Constitution of Binary Alloys* (McGraw-Hill).

HEAVENS, O. S., 1950, *J. Phys. Radium*, **11,** 355.

HEAVENS, O. S., and COLLINS, L. E., 1952, *J. Phys. Radium*, **13,** 658.

HILL, R. M., and WEAVER, C., 1958 a, *Trans. Faraday Soc.*, **54,** 1140 ; 1958 b, *Ibid.*, **54,** 1464.

HOLLAND, L., 1956, *Vacuum Deposition of Thin Films* (London: Chapman & Hall), p. 341.

HUME-ROTHERY, W., 1954, *The Structure of Metals and Alloys* (London: Institute of Metals), p. 87.

LE CLAIRE, A. D., 1949, *Progress in Metal Physics*, **1,** 306 (London: Butterworths Scientific Publications).

MEHL, R. F., 1936, *Trans Amer. Inst. min. (metall.) Engrs*, **122,** 11.

STRONG, J., 1935, *Rev. sci. Instrum.*, **16,** 143.

VAN VLECK, J. H., 1932, *Theory of Electric and Magnetic Susceptibilities* (Oxford: Clarendon Press), p. 225.

WEAVER, C., and HILL, R. M., 1958, *Phil. Mag.*, **3,** 1402 ; 1959, *Ibid.*, **4,** 253.

The Magnetic Susceptibility of Vanadium between 20 and 293°K†

By B. G. Childs, W. E. Gardner and J. Penfold
Atomic Energy Research Establishment, Harwell, Berks

[Received June 11, 1959]

Abstract

The magnetic susceptibility of four samples of pure vanadium metal, prepared by different methods, has been measured at 20, 77 and 293°K. The most reliable values obtained are 5·89, 5·88 and $5{\cdot}81 \times 10^{-6}$ e.m.u./g respectively. There appears to be no systematic dependence of susceptibility on the method of preparation but the values obtained are appreciably larger than those reported by previous workers. The reason for this difference is discussed in terms of the impurity contents of the vanadium used in the earlier work.

§ 1. Introduction

The mass susceptibility of vanadium at room temperature was first measured by Honda (1910) who obtained a value of $1{\cdot}50 \times 10^{-6}$ e.m.u./g. In a later measurement Owen (1912) obtained values of $2{\cdot}40 \times 10^{-6}$ and $4{\cdot}15 \times 10^{-6}$ e.m.u./g, on two specimens of different iron contents. Klemm (1939) concluded that the susceptibility was very sensitive to impurities and obtained specimens of pure vanadium from three different sources. He made measurements by the Gouy method at two temperatures, 293 and 90°K, corrected his results for ferromagnetic impurity, and obtained the values given in table 1. The purities of his specimens are given in the second column.

Table 1

Observer	Purity (wt %)	Susceptibility (χ) × 10^6 e.m.u./g	
		Room temperature	90°K
Honda	—	1·50	—
Owen	—	2·40, 4·15	2·40
Klemm	99·85	3·95	3·95
,,	99·8	5·8 (5·0)	7·3 (5·0)
,,	99·7	4·6	4·8
Kriessman	99·8	5·00	—

---

† Communicated by the Author.

Since his second specimen showed a considerable temperature dependence he further corrected his results (figures in brackets) by assuming the presence of a paramagnetic impurity obeying Curie's law. Despite this correction it can be seen that his results show a considerable variation and so his usually quoted mean figure of $4{\cdot}5 \times 10^{-6}$ e.m.u./g for the room temperature susceptibility is rather misleading.

Kriessman (1953) measured the susceptibility of vanadium, described as 99·8% pure, from 298°K to 1973°K and observed a decrease from $5{\cdot}00 \times 10^{-6}$ to $4{\cdot}57 \times 10^{-6}$ e.m.u./g. His results were corrected for the presence of a ferromagnetic impurity.

Our interest in this problem arises from a study of the effect on the susceptibility of vanadium of other transition metals of the first period present in solid solution. For this work we obtained samples of vanadium, which had been prepared by different methods, from four different sources, the U.K.A.E.A. laboratories, Culcheth, Johnson, Matthey and Company (J.M.), the Battelle Memorial Institute, Columbus, Ohio (B.M.I.) and the U.S. Bureau of Mines Electrometallurgical Station (U.S.B.M.).

The Culcheth and J. M. samples were prepared by the calcium reduction of vanadium pentoxide, the Culcheth metal receiving an additional high-temperature degassing treatment. The B.M.I. vanadium was produced from vanadium iodide by the Van Arkel process and the U.S.B.M. metal was prepared electrolytically.

§ 2. EXPERIMENTAL DETAILS

Since all the samples, except that from B.M.I., were granular in form they were arc-melted into buttons on a water-cooled copper hearth in a purified argon atmosphere. From these buttons and the original B.M.I. metal, specimens approximately 8 mm × 1·5 mm × 1·5 mm weighing about 0·070 g were cut with a new carborundum slitting wheel. These specimens were degreased in alcohol, cleaned in dilute hydrochloric acid, and finally washed in distilled water. This process was repeated if subsequent measurements indicated any ferromagnetic contamination.

The susceptibility was measured by the Faraday method using a Sucksmith ring balance with tantalum as a standard (Childs and Penfold 1957). Measurements were made at three temperatures : 20, 77 and 293°K.

§ 3. RESULTS

The results obtained are given in table 2. The standard deviation of the susceptibility values is $0{\cdot}10 \times 10^{-6}$ e.m.u./g. The range of the variation in the room temperature susceptibility values for the different specimens is not large—from 5·64 to $5{\cdot}83 \times 10^{-6}$ e.m.u./g. The temperature dependence for individual specimens is also small, the susceptibility increasing slightly with decreasing temperature (cf. Kriessman and Callen 1954).

Table 2 contains, in addition, the Vickers hardness number and the lattice parameter of each specimen. Most impurities increase the hardness of vanadium (Rostoker 1958) ; the lattice parameter however decreases for

Table 2

Specimen	Source	$\chi \times 10^6$ e.m.u./g			Vickers hardness number (5 kg load)	Lattice parameter (Å)
		20°K	77°K	293°K		
A	Culcheth	5·90	5·90	5·77	220 ± 5	$3{\cdot}032 \pm 0{\cdot}002$
B	Johnson, Matthey & Co.	5·94	5·96	5·83	211 ± 5	$3{\cdot}031^5 \pm 0{\cdot}001$
C1	U.S. Bureau of Mines	5·76	5·75	5·64	118 ± 5	$3{\cdot}029 \pm 0{\cdot}001$
C2	U.S. Bureau of Mines	5·83	5·86	5·77	111 ± 5	$3{\cdot}029 \pm 0{\cdot}001$
D	B.M.I.	5·89	5·88	5·81	90 ± 5	$3{\cdot}025 \pm 0{\cdot}001$

Table 3

Metal	Source	Purity (wt %)	$\chi \times 10^6$ e.m.u./g at 293°K		Reference
			Present work	Previous value	
Platinum	Johnson, Matthey & Co.	99·99	0·979	0·971	Hoare and Walling (1951)
Titanium	Johnson, Matthey & Co.	99·9	3·34	3·31	Denney (1955)
Chromium	Johnson, Matthey & Co. (0·35 wt % oxygen)	99·6	3·51	3·56	McGuire and Kriessman (1952)
Chromium	Aeronautical Res. Labs. Melbourne (0·003 wt % oxygen)	99·9	3·17	3·17	Lingelbach (1958)
Manganese	Johnson, Matthey & Co.	99·9	9·64	9·9	Kriessman and McGuire (1955)

some impurities in substitutional solution but increases for most *interstitial* impurities such as oxygen, nitrogen and carbon (Seybolt and Sumsion 1953). These two quantities taken together are therefore a good guide to the purity of the metal.

Comparing table 1 with table 2 it can be seen that we have obtained a consistent value for the susceptibility which is larger than the value previously accepted. The difference is not associated with experimental errors. We have made measurements on four other transition metals and our results are compared in table 3 with values obtained previously on specimens of comparable purity.

We therefore believe that the discrepancy in the case of vanadium between our results and the earlier work may be associated with the different purities of the samples used. Table 4 lists the principal impurities in our samples as given by the manufacturers and supplemented by further analyses performed in this laboratory.

Table 4. Analysis of Principal Impurities (wt %)

	Purity	C	Si	Cr	Fe	Al	Cu	H	N	O
A	99·6	0·03	—	—	0·10	—	—	0·003	0·01	0·15–0·20
B	99·6	0·044	0·024	0·005	0·10	0·019	0·002	0·001	0·06	0·12
C1	99·7^5	—	0·001	0·003	0·09	0·002	0·002	—	0·003	0·083
C2	99·8^5	—	0·001	—	0·09	0·002	0·003	—	—	0·055
D	99·9	0·005	0·001	0·001	0·04	0·005	0·001	0·001	0·008	0·020

(— Data not available.)

The nominal purities of our samples are about the same as those quoted by the earlier workers. It is possible however that the gas content of the vanadium was not allowed for in their figures. We have observed, for example, that the presence in vanadium of 7 wt % of oxygen decreases its susceptibility to $4{\cdot}8 \times 10^{-6}$ e.m.u./g.

§ 4. CONCLUSION

The physical properties of vanadium are clearly affected by small amounts of impurities, particularly oxygen and nitrogen. It appears that the magnetic susceptibility may be similarly affected. Our specimen D (Van Arkel) contains the least amount of impurity and so gives our best value for the susceptibility of vanadium at room temperature, namely $(5{\cdot}81 \pm 0{\cdot}10) \times 10^{-6}$ e.m.u./g or $(296 \pm 5) \times 10^{6}$ e.m.u./g atom.

ACKNOWLEDGMENTS

We wish to thank Mr. A. D. Le Claire and Dr. P. C. L. Pfeil for helpful advice, Messrs. C. E. Austing, T. W. Baker and members of the alloys section for assistance in the preparation and examination of the specimens. Dr. A. Wexler of the Westinghouse Research Labs. and Dr. D. H. Baker of the U.S. Bureau of Mines kindly supplied us with some of the samples.

REFERENCES

CHILDS, B. G., and PENFOLD, J., 1957, *Phil. Mag.*, **2,** 389.
DENNEY, J. M., 1955, *Phys. Rev.*, **99,** 1640.
HOARE, F. E., and WALLING, J. C., 1951, *Proc. phys. Soc. Lond.* B, **64,** 337.
HONDA, K., 1910, *Ann. Phys., Lpz.*, **32,** 1027.
KLEMM, LI, 1939, *Z. Electrochem.*. **45,** 354.
KRIESSMAN, C. J., 1953, *Rev. mod. Phys.*, **25,** 122.
KRIESSMAN, C. J., and CALLEN, H. B., 1954, *Phys. Rev.*, **94,** 837.
KRIESSMAN, C. J., and MCGUIRE, T. R., 1955, *Phys. Rev.*, **98,** 936.
LINGELBACH, R., 1958, *Z. Phys. Chem.* (Neue Folge), **14,** 1.
MCGUIRE, T. R., and KRIESSMAN, C. J., 1952, *Phys. Rev.*, **85,** 452.
OWEN, M., 1912, *Ann. Phys., Lpz.* **37,** 657.
ROSTOKER, W., 1958, *The Metallurgy of Vanadium* (London : Chapman and Hall).
SEYBOLT, A. U., and SUMSION, H. T., 1953, *Trans. Amer. Inst. min. (metall.) Engrs*, **197,** 292.

Crystal Fine Structure, Conductivity and Cation Self-diffusion in Sodium Chloride†

By I. M. Hoodless‡ and S. J. Thomson‡
Londonderry Laboratory for Radiochemistry,
University of Durham Science Laboratories, South Road, Durham

[Received June 8, 1959]

Abstract

The Na^+ self-diffusion and ionic conductivity have been measured in single crystal plates of sodium chloride in the low temperature range. These plates, which were taken from the same sodium chloride boule, were subjected to either chilling in liquid nitrogen or annealing at 600°–620°c prior to the measurements. Both treatments produced increases in the ionic conductivity while the self-diffusion was relatively unchanged. The results are explained in terms of space charge and impurity effects.

§ 1. Introduction

Two ranges of diffusion exist in the alkali halides (Seitz 1954); the same is true of conductivity, which is, in effect, the diffusion of ions under the influence of an electric field. In sodium chloride the high temperature range occurs above 550°c and here conductivity and diffusion are independent of the past history of the crystal specimen. The movement of the ions is attributed to the presence of Schottky type vacancies, which are thermally created. The Einstein relationship has been found to be valid in this region (Mapother *et al.* 1950). In the lower temperature range the diffusion (and conductivity) of the sodium ion is strongly dependent on the presence of impurities in the crystal. Mapother *et al.* (1950) have explained the invalidity of the Einstein relationship in this region by proposing that a fraction of the aliovalent positive impurity ions are associated with positive ion vacancies. These 'complexes' are effectively neutral and will not therefore contribute to the conductivity but it is assumed that they are sufficiently mobile to contribute to the diffusion. This view is supported by conductivity measurements on cadmium-doped single crystals of sodium chloride (Etzel and Maurer 1950).

The general picture of ion movement in sodium chloride seems therefore to be attributed to movement via vacancies, which are either thermally created or introduced by the presence of aliovalent impurities. Another factor might well be considered, namely the influence of substructure, i.e. grain boundaries and dislocations. Grain-boundary and surface diffusion usually require a lower activation energy than bulk diffusion (Barrer 1951), so it might be expected that these types of diffusion would be important, especially in the low temperature range. Recently the substructure of single crystals of sodium chloride has been investigated by light scattering (Humphreys-Owen 1955), x-ray methods (Jones and Smith 1956) and by etching (Amelinckx 1954), but few experiments have been made to determine its effect on ion movement. Cunnel and Schneider (1954), Caffyn and Schneider (1955), Ewles and Stead (1956) and Ewles and Jain (1958) have measured the ionic conductivity in quenched alkali halide crystals but their results have not completely resolved the role of grain boundaries etc. Measurements of the self-diffusion of both the ions in crystal compacts of sodium chloride have shown the Cl^- ion movement to be strongly dependent on grain size whereas Na^+ ion movement was unchanged. These observations were, however, confined to the high temperature range (Laurent and Bénard 1955).

---

† Communicated by the Authors.

‡ Present address: Department of Chemistry, The University of Glasgow, Glasgow, W.2.

The purpose of the present experiments was to determine the effects of changes in the mosaic structure on the low temperaure Na^+ diffusion and conductivity in single crystals of sodium chloride. It was considered to be essential that all studies should be made on pieces of crystal from the same boule and that the method for measurement of diffusion should be such that several measurements could be made on a single specimen. It was decided also to investigate briefly the surface mobility of Na^+ ions and to examine the possibility of preferential penetration of labelled Na^+ ions in grain boundaries.

§ 2. EXPERIMENTAL

2.1. *Crystal Growth*

Single crystals were grown from a melt of Messrs. B. D. H. Ltd. Analar sodium chloride in a platinum vessel using the Kyropoulos technique. They were allowed to cool from the melting point to room temperature over a period of sixteen hours.

2.2. *Conductivity*

The conductivity was measured by a d.c. pulse method using a circuit similar to that of Mapother *et al.* (1950). Mercury contact switches were used wherever possible and the complete apparatus was mounted on paraffin wax to prevent leakage currents. The crystal, whose contact faces were suitably coated with a conducting material, was held between nickel electrodes and surrounded by a furnace. An Iron-constantan thermocouple, mounted in the lower electrode, measured the crystal temperature. The assembly was enclosed in a Pyrex vessel, through which a stream of dry, oxygen-free nitrogen was continuously passed.

Special care was taken in selecting a conducting material to coat the contact faces; trial experiments were carried out using 'Dag', gold, platinum and silver coatings, the latter proving the most satisfactory. 'Dag', a colloidal suspension of graphite in alcohol, was quite satisfactory for temperatures below 450°c but at higher temperatures it disappeared from the crystal faces. The gold films, which were prepared by evaporation onto the crystal, readily sintered at temperatures above 400°c. The results, using platinum coatings, were also very difficult to interpret and it appeared that the crystal and electrodes acted like a semi-conductor, for the magnitude of the conductivity was dependent on the direction of the current. The measurements, described in this paper, were carried out using a silver coating; this is obtained as a suspension (Melton 'Liquid Silver' Q 50 grade) which can be applied to the crystal.

2.3. *Bulk Diffusion*

These measurements were carried out using a radio-isotope surface counting technique. In this method the β-activity of sodium-22 ions on the surface was measured in a G–M counter. Diffusion of the sodium was allowed to take place into the crystal and the absorption of β's in the sodium chloride resulted in a diminution in the count rate observed at the surface. From this change in count rate, the diffusion coefficient could be calculated. The advantages of this method over sectioning techniques were that more than one measurement could be made on the same crystal and there was less chance of contamination of inactive parts of the crystal.

The $^{22}NaCl$ was evaporated, under vacuum, from an electrically heated platinum boat onto one face of the NaCl crystal, 2 cm × 2 cm × 0·2 cm in size. The crystal was shielded so that a rectangular deposit, 1·5 cm × 0·2 cm, of active material was obtained on the face. The crystal was then mounted on a steel plate, fitted with a bracket and screw clamp to ensure that the crystal could be replaced in a reproducible position for each count. The activity of the sample was determined with a thin end-window Geiger counter, mounted directly above the crystal. Precautions were taken to prevent any water vapour being present.

The crystal was transferred to a Pyrex diffusion vessel and an inactive crystal was mounted 0·2 cm above the active face. Any evaporation from the active deposit could then be detected but in none of the experiments was any evaporation observed. The vessel was evacuated and then filled with slightly less than one atmosphere of dry, oxygen-free nitrogen. The vessel was sealed off and transferred to a pre-heated furnace, the temperature of which could be maintained at ± 2°c of the desired value over periods of 200–300 hours. After allowing diffusion to take place the vessel was removed, cooled to room temperature and the surface activity of the crystal determined under the same conditions as the initial counting. A standard $^{22}NaCl$ source was measured before and after each count and the results were referred to this standard.

In order to evaluate the diffusion coefficients it was necessary to know the extent of absorption of the ^{22}Na radiations in sodium chloride. As it was not possible to prepare thin enough sections of crystal for this purpose, measurements were made with standard aluminium absorbers and the corresponding absorption in sodium chloride calculated from a comparison of the densities. The ^{22}NaCl source used for these measurements was mounted on a crystalline sodium chloride substrate, consequently any β^+ back-scattering effects would be the same in the absorption determinations and in the diffusion experiments.

From a knowledge of the absorption of ^{22}Na radiations and from the decrease in count rates due to diffusion it was possible to calculate D, the self-diffusion coefficient. The solution of Fick's law applicable to this particular case is given by (Jost 1952)

$$C_x = \frac{Q}{(\pi Dt)^{1/2}} \exp\left(-\frac{x^2}{4Dt}\right)$$

where C_x is the concentration of active material at a depth x, Q is the quantity of active material on the surface initially and t the diffusion time. It has been found in these experiments that a 2·6% change in the counting rate is equivalent to 13·3% change in D.

2.4. *Surface Movement*

If surface movement was the dominant process compared with bulk diffusion, then a surface scan of the radioactivity on the surface should show evidence of lateral movement of sodium ions.

An active deposit was placed on the crystal by the method described in § 2.3, and the crystal mounted in a reproducible position on a steel plate. A calibrated screw, fitted to the plate, allowed the crystal to move under the field of view of a thin end-window Geiger counter. A lead slit restricted the vision of the counter so that the activity of a strip of crystal, 0·13 cm in width, could be determined by each count. The accuracy of this type of apparatus has been demonstrated by Sherwood (1957, private communication), who, on a similar apparatus, compared the distance travelled by a very thin radioactive wire in the field of view with that measured geometrically. They were found to be identical.

The distribution of activity on the surface was determined by the scanning technique and the crystal transferred to the diffusion vessel, described in § 2.3. After allowing diffusion to take place the active face was again scanned, and the counts referred to the standard source.

2.5. *Grain Boundary Diffusion*

An attempt was made to study grain-boundary diffusion of ^{22}Na ions by an autoradiographic technique. The preparation and heating of the sample were the same as described in § 2.3 but, after diffusion, layers of the crystal were removed by grinding the face, opposite to the active deposit, with sira powder. The ground face was then exposed to an Ilford G5 nuclear plate of emulsion thickness 50 μ. If rapid diffusion had taken place along grain boundaries this would be easier to detect in regions of the crystal furthest away from the initial active deposit. The procedure was repeated at various thicknesses of the crystal. The nuclear plates were developed and examined under a microscope with a 450 × magnification.

Since β-particles coming from a point source of matter emerge in all directions and are randomly scattered in an absorbing medium there must necessarily be a limit to the proximity of two sources without their images becoming indistinguishable on a nuclear plate. An artificial specimen was therefore prepared to determine the limits of proximity. This was carried out by preparing a synthetic 'crystal' from microscope cover slides of varying thicknesses. Each of these slides had an active solution of ^{22}NaCl deposited on one face. The slides were glued together to form a sandwich and this was placed edge downwards on a nuclear plate. Development of the plate showed it was just possible to distinguish two active sources separated by a distance of $200\,\mu$ and therefore grain boundary diffusion would only be detected if the boundaries were at least $200\,\mu$ apart.

2.6. *Thermal Treatment of the Crystals*

The conductivity and self-diffusion measurements, quoted here, have all been carried out on slices of the same single crystal. The procedure was to subject a slice of the crystal to a particular treatment and then to split the slice so that one-half could be used for the conductivity and the other half for the diffusion measurement.

The annealing was carried out by sealing the crystal in a silica vessel under slightly less than one atmosphere of dry, oxygen-free nitrogen and then heating to temperatures of 600°–620°c. The crystal was allowed to cool to room temperature over a period of four hours and the electrodes applied. Chilling was brought about by suspending the crystal in a thin Pyrex stoppered vessel and then immersing in liquid nitrogen for five minutes.

§ 3. RESULTS

3.1. *Conductivity*

Theory predicts that the variation of ionic conductivity (σ) with temperature is given by the equation

$$\sigma = (A/T)\exp(-E/kT)$$

where A is a constant and E is the energy of activation. Since the exponential term varies much more rapidly than $1/T$ it is convenient to express the conductivity graphically as $\log\sigma$ against $1/T$.

The results of the conductivity measurements on crystal 5 are shown in fig. 1. This crystal was grown from a melt of previously grown crystals in order to increase the purity. Both the chilling and the annealing of the crystal produced increases in the conductivity. A typical result taken at 441°c ($1/T = 1{\cdot}4 \times 10^{-3}$) shows that the chilling of a crystal section increased the conductivity by 50% while the annealing of a section for 69 hours and 256 hours at 620°c produced increases of 76% and 90% respectively.

Similar increases have been observed in other single crystals, when they were chilled or annealed, and the results from these have been combined with the results of crystal 5 to obtain values of the activation energy (table 1).

Fig. 1

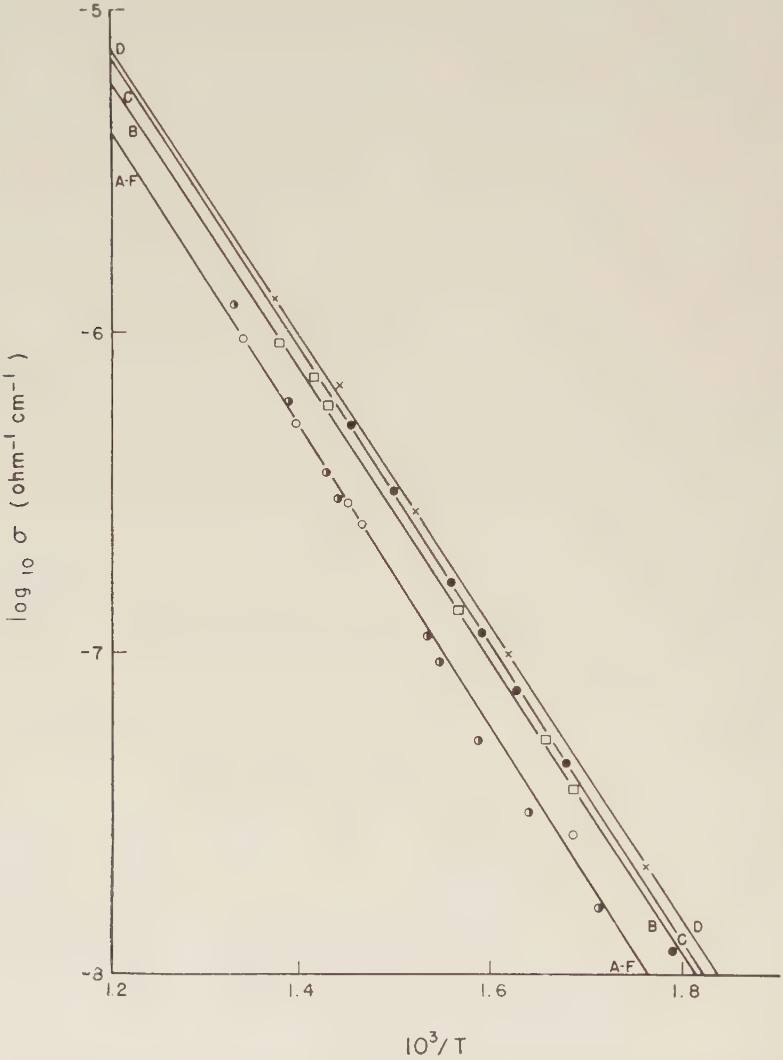

The variation of the conductivity with the absolute temperature for single crystal specimens of sodium chloride taken from one crystal boule.

○ 5A, untreated specimen;
□ 5B, specimen cooled in liquid nitrogen;
● 5C, specimen annealed at 600°C for 69 hours;
× 5D, specimen annealed at 620°C for 254 hours;
◑ 5F, untreated specimen.

Table 1

Crystal	Number of experiments	E_A (ev)
Untreated	4	$0{\cdot}94 \pm 0{\cdot}025$
Chilled	2	$0{\cdot}91 \pm 0{\cdot}020$
Annealed	2	$0{\cdot}92 \pm 0{\cdot}020$

It should be noted that these results were obtained when the electrode material was applied to the crystal after the annealing or chilling process. In contrast to this when a series of annealing studies were made at 600°c with electrodes applied prior to the heat treatment, the conductivity was found to decrease; this decrease depended on the annealing time. The activation energy (0·93 ev) was unchanged by the annealing. It seems probable that this decrease must be attributed to some electrode effect. A similar phenomena was observed by Etzel and Maurer (1950) with cadmium-doped sodium chloride crystals.

3.2. *Bulk Diffusion*

The results are given in table 2.

Table 2

Crystal	Thermal treatment	Diffusion time (hrs)	Diffusion temp. (°c)	D (cm² sec⁻¹)
5A	Untreated	189	511	$7{\cdot}90 \times 10^{-11}$
5A		$443\frac{1}{2}$	511	$9{\cdot}00 \times 10^{-11}$
5B	Chilled in liquid nitrogen	189	511	$8{\cdot}70 \times 10^{-11}$
5B		$443\frac{1}{2}$	511	$9{\cdot}37 \times 10^{-11}$
5C	Annealed at 620°c for 265 hrs	$254\frac{1}{2}$	511	$9{\cdot}28 \times 10^{-11}$

There was no appreciable difference in the final value of D for the untreated, chilled and annealed crystals. There is an indication, however, that D increases with time of heating; D for the untreated crystal increased by 14% during the second heating while D for the chilled crystal increased by 7·7%.

3.3. *Surface Movement*

Experiments at 400°c and 500°c with heating times of 100 to 200 hours showed no evidence of surface diffusion. Figure 2 shows an example of the activity plots before and after diffusion. The bulk diffusion measurements indicated a rapid movement of sodium ions into the crystal.

3.4. *Grain Boundary Diffusion*

The autoradiographic experiments, which were carried out on crystals 5A and 5B after bulk diffusion measurements, showed no positive evidence of grain-boundary diffusion. It should be pointed out that the diffusion was measured after long periods of heating at 511°c. This represented a considerable annealing treatment of the crystal and it is therefore not possible to say if grain-boundary diffusion occurred in chilled crystals.

Fig. 2

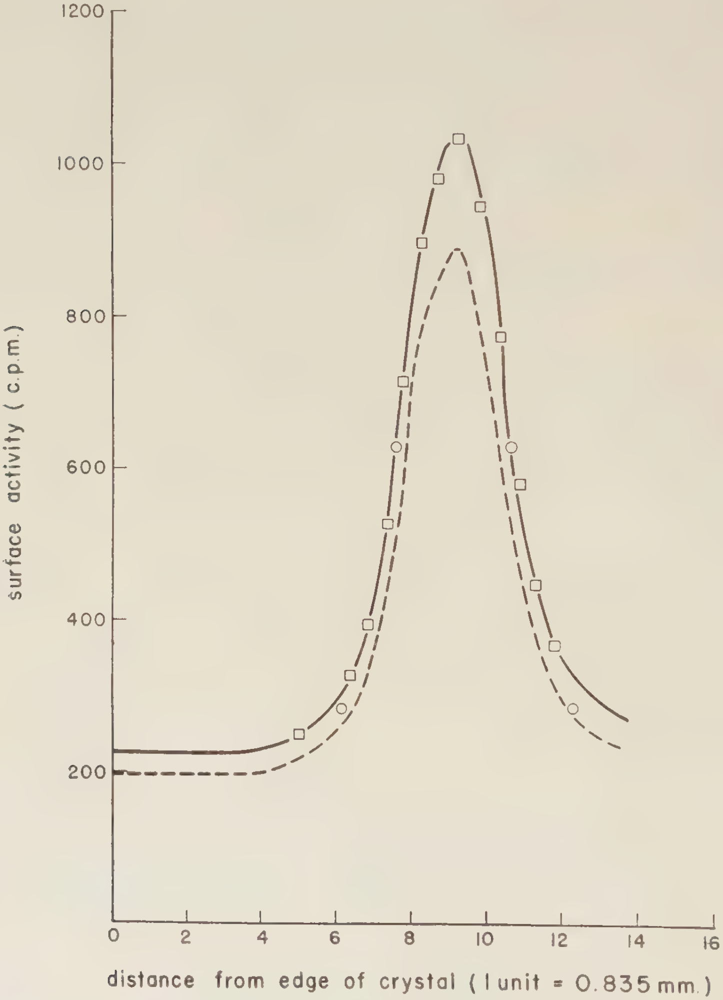

Distribution of activity over the crystal surface before and after diffusion.

—○—□— Initial surface activity;

– – – – – Final surface activity after heating for 214 hours at 506°c.

3.5. *Appearance of Mosaic Patterns in the Crystals*

A film of inactive sodium chloride was evaporated onto the face of a single crystal of sodium chloride and the crystal then heated in air at 400°c for several hours. On examination under a microscope, with 200 × magnification a mosaic pattern was observed, (fig. 3, Pl. 136). The crystal was then chilled in liquid nitrogen, cleaved and the film again prepared. Figure 4 (Pl. 137) shows the appearance of the evaporated film on the chilled crystal. The average area of the domains in the chilled specimen was 8×10^{-6} cm^2, while the domains in the untreated crystal varied from $2{\cdot}4 \times 10^{-4}$ cm^2 to $3{\cdot}2 \times 10^{-5}$ cm^2 in area. Annealed crystals gave patterns similar to the untreated specimen.

§ 4. CONCLUSION

The diffusion coefficient of Na^+ ions in single crystals, whose boundary structure has been greatly increased by chilling in liquid nitrogen, does not differ substantially from that in the untreated specimen. Annealing at 620°c has also only a very small effect on the rate of diffusion. Now the experiments on grain-boundary diffusion indicated that facile diffusion along boundaries separated by more than 200 μ could not be detected, and that conductivity and diffusion changes on annealing must therefore be interpreted along other lines.

In contrast to the diffusion results, both the annealing and the chilling of the crystals brings about substantial increases in the conductivity. It should be pointed out, however, that the diffusion and the conductivity measurements are not strictly comparable. The practical measurement of diffusion involved long periods of heating and hence the crystal was subject to an unavoidable annealing process. The conductivity measurements, on the other hand, could be completed in 4 hours. The activation energy for conduction is unchanged by the heat treatments and this indicates that the increases in conductivity are due to increases in the number of charge carriers rather than to a change in mechanism.

Annealing of a crystal at 620°c increased the conductivity by a factor of about 2 over the untreated crystal. Similar observations have been made by Russell and Maurer (1954) and by Fishbach and Nowick (1957). The latter authors have ascribed this change in conductivity to an increased dispersion of aliovalent cation impurities in the annealed crystals. Our results tend to support this view. The crystal, on which our measurements were made, was grown from a melt of sodium chloride, then cooled from the melting point to room temperature over a period of 16 hours and allowed to stand at room temperature for several weeks prior to the measurements. It is estimated, from the concentration of impurities in the melt, that this crystal contains 1 part in 10^6 of aliovalent cation impurity. On cooling from the melting point some of this impurity will precipitate out at the boundaries, thus reducing the number of positive-ion vacancies in the crystal. This precipitation behaviour has been observed by Amelinckx *et al.* (1955) and by Mikaye and Suzuki (1954) in 'doped' crystals of sodium chloride. Also Schulman *et al.* (1950) have shown that certain impurities in sodium chloride precipitate out on standing at room temperature. Annealing of the crystal at 620°c will cause these precipitated impurities to go into solution and it is believed that the rate of cooling, the crystal was cooled over a period of 4 hours, was too rapid to allow appreciable reprecipitation of the impurities. The crystal would therefore contain more impurities in solution than the untreated crystal and hence would have a larger conductivity because of these extra impurity-induced positive-ion vacancies.

Chilling of a crystal in liquid nitrogen would produce a sharp temperature gradient in the specimen since it is unlikely that the interior of the crystal would be near -195°c with the short chilling time of five minutes. Measurements of the density change of sodium chloride when it is cooled from room temperature to -195°c show that there would be a volume contraction of 2·5% (Henglein 1925). In the present experiments the outer layers would be unable to contract fully and, as a result, plastic flow would be produced in the crystal. It is possible that this process could cause dispersion of the precipitated impurity thus giving rise to an increase in conductivity. Alternatively the increase could be accounted for by the increase in boundary structure. Lehovec (1953) and Eshelby *et al.* (1958) have pointed out that dislocations, grain and mosaic boundaries in sodium chloride are electrically charged; there is an excess of vacancies of one sign at the surface of the boundary balanced by a corresponding excess of vacancies of the other sign in the boundary regions. This will give rise to an extra 'surface' conduction. Estimates, from the surface patterns, of the increase in boundary structure on chilling indicate that the increase in conductivity could be accounted for on this basis. It is surprising, however, that the activation energy is the same as in the untreated specimen.

ACKNOWLEDGMENTS

The authors wish to thank Mr. G. R. Martin for his advice on conductivity measurements and Mr. J. V. Major for his help and advice with the autoradiography experiments. One of us (I. M. H.) is indebted to the Durham Colleges in the University of Durham for the award of a Research Studentship, during the tenure of which this work was carried out.

REFERENCES

AMELINCKX, S., 1954, *Acta Met.*, **2,** 848.

AMELINCKX, S., VAN DER VORST, W., GEVERS, R., and DEKEYSER, W., 1955, *Phil. Mag.*, **46,** 450.

BARRER, R. M., 1951, *Diffusion in and through Solids* (Cambridge: University Press), p. 312.

CAFFYN, J. E., and SCHNEIDER, E. E., 1955, *Rep. Conf. on Defects in Crystalline Solids* (London: The Physical Society), p. 74.

CUNNEL, F. A., and SCHNEIDER, E. E., 1954, quoted by Seitz, F., 1954, *Rev. mod. Phys.*, **26,** 7.

ESHELBY, J. D., NEWEY, C. W. A., PRATT, P. L., and LIDIARD, A. B., 1958, *Phil. Mag.*, **3,** 75.

Ewles, J., and Stead, K. C., 1956, *Proc. phys. Soc. Lond.*, B, **69,** 396.
Ewles, J., and Jain, S. C., 1958, *Proc. roy. Soc.* A, **243,** 353.
Etzel, H. W., and Maurer, R. J., 1950, *J. chem. Phys.*, **18,** 1003.
Fishbach, D. B., and Nowick, A. S., 1957, *J. Phys. Chem. Solids*, **2,** 226.
Henglein, F. A., 1925, *Z. Phys. Chem.*, **115,** 91.
Humphreys-Owen, S. P. F., 1955, *Proc. phys. Soc. Lond.*, B, **68,** 325.
Jones, D. A., and Smith, T., 1956, *Proc. phys. Soc. Lond.*, B, **69,** 878.
Jost, W., 1952, *Diffusion in Solids, Liquids and Gases* (Academic Press Inc.).
Laurent, J. F., and Bénard, J., 1955, *C.R. Acad. Sci. Paris*, **241,** 1204.
Lehovec, K., 1953, *J. chem. Phys.*, **21,** 1123.
Mapother, D., Crooks, H. N., and Maurer, R. J., 1950, *J. chem. Phys.*, **18,** 1231.
Mikaye, S., and Suzuki, K., 1954, *Acta Cryst.*, **7,** 514.
Russell, G. A., and Maurer, R. J., 1954, Technical Report No. 12, NRO17-412, University of Illinois.
Schulman, J. H., Ginther, R. J., and Klick, C. C., 1950, *J. opt. Soc. Amer.*, **40,** 854.
Seitz, F., 1954, *Rev. mod. Phys.*, **26,** 7.

Dislocation Etch Pits in Zinc Crystals†

By JOY GEORGE
National Research Fellow, Department of Physics, University College,
Trivandrum, Kerala, India

[Received June 3, 1959]

ABSTRACT

Star-shaped terraced etch pits at the sites of dislocations have been produced on the (0001) plane of crystals of vapour grown zinc, using Superoxol etch. The same etch pattern is also observed on the (0001) basal facets of crystals grown by the droplet method. Closely spaced etch pits suggestive of low-angle tilt boundaries are also observed. Evidence has also been presented of spiral growth mechanism from a Frank–Read source.

§ 1. INTRODUCTION

ETCH pits which are sites of dislocations have been produced on (100) and (111) planes of silicon (Vogel and Lovell 1956), on (100) planes of lithium fluoride (Gilman *et al.* 1958) and on the cleavage planes (111) of antimony (Wernick *et al.* 1958). Gilman (1956) and Meleka (1956) etched single crystals of zinc and etch pits have been produced at the sites of dislocations. Servi (1958) observed spiral etch patterns and Frank and Vreeland (1958) explained the patterns in terms of Frank–Read sources.

In most of these cases the surfaces were treated with a polish etch solution before using the dislocation etch techniques. It has been felt worthwhile to extend the dislocation etch techniques to virgin surfaces of zinc grown from vapour, using as a suitable reagent Superoxol‡ and hitherto unreported etch figures have been observed.

§ 2. EXPERIMENTAL

The sample of pure metal of zinc was melted and drawn through a narrow constriction under vacuum, to be collected inside a Pyrex tube closed at one end with a clean glass plate supported across the tube at that end with the open end sealed while in vacuum. This was then introduced in a vertical furnace such that the metal was at a temperature of about 400°C and zinc crystals were deposited on the glass plate as well as on the sides of the tube near it after a few hours. The collecting of these fine crystals on a horizontal detachable glass plate has the added advantage of permitting examination of the crystals under high magnification. The crystals were subsequently etched in Superoxol and rinsed with water and acetone in turn being dried by a current of warm air.

---

† Communicated by Professor S. Tolansky, F.R.S.

‡ One part 30% H_2O_2, one part 40% HF, four parts H_2O (H. C. Theuerer, U.S. patent 2542727).

§ 3. OBSERVATIONS

Several of the crystals have been etched and examined and some typical cases are described here. Figure 1 (× 1230)† shows an etch pattern on the (0001) plane. The star shape of the etch pit changes gradually from the outside and takes the shape of a regular hexagon as the centre is approached. This is because the etching is preferential, being greater in the [11$\bar{2}$0] directions and occurs in the direction of the C axis as can be seen from the hexagonal symmetry. The light-profile (Tolansky 1952) across this terraced etch pit (fig. 2) reveals that the shape of the pit is conical (axis of the cone coinciding with the C axis) though the shift due to each terrace is too small to be resolved by the profile. The inner and outer terraces are all regularly spaced and are concentric with the central depression.

Identical etch pits are also observed on the basal facets of crystals grown by the droplet method (Forty 1952). Figure 3 (× 570) shows the etch pit on such a crystal. The 'star-shaped terraced' pattern is gradually developing, the centre showing regular hexagons. A double profile across this etch pit shows, as before, the slope at the centre, and the sides of the arms lying along [11$\bar{2}$0] are also inclined (fig. 3). The same pit under higher magnification (fig. 4) (× 1230) reveals more interesting details. Between the arms can be seen small crystallites stacked one over the other, the stacking direction being parallel to the arms, a phenomenon usually observed in zinc during growth from the vapour, when small platelets stack one above the other.

There also appear closely spaced etch pits (fig. 5) (× 570) resembling the low-angle tilt boundaries observed in germanium and silicon.

§ 4. CONCLUSIONS

According to Forty (1952), though there is no direct evidence of screw dislocations in the growth of zinc crystal as in the case of other hexagonal metals, the termination of growth steps in the surface indicates the presence of dislocations. It can be believed that the randomly distributed 'star-shaped terraced' etch pits are at the sites of dislocations. Since the pattern is symmetrical the dislocation must be normal to the surface along the axis of the cone and screw component of the Burgers vector which is normal to the surface. Evidence of spiral growth mechanism is presented by one observation (fig. 6) (× 570) which shows the formation of a closed loop from a pair of dislocations, the mechanism being similar to a Frank–Read source. Servi (1958) has by etching shown evidence of operative Frank–Read source in zinc crystals.

---

† All figures are as plates.

The closely spaced etch pits are at the sites of dislocations as they have been found in linear arrays suggestive of small angle tilt boundaries.

ACKNOWLEDGMENTS

The author wishes to make acknowledgment to the Government of India for a research fellowship. Thanks are due to my colleagues Mr. A. O. Mathai of the Physics Department and Mr. C. Surendranath of the Chemistry Department for helpful suggestions.

REFERENCES

FORTY, A. J., 1952, *Phil. Mag.*, **43**, 949.
FRANK, F. C., and VREELAND, THAD, Jr., 1958, *Phil. Mag.*, **3**, 419.
GILMAN, J. J., 1956, *Trans. Amer. Inst. min. (metall.) Engrs.*, **206**, 998.
GILMAN, J. J., JOHNSTON, W. G., and SEARS, G. W., 1958, *J. appl. Phys.*, **29**, 747.
MELEKA, A. H. A., 1956, *Phil. Mag.*, **1**, 803.
SERVI, I. S., 1958, *Phil. Mag.*, **3**, 63.
TOLANSKY, S., 1952, *Z. Elektrochem.*, **56**, 263.
VOGEL, F. L., and LOVELL, L. C., 1956, *J. appl. Phys.*, **27**, 1413.
WERNICK, J. H., HOBSTETTER, J. N., LOVELL, L. C., and DORSI, D., 1958, *J. appl. Phys.*, **29**, 1013.

3d Band Structure of some Transition Elements†

By Ellinor F. Belding
Vassar College, Poughkeepsie, N.Y.

[Received June 2, 1959]

Abstract

Tight-binding calculations of the structure of the 3d band for Cr, Fe and Ni, using the interaction of both nearest and second nearest neighbours show a broadening of the 3d band at the lower energy limit for the body-centred cubic elements due to the second nearest neighbour interaction but a negligible effect on face-centred cubic Ni.

§ 1. Introduction

Fletcher (1952) calculated by the tight-binding approximation the structure of the upper part of the 3d band of nickel, taking into account the interaction of nearest neighbours only. His paper gives a clear description of the method of calculation used in the present paper. Slater and Koster (1954) used Fletcher's values for the overlap integrals of nickel to calculate the structure of the entire 3d band for a body-centred lattice, showing the symmetrical character of the band when only nearest neighbour interaction is assumed.

The work of Löwdin and Appel (1956) on interpolated analytic SCF functions for the first transition group of elements suggested that a further calculation by the tight-binding approximation using these functions as starting functions and extending the calculation to include the interaction of second nearest neighbours would give a better idea of the width and shape of the 3d bands for chromium, iron and nickel. The calculations of the potentials of the three atoms, the overlap integrals for not only nearest and second nearest neighbours, but also for the two next nearest neighbours for Cr and Ni, and the solutions of the determinants were carried out on the I.B.M. 704 computer. The final determinations of the density of states curves were made by graphical integration of constant energy surfaces in k-space.

§ 2. Details of the Calculation

Since the wave functions are in analytic form the potentials for the three elements were put in the form

$$V=\left(1+\sum_i A_i \exp(-a_i r)\right)\Big/ r \quad (i=1,\ 4)$$

---

† Communicated by the Author. This study was carried out while a summer employee of the Computing Center, International Business Machines Corporation Research Laboratory, Poughkeepsie, N.Y.

for the calculation of the overlap integrals. Table 1 gives the values used to fit the potential curves.

Table 1. Values for Fitting Potential Curves

	Cr	Fe	Ni
A_1	17·571	23·324	27·678
A_2	468·70	1814·1	1024·5
A_3	−1505·7	−5333·0	−2568·5
A_4	1042·4	352·06	1544·7
a_1	1·2992	1·5566	1·8101
a_2	4·8648	6·1153	5·9765
a_3	6·7754	7·4862	7·4956
a_4	8·3754	8·5822	9·3185

The sides of the unit cell fixed the coordinate axes and the orientation of the wave functions. When transforming to prolate spheroidal coordinates for the integration, there are only four angular functions possible for the components of the overlap integrals. These four functions were integrated with the appropriate interatomic separations and then combined to give the integrals of the matrix components. Slater and Koster give tables for the matrix components. The four angular functions which appear in the integrals are:

$$\text{(A)}\quad \sin^2\theta_1 \sin^2\theta_2, \qquad \text{(B)}\quad \cos^2\theta_1 \cos^2\theta_2,$$

$$\text{(C)}\quad (\sin^2\theta_1 \cos^2\theta_2 + \cos^2\theta_1 \sin^2\theta_2), \qquad \text{(D)}\ \sin\theta_1 \sin\theta_2 \cos\theta_1 \cos\theta_2,$$

where 1 refers to the first atom, 2 the second, θ the usual spherical coordinate, and A, B, C, D designate the integrals involving these functions.

Table 2. Components of Overlap Integrals (in ev × 10^{-3})

Element	Component	Nearest neighbour	2nd neighbour	3rd neighbour	4th neighbour
Cr	A	5·587	2·410	0·1746	0·05954
	B	46·48	25·79	3·690	0·1528
	C	74·55	39·53	5·030	0·2082
	D	−6·056	−3·121	−0·3490	−0·01364
Fe	A	2·959	1·123		
	B	33·98	16·86		
	C	52·99	25·22		
	D	−3·830	−1·734		
Ni	A	1·422	0·07297	0·007213	0·001014
	B	21·66	2·217	0·3315	0·06243
	C	33·06	3·094	0·4427	0·08118
	D	−2·147	−0·1677	−0·02100	−0·003473

Table 2 shows the results of the calculations for these components of the overlap integrals. It is clear that whereas the values for the integrals for the second nearest neighbours for nickel are only about 10% of those for the nearest neighbours this is not true for the body-centred elements. The second nearest neighbour interaction cannot be neglected for chromium and iron. The effects of other neighbours are small for all of these elements.

§ 3. DISCUSSION OF RESULTS

A complete density of states curve was calculated for iron using constant energy surfaces for every 0·2 ev in k-space. This is shown in the figure. The general shape of the curve is similar to that of Slater and Koster, two principal maxima separated by a minimum, but the effect of the second nearest neighbour is to shift a number of states to the upper maximum and to broaden the lower edge of the band by 1·01 ev. The long tail however accommodates but 0·287 states per atom. A calculation of the corresponding portion of the density of states curve for chromium shows a tail with a width of 1·57 ev accommodating 0·345 states per atom.

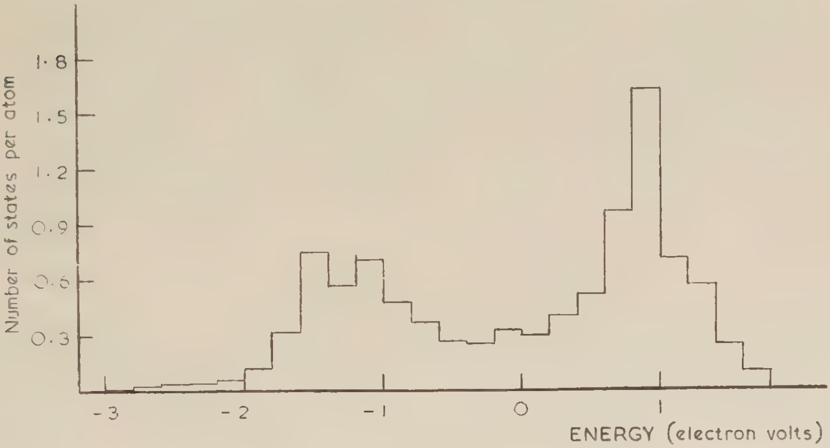

Density of states curve for Fe.

No such tail appears in the density of states curve for the face-centred cubic lattice when the second nearest neighbour interaction is taken into account. The band remains compact.

This study suggests that the 3d band for the body-centred cubic elements iron and chromium is broader than previously thought, that the density of states is highest near the top of the band, and that the bottom of the 3d band is comparatively wide and has very few states available for occupancy.

ACKNOWLEDGMENTS

I wish to express my gratitude to the International Business Machines Corporation for the privilege of working in the Computing Center and to thank the members of the Computing Center for their generous aid in computing problems. I also wish to thank Professor N. F. Mott, F.R.S. and Dr. R. E. Behringer for extremely helpful criticism.

References

Fletcher, G. C., 1952, *Proc. phys. Soc. Lond.*, **65,** 192.
Löwdin, P., and Appel, K., 1956, *Phys. Rev.*, **103,** 1746.
Slater, J. C., and Koster, G. F., 1954, *Phys. Rev.*, **94,** 1498.

Extension of the Theory of the Effects of Anisotropic Relaxation Times on the Hall Coefficients of some Dilute Alloys of Silver†

By J. R. A. COOPER‡ and S. RAIMES
Department of Mathematics, Imperial College, London

[Received May 15, 1959]

ABSTRACT

The recent work of the authors (1959) on the effects of anisotropic relaxation times and non-spherical energy surfaces on the Hall coefficients of some dilute alloys of silver is extended to permit the impurity relaxation time, as well as the thermal relaxation time, to be anisotropic. Also the sixth-order cubic harmonic is included in all the expansions, which had previously stopped at the fourth order harmonic. It is found that agreement with experiment may be improved or, alternatively, the same agreement as before may be obtained with more reasonable values of the empirically determined parameters, provided the thermal and impurity relaxation times can have opposite anisotropies, that is, if the minima of the one occur in the directions of the maxima of the other. It is also possible to explain the experimental results for the silver–gold system, which were at variance with the previous theory. The effects of the inclusion of the sixth-order harmonic are found to be slight, and, in particular, the distance of closest approach of the Fermi surface to the Brillouin zone boundary in pure silver is very little changed.

§ 1. GENERAL THEORY

IN this note we give the results of an extension of the theory described in a recent paper (Cooper and Raimes 1959, hereafter denoted by CR) concerning the effects of anisotropic relaxation times and non-spherical energy surfaces on the Hall coefficients of some dilute alloys of silver. In that work the total relaxation time was assumed to be compounded of a thermal relaxation time τ_t, taken to be anisotropic, and an impurity relaxation time τ_i, taken to be isotropic. Both τ_t and the wave number k of a one-electron state were expanded in series of surface harmonics with cubic symmetry, as far as that of the fourth order; thus

$$\tau_t=\tau_0(E)+\tau_1(E)\,Y_4{}^c(\theta,\phi), \qquad . \quad . \quad . \quad . \quad . \quad . \quad . \quad (1)$$

$$k=\alpha_0(E)+\alpha_1(E)\,Y_4{}^c(\theta,\phi). \qquad . \quad . \quad . \quad . \quad . \quad . \quad . \quad (2)$$

The impurity relaxation time was taken to be, simply,

$$\tau_i=\gamma(E)/x, \qquad . \quad . \quad . \quad . \quad . \quad . \quad . \quad . \quad . \quad . \quad (3)$$

where x is the atomic fraction of solute.

---

† Communicated by the Authors.

‡ Now at the National Physical Laboratory, Teddington.

In the present work we have permitted τ_i to be anisotropic also, and have included the sixth-order cubic harmonic in all the expansions. In the final expression for n^*, defined in eqn. (2) of CR, all the functions occurring have to be evaluated at E_0, the energy at the Fermi surface. We may therefore demonstrate our extended notation by giving our expansions for energy E_0; thus

$$k=\alpha_0(1+AY_4^c+A_1Y_6^c), \qquad \dots\dots \qquad (4)$$

$$\partial k/\partial E=\alpha_0'(1+BY_4^c+B_1Y_6^c), \qquad \dots\dots \qquad (5)$$

$$\tau_t=\tau_0(1+CY_4^c+C_1Y_6^c), \qquad \dots\dots \qquad (6)$$

$$\tau_i=\gamma(1+DY_4^c+D_1Y_6^c)x, \qquad \dots\dots \qquad (7)$$

where all the functions occurring are assumed to be evaluated at the Fermi surface. The definitions of α_0, τ_0, γ, A, B and C are as in CR. Here, however, we have five additional parameters, A_1, B_1, C_1, D and D_1, which are really functions of E_0, although we may assume that they do not vary significantly over the range of x in which we are interested. The sixth-order cubic harmonic is given by

$$\begin{aligned}Y_6^c(\theta,\phi)&=P_6(\cos\theta)-\cos 4\phi P_6^4(\cos\theta)/360\\ &=\tfrac{1}{16}[231z^6-315z^4+105z^2-5\\ &\qquad -21\cos 4\phi(1-z^2)^2(11z^2-1)],\end{aligned}$$

where $z=\cos\theta$.

The formula for n^* is now found to be

$$\begin{aligned}n^*=(1+xZ)\Big[\,1&+\tfrac{4}{21}\{9A^2-18A[(C-D)U-(B-D)]\\ &-[(C-D)U-(B-D)]^2\}+\tfrac{8}{13}\{20A_1^2\\ &-40A_1[(C_1-D_1)U-(B_1-D_1)]\\ &-[(C_1-D_1)U-(B_1-D_1)]^2\}\Big], \qquad \dots \qquad (8)\end{aligned}$$

where, as before,

$$U=1/(1+\lambda x), \quad \text{with} \quad \lambda=\tau_0(E_0)/\gamma(E_0).$$

This expression is correct as far as terms of the second order in the coefficients of Y_4^c and Y_6^c. We have obtained the third-order terms also, but they are so complicated that there seems little point in including them. As it is, the expression is considerably more complicated than our previous one—eqn. (22) of CR. An exhaustive attempt will not be made to determine those values of the parameters which give best agreement with experiment, but we will content ourselves with some general observations. Indeed, since perfect agreement with experiment cannot be attained, what constitutes *best* agreement is to some extent a matter of choice—we can, as will be seen, obtain the minima of the n^* curves at the correct value of x, or we can obtain the correct depths of the minima, but we cannot obtain both simultaneously.

§ 2. THE EFFECTS OF THE ANISOTROPY OF THE IMPURITY RELAXATION TIME

If the sixth-order harmonic is dropped from every expansion, that is, if A_1, B_1, C_1 and D_1 are put equal to zero, the formula for n^* reduces to

$$n^* = (1+xZ)\Big[1 + \tfrac{4}{21}\{9A^2 - 18A[(C-D)U-(B-D)] - [(C-D)U-(B-D)]^2\}\Big], \quad . \; . \; . \quad (9)$$

which is the same as our original one, eqn. (22) of CR, except that $(B-D)$ replaces B and $(C-D)$ replaces C. The appearance of D is a result of our now permitting τ_i to be anisotropic as well as τ_l. One effect of this can be deduced immediately from our previous work. If τ_l and τ_i must have their maxima in the same directions, so that C and D have the same sign, then agreement with experiment cannot be improved (except for the silver–gold system, which will be discussed below), but must be worsened, by the introduction of D. However, if τ_l and τ_i have *opposite* anisotropies, so that the maxima of one are in the directions of the minima of the other, and C and D have opposite signs, then the same experimental agreement as before can be obtained with more reasonable values of the parameters B and C. Thus, if we now set

$$A = -0{\cdot}133, \quad B = 3A = -0{\cdot}399, \quad C = 0{\cdot}178, \quad D = -0{\cdot}266,$$

so that

$$B-D = A = -0{\cdot}133, \quad C-D = 0{\cdot}444,$$

it is easily seen that our formula for n^* is exactly the same as in CR, with the values given in eqn. (26) of that work. But now $B = 3A$, as suggested by inversion of the expansion of E in terms of **k**. Also, $C = 0{\cdot}178$, instead of $0{\cdot}444$, so that the variation of τ_l over the Fermi surface is now less than half of what it was previously.

In CR we chose our parameters so that the theoretical n^* curve for the silver–tin system had its minimum at the same value of x as did the experimental curve. The minimum was found to be too shallow, however, and it was not possible to deepen it significantly, even permitting a displacement of its position, except by assuming unreasonable values for the parameters. It was, of course, necessary for our various expansions that C be small compared with unity, so that we have rejected values of C greater than $0{\cdot}5$. The parameter A is limited to much smaller magnitudes if the Fermi surface is not to touch the zone boundary, and, as explained in CR, it is certainly unreasonable to take B less than A. Now that $(C-D)$ replaces C and $(B-D)$ replaces B, however, even though the same restrictions apply to C and B, and the magnitude of D is limited in the same way as C, we can obtain results which were outside the range of our previous theory. In particular, we can obtain theoretical minima of the correct depth, provided the value of x at which a minimum occurs is permitted to be slightly larger than the experimental value. Figure 1 shows the theoretical n^* curve for the silver–tin system, obtained from eqn. (9) with the following values of the parameters:

$$A = B = -0{\cdot}133, \quad C = 0{\cdot}444, \quad D = -0{\cdot}230.$$

A similar result can be obtained with a wide range of equally permissible values—for example, it can be seen immediately that the values

$$A = -0{\cdot}133, \quad B = 3A = -0{\cdot}399, \quad C = 0{\cdot}178, \quad D = -0{\cdot}496,$$

will give exactly the same result. The experimental points of Dorfman and Zhukova (1939) are also shown in fig. 1, and, remembering that these are unlikely to be absolutely accurate, we see that the agreement between theory and experiment is quite good.

Fig. 1

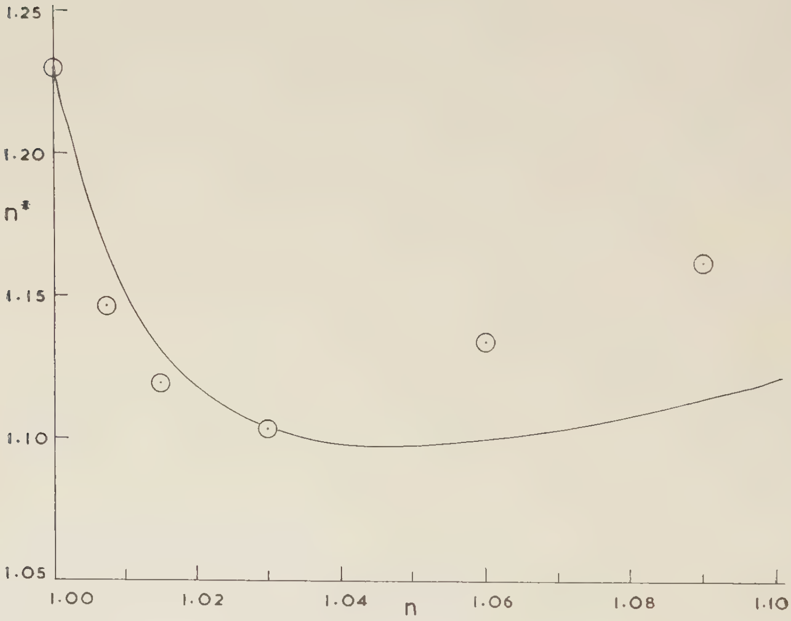

Theoretical curve of n^* against n for the silver–tin system, obtained from eqn. (9), with $A = B = -0{\cdot}133$, $C = 0{\cdot}444$, $D = -0{\cdot}230$. The encircled points are the room temperature measurements of Dorfman and Zhukova (1939).

It is important to realize that, whereas λ was previously the only parameter which varied from system to system, we now expect D also to vary. The parameter D represents the anisotropy of the impurity scattering and so will undoubtedly have different values for different solutes. This means that, having chosen A, B, C and D to fit the silver–tin system, say, the results for the other systems are not rigidly fixed, but may be adjusted by choosing different values of D. This additional latitude is found to be of little significance except in the case of the silver–gold system, where it is of great importance. We pointed out, in CR, that Onnes and Beckman (1912) had found n^* to be initially an *increasing* function of x for the silver–gold system, and it was impossible in our previous theory to choose values of A, B and C which would permit this and simultaneously give curves with minima for other systems. Now it is possible to do so, by suitable choice of D. It may be seen in eqn. (9) that, since $Z=0$ for silver–gold, x only appears in the function U. Hence, if $C=D$, n^* will not vary with x, and it is easy to show, further, that n^* will *increase* with x if $D>C$, so that this is the condition for at least qualitative agreement with the results of Onnes and Beckman. The parameter C is positive, of course, which implies that for the silver–gold system D must be positive, whereas it is negative for the other systems. In other words, it seems that for the silver–gold system τ_t and τ_i must have similar anisotropies, whereas for the other systems they must have opposite anisotropies. Although the scattering for homovalent impurities will certainly be very different from that for heterovalent impurities, it is difficult to see why they should lead to impurity relaxation times with opposite anisotropies. None the less, this question, and that of whether τ_t and τ_i may have opposite anisotropies, deserve detailed investigation.

§ 3. THE SIXTH-ORDER HARMONIC AND THE FERMI SURFACE

In order to estimate the effect of the sixth-order harmonic, we have repeated the work of CR, using the sixth-order harmonic, and *not* the fourth-order harmonic, in the expansions. The formula for n^* is obtained from eqn. (8) by setting A, B, C, D and D_1 equal to zero, thus:

$$n^*=(1+xZ)[1+\tfrac{8}{13}\{20A_1^2-40A_1(C_1U-B_1)-(C_1U-B_1)^2\}], \qquad (10)$$

which may be compared with eqn. (22) of CR. Following our previous method, we set $A_1=B_1$ and fit formula (10) to the value of n^* for pure silver and also to the value of x corresponding to the minimum of n^* in the silver–tin system. In this way we obtain the values

$$A_1=B_1=0{\cdot}046, \quad C=-0{\cdot}158.$$

The resulting curves of n^* against n are very similar to those shown in fig. 1 (b) of CR, the minima being slightly deeper but not significantly so. We find also that the minima become shallower as the value of B_1/A_1 is increased from unity, just as in the case of B/A for the fourth-order harmonic. Since the results of using the fourth-order harmonic only and of using the sixth-order harmonic only are so very similar, we conclude that the results will not be significantly improved when both harmonics are included in the expansions.

The magnitude of C_1 is much smaller than that of C, which we found to be 0·444. This might, at first sight, be thought to imply that use of the sixth-order harmonic instead of the fourth can provide similar results with a smaller variation of τ_t over the Fermi surface. This is not so, however, because the maximum and minimum values of Y_6^c are 16/9 and −13/8 respectively, while those of Y_4^c are 1 and −2/3 respectively, so that in both cases the maximum value of τ_l on the Fermi surface is about twice its minimum value. In the same way, although A_1 is much smaller than $|A|$, which we found to be 0·133, the Fermi surface bulges about the same amount in both cases.

Fig. 2

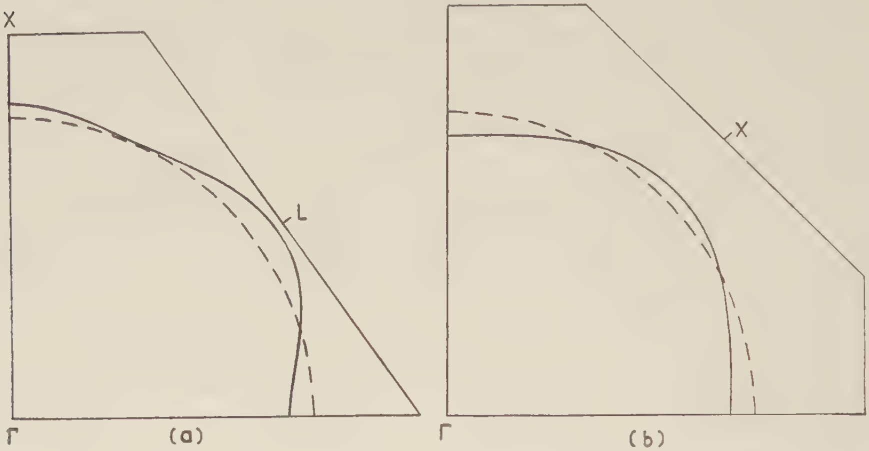

Sections of the Fermi surface in pure silver (according to eqn. (4), with $A=0$ and $A_1=0{\cdot}046$), and the Brillouin zone: (*a*) in the plane $k_1=k_2$; (*b*) in the plane $k_1=0$. Γ is the centre of the zone, L is the centre of a hexagonal face, and X is the centre of a square face. The broken circles are sections of the sphere which would contain one electron per atom—the distance ΓL is 1·107 times the radius of this sphere.

It should be noted that, although expression (10) is unchanged when the signs of A_1, B_1 and C_1 are *all* changed, we choose A_1 to be positive. This is in order that the Fermi surface will bulge towards the hexagonal faces of the Brillouin zone. We chose A to be negative in the case of the fourth-order harmonic for the same reason. Now, however, using the sixth-order harmonic only, we find that the Fermi surface bulges in the directions of the square faces also. Two cross sections of the Fermi surface for pure silver, with $A_1=0{\cdot}046$, are shown in fig. 2, which may be compared with fig. 2 of CR. The true Fermi surface, if the present theory is correct, must lie somewhere between the two. Since the distance of closest approach to the zone boundary is about the same in the two cases, we may assume that it will be little changed when both the fourth and the sixth-order harmonics are included in the expansions.

REFERENCES

Cooper, J. R. A., and Raimes, S., 1959, *Phil. Mag.*, **4**, 145.
Dorfman, Y. G., and Zhukova, P. N., 1939, *Zhur. Eksptl. i Teort. Fiz.*, **9**, 51.
Onnes, K., and Beckman, B., 1912, *Proc. Acad. Sci. Amst.*, **15**, **307**, 319, 664, 988.

Coulomb Scattering in a Magnetic Field†

By P. A. Sweet
University of London Observatory, Mill Hill Park, N.W.7

[Received June 9, 1959]

Abstract

It is shown that the contributions of distant encounters to the velocity diffusion coefficients in Coulomb scattering are convergent when a magnetic field is present, and that no cut-off is required in the impact parameter. A cut-off is, however, required in the coefficient which defines space diffusion across the field.

In a plasma the diffusion coefficients are slightly reduced when the typical gyromagnetic radius of the particles is less than the Debye length.

§ 1. Introduction

In the Boltzmann equation for an ionized gas it is well known that a magnetic field makes itself felt principally through the Lorentz force term $e(\mathbf{v}\wedge\mathbf{B})\,.\,\partial f/\partial\mathbf{v}$, in the usual notation. It is not generally appreciated, however, that the collision term $(\partial f/\partial t)_{\text{coll}}$ is also affected, independently, by the field. This is because the field affects the dynamics of ion encounters, angular momentum no longer being conserved. It is shown in the present paper that a magnetic field causes the scattering of ions on ions to fall off faster with increasing impact parameter than in the absence of a field. The velocity diffusion coefficients can therefore be defined without introducing a cut-off in the impact parameter, as is normally required in Coulomb scattering.

§ 2. The Scattering of an Electron by a Fixed Proton in a Uniform Magnetic Field

The treatment will be classical and non-relativistic. The equations of motion are then

$$m\,\frac{d^2\mathbf{r}}{dt^2}=-\frac{e}{c}\,\frac{d\mathbf{r}}{dt}\wedge\mathbf{B}-\frac{e^2\mathbf{r}}{r^3}, \qquad \ldots\ldots \quad (1)$$

where $\mathbf{r}$ is the radius vector of the electron relative to the proton, $\mathbf{B}$ is the magnetic field strength, m is the mass of the electron, e is the charge of a proton and c is the velocity of light. Take rectangular axes through the proton, with the z-axis parallel to the field. At large distances from the proton the electron describes a spiral of constant pitch and radius about an axis parallel to the z-axis. Before the encounter suppose that the gyromagnetic axis lies in the y-plane at a distance p from the z-axis. Let the resultant velocity be v, inclined at an angle θ to the z-axis. It is required to determine the displacement of the gyromagnetic axis and the change in θ due to the encounter; the resultant velocity, at large distances from the proton, will be unaltered by the encounter since the magnetic field does no work on the electron. An angular momentum integral of (1) also exists, but will not be used in the analysis. On reducing the variables to dimensionless form by substituting

---

† Communicated by Professor V. C. A. Ferraro.

$$t=\mu p\tau/v;\quad \mathbf{r}=p\mathbf{s}=p(\xi,\eta,\zeta),$$

(1) can be written

$$\left.\begin{aligned}\ddot{\varpi}&=i\dot{\varpi}/\lambda-\lambda\mu\varpi/s^3;\\ \ddot{\zeta}&=-\lambda\mu\zeta/s^3,\end{aligned}\right\}\quad\ldots\ldots\quad(2)$$

where $\varpi=\xi+i\eta$, and the differentiations are with respect to τ. λ and μ are given by

$$\lambda=p_1/p;\quad \mu=p_1/p_0;\quad a=mcv/eB;\quad p_0=e^2/mv^2;\quad p_1=(ap_0)^{1/2}.$$

a is the gyromagnetic radius of an electron with velocity v at right angles to the field, and p_0 is the impact parameter for a 90° deflection in the absence of the field. p_1 is the distance from the origin at which the Lorentz and Coulomb forces on the electron would have equal strengths. As $p\to\infty$ with a fixed v and B, $\lambda\to 0$ and μ remains constant.

In the problem of distant encounters, the Coloumb force is weak compared with the Lorentz force, and it can be regarded as a perturbation of the gyromagnetic spiral. The characteristic time of variation of the perturbation is much longer than the gyromagnetic period. The perturbation must therefore be treated by a method similar to the WKB method. ϖ and ζ are expanded in ascending powers of λ, regarding μ as a constant parameter of unit order of magnitude, in the form

$$\left.\begin{aligned}\varpi&=\sum_{m=0}^{\infty}\sum_{n=-\infty}^{\infty}\alpha_{mn}(\tau)\lambda^m\exp(in\tau/\lambda);\\ \zeta&=\sum_{m=0}^{\infty}\sum_{n=-\infty}^{\infty}\beta_{mn}(\tau)\lambda^m\exp(in\tau/\lambda).\end{aligned}\right\}\quad\ldots\quad(3)$$

ζ is real, hence $\beta_{m,-n}=\overline{\beta_{m,n}}$. The α's and β's vary in a time scale of unit order of magnitude, independently of λ.

Before the encounter the gyromagnetic radius is $\lambda\sin\theta$, in the dimensionless variables, and the gyromagnetic axis is in the η-plane at unit distance from the ζ-axis. Time will be measured from the instant that the electron crosses the ζ-plane. The boundary conditions for the α's and β's are therefore:

$$\left.\begin{array}{ll}\alpha_{00}\to 1 & \\ \alpha_{11}\to\sin\theta\exp(i\phi) & \\ \alpha_{mn}\to 0 & (m,n)\neq(0,0)\text{ or }(1,1)\\ \dot{\beta}_{00}\to\mu\cos\theta & \\ \dot{\beta}_{mn}\to 0 & (m,n)\neq(0,0)\end{array}\right\}\text{ as }\tau\to-\infty,\qquad(4)$$

$$\sum_{n=-\infty}^{\infty}\beta_{mn}=0\qquad\text{all } m\qquad\text{at }\tau=0,$$

where ϕ is an arbitrary parameter determining phase in the spiral orbit. The α's and β's are determined by substituting the expansions (3) into the equations of motion (2) and equating coefficients of $\lambda^m \exp(in\tau/\lambda)$. This produces a set of ordinary linear differential equations of the second order, in which the boundary conditions (4) are sufficient to determine unique solutions. α_{0n}, α_{1n} and β_{0n} for all n can be obtained independently of the higher terms. The coefficients α_{2n}, for all n, are then obtainable in terms of the α_{0n}, etc. All the α's and β's are derivable successively in this way. The expansions (3) are found to be

$$\left.\begin{aligned} \varpi &= 1+\lambda\sin\theta\exp\,[i(\tau/\lambda+\phi)]-\lambda^2 i\sec\theta(1+hk)+\dots\,; \\ \zeta &= h+\lambda\mu^{-1}\sec^2\theta\sinh^{-1}h-\lambda^2\mu^{-2}\sec^4\theta[(2k^{-1}+k)\sinh^{-1}h \\ &\qquad\qquad + 2h\log_e k-\tfrac{7}{2}\tan^{-1}h-2h\log_e 2]+\dots, \end{aligned}\right\} \qquad (5)$$

where $h=\tau\mu\cos\theta$ and $k=(1+h^2)^{-1/2}$. The higher order terms rapidly increase in complexity.

§ 3. THE DISPLACEMENT OF THE GYROMAGNETIC SPIRAL

The spiral orbit after the encounter is given by

$$\left.\begin{aligned} \varpi_\infty &= \sum_{m=0}^{\infty}\alpha_{m0}(\infty)\lambda^m+\exp(i\tau/\lambda)\sum_{m=0}^{\infty}\alpha_{m1}(\infty)\lambda^m; \\ \dot{\zeta}_\infty &= \sum_{m=0}^{\infty}\dot{\beta}_{m0}(\infty)\lambda^m. \end{aligned}\right\} \qquad (6)$$

The gyromagnetic axis is therefore displaced, due to the encounter, by an amount given by

$$\Delta\varpi = \sum_{m=0}^{\infty}\Delta\alpha_{m0}\lambda^m, \quad . \quad . \quad . \quad . \quad . \quad . \quad . \quad . \quad (7)$$

where $\Delta\alpha_{m0}=\alpha_{m0}(\infty)-\alpha_{m0}(-\infty)$. The change in velocity along the field is given by

$$\Delta\dot{\zeta} = \sum_{m=0}^{\infty}\Delta\dot{\beta}_{m0}\lambda^m, \quad . \quad . \quad . \quad . \quad . \quad . \quad . \quad . \quad (8)$$

where $\Delta\dot{\beta}_{m0}=\dot{\beta}_{m0}(\infty)-\dot{\beta}_{m0}(-\infty)$. From the expansions (5)

$$\Delta\varpi = -2\lambda^2 i\sec\theta+0(\lambda^3)\,; \quad . \quad . \quad . \quad . \quad . \quad . \quad . \quad . \quad (9)$$

$$\Delta\dot{\zeta} = 12\lambda^6\mu^2\sin\theta+0(\lambda^8). \quad . \quad . \quad . \quad . \quad . \quad . \quad . \quad (10)$$

§ 4. CONVERGENCE OF THE DIFFUSION COEFFICIENTS

Consider an electron moving among fixed protons at a density n per cm^3, in the presence of a uniform magnetic field. Suppose that the Debye length in the plasma is large compared with the gyromagnetic radius of the electron, so that the motion of the electron is a series of encounters, between which steady gyromagnetic spirals are described. The statistical behaviour of the electron is then describable by three quantities, namely the diffusion of the gyromagnetic axis in space, the mean rate of decrease of velocity along the field, and the diffusion, in velocity space, of the velocity perpendicular to the field.

Dealing first with the gyromagnetic axis, by symmetry there will be no mean drift, but there will be a statistical spread radially outwards from an initial position. The mean number of encounters per second in which the encounter parameters lie within the ranges $(\phi, \phi+d\phi)$, $(\theta, \theta+d\theta)$, $(v, v+dv)$ and $(p, p+dp)$ is $n \sin\theta\cos\theta\, vf(v)p\, dp\, dv\, d\theta\, d\phi$, where f is the probability of an electron having a resultant velocity within the range $(v, v+dv)$. Suppose that the gyromagnetic axis is at some specified point at a given instant. Then the mean square displacement from this position, after a time dt is given by

$$\langle|\Delta w|^2\rangle\, dt = n\, dt \int_{v=0}^{\infty}\int_{p=0}^{p_m}\int_{\theta=0}^{\pi/2}\int_{\phi=0}^{2\pi} |\Delta w|^2 vfp \sin\theta\cos\theta\, d\phi\, d\theta\, dp\, dv, \quad (11)$$

where p_m is the maximum value of the impact parameter beyond which encounters cannot be taken as binary. It has been shown (Spitzer 1956) that in a plasma p_m is of the order of magnitude of the Debye length. $\langle|\Delta w|^2\rangle$ is the rate of increase of the mean square displacement. In distant encounters Δw, as determined by (9), is given by

$$w = -2iap_0p^{-1}\sec\theta, \quad . \quad . \quad . \quad . \quad . \quad . \quad . \quad . \quad (12)$$

provided that θ is not arbitrarily near $\pi/2$. The expression on the right-hand side of (11) therefore increases indefinitely as p_m increases. The diffusion coefficient therefore cannot be defined without introducing this cut-off parameter.

The mean rate of change of velocity parallel to the field, i.e. the dynamical friction, is given by

$$\langle\Delta v_{\parallel}\rangle = n\int_{v=0}^{\infty}\int_{p=0}^{p_m}\int_{\theta=0}^{\pi/2}\int_{\phi=0}^{2\pi} \Delta\dot{z} vfp \sin\theta\cos\theta\, d\phi\, d\theta\, dp\, dv.$$

In considering the contribution from distant encounters $\Delta\dot{z}$ can be obtained from (10), thus

$$\Delta\dot{z} = 12a^{7/2}vp_0^{5/2}p^{-6}\sin\theta. \quad . \quad . \quad . \quad . \quad . \quad . \quad . \quad . \quad (13)$$

$\langle\Delta v_{\parallel}\rangle$ therefore tends to a finite limit as $p_m \to \infty$. The coefficient of dynamical friction can therefore be defined without introducing the Debye cut-off parameter, thus

$$\langle\Delta v_{\parallel}\rangle = n\int_{v=0}^{\infty}\int_{p=0}^{\infty}\int_{\theta=0}^{\pi/2}\int_{\phi=0}^{2\pi} \Delta\dot{z} vfp \sin\theta\cos\theta\, d\phi\, d\theta\, dp\, dv. \quad (14)$$

The mean square diffusion coefficients $\langle(\Delta v_{\parallel})^2\rangle$ and $\langle(\Delta v_{\perp})^2\rangle$, in velocity space, parallel and perpendicular to the field, respectively, can be similarly defined without a cut-off parameter.

§ 5. CONCLUSIONS

If the magnetic field in a plasma is so strong that the typical gyromagnetic radius of the particles is small compared with the Debye length then the particles, between collisions, describe well-defined gyromagnetic spirals. The statistical behaviour of the plasma can then be described in terms of the diffusion of the axes of the gyromagnetic spirals, due to encounters, together with the usual velocity diffusion coefficients $\langle \Delta v_{\parallel} \rangle$, $\langle (\Delta v_{\parallel})^2 \rangle$ and $\langle (\Delta v_{\perp})^2 \rangle$. The space diffusion coefficient for the axes is not convergent for large values of the impact parameter in encounters, and it requires a Debye cut-off. The velocity diffusion coefficients, however, are convergent and can be defined without a cut-off. They are, moreover, reduced by the magnetic field, as compared with the values computed for pure Coulomb scattering. The transport phenomena, derived with the use of Boltzmann's equation, will therefore be modified. The Debye length in a plasma is $(kT/4\pi n_e e^2)^{1/2}$, where k is Boltzmann's constant, n_e is the electron density and T is the temperature. The gyromagnetic radius for an electron at the mean thermal velocity

$$\bar{v} = (3kT/m)^{1/2} \quad \text{is} \quad (mc/eB)(3kT/m)^{1/2};$$

it is therefore less than the Debye length if $B > c(12\pi m n_e)^{1/2}$. In the solar chromosphere, at a level where $n_e = 10^{11}$, the condition is $B > 2 \times 10^3$ gauss. This is the typical field strength in a sunspot. At a density $n_e = 10^{14}$, $B > 6 \times 10^4$ gauss. Such a situation could arise in laboratory discharges. The modification to the diffusion coefficients, under these conditions, would only be slight. Close electron–proton encounters, namely those where $p \sim p_0$, are seriously affected by the field only if $p_1 \sim p_0$, i.e. if $a \sim p_0$. Taking v to be the mean thermal velocity of the electrons this requires $B \sim m^{1/2} c (3kT)^{3/2}/e^3 \simeq 100 T^{3/2}$. Under astrophysical and laboratory conditions this would involve impossibly high field strengths.

REFERENCE

Spitzer, L., 1956, *Physics of Fully Ionized Gases*, Ch. 5 (New York: Interscience Publishers).

The Effect of Added Titanium on the Magnetic Behaviour of Haematite†

By D. M. Finlayson and T. Smith
Department of Natural Philosophy, Marischal College, Aberdeen

[Received June 15, 1959]

Abstract

It is shown that the solution of about 1% titanium in α-haematite does not suppress the rapid change in either the susceptibility or the parasitic ferromagnetism which are associated with the change in the direction of the antiferromagnetic axis near 260°K.

The results also suggest that the variation with temperature of the room temperature remanent magnetization is not always a reliable indication of whether an axial switch has taken place.

§ 1. Introduction

At about 260°K the antiferromagnetic axis in haematite moves from the trigonal axis to the basal plane. At the same temperature there is a marked change in the parasitic ferromagnetism. The transition is of considerable importance in rock magnetism, as many sedimentary rocks contain haematite with up to 5% of Ti. Unfortunately the evidence concerning the effect of the Ti on the transition is not conclusive. Thus Morin (1950) found the transition to be suppressed by 1% Ti, while Haigh (1957) found that the added Ti simply moved the transition to a slightly lower temperature. Haigh detected the transition by measuring the room temperature remanent magnetization of the material at different temperatures, and thus observed a quantity associated with the parasitic ferromagnetism: Morin, however, measured the force on a specimen suspended in a non-uniform magnetic field. The discrepancy could be resolved if the Ti suppressed the transition in the susceptibility (which might have accounted for most of the force measured by Morin), but not the transition in the ferromagnetism. To test this possibility, both susceptibility and ferromagnetic intensity have been measured in the transition region for some of the powders used by Haigh. It was thought worth while extending the measurements to lower temperatures as the origin of the ferromagnetism is incompletely understood, and data in this region are meagre.

---

† Communicated by the Authors.

§ 2. Experimental Results

Measurements were made with a Sucksmith balance incorporated in a Jones liquefier. At each temperature the deflection of the specimen was found for six field strengths. In each case the force can be represented by

$$F = H\frac{dH}{dx}\left(\chi + \frac{\sigma}{H}\right)$$

Fig. 1

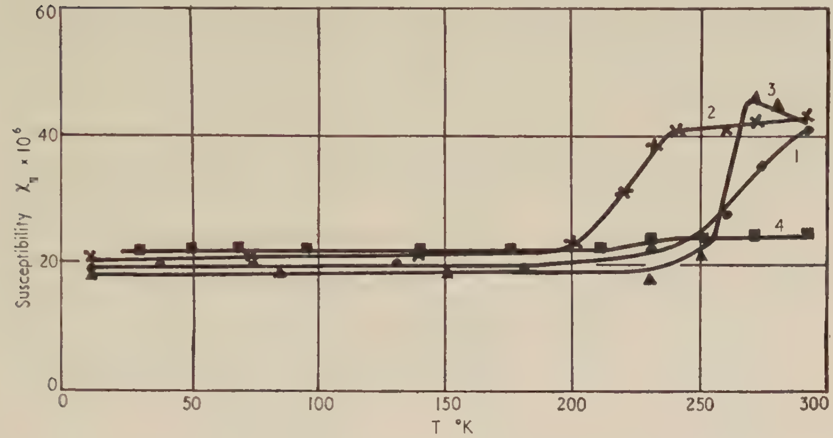

Variation of susceptibility of α Fe_2O_3 powders with temperature.

Curve 1. ● Pure powder (99·9% after heating for 16 hrs in oxygen).
Curve 2. × Powder containing 0·98% Ti.
Curve 3. ▲ High purity material (99·99% after heating 16 hrs in oxygen).
Curve 4. ■ Commercially produced α Fe_2O_3.

Fig. 2

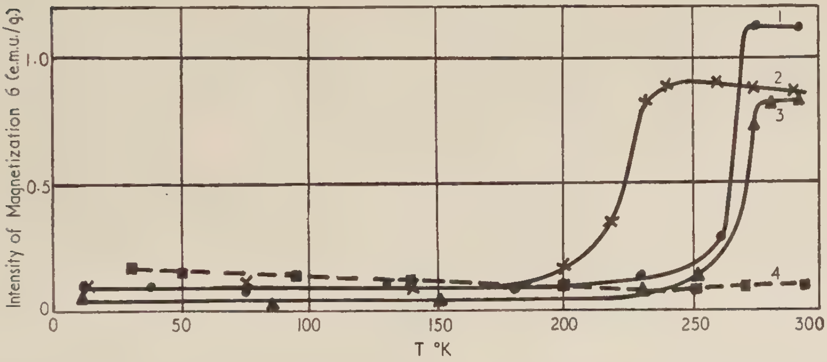

Variation of intensity of magnetization of α Fe_2O_3 powders with temperature.

Curve 1. ● 99·9% powder after heating for 16 hrs in oxygen.
Curve 2. × Powder containing 0·98% Ti.
Curve 3. ▲ 99·99% powder after heating for 16 hrs in oxygen.
Curve 4. ■ Commercially produced α Fe_2O_3.

where χ is the susceptibility and σ is the intensity of magnetization. $H(dH/dx)$ was found by using a material of known susceptibility and H by a fluxmeter. Thus, if σ is independent of field, a plot of F against $1/H$ gives χ and σ. The best straight line was found for each temperature by doing a regression of the appropriately weighted F against $1/H$.

It will be seen from curves 1 in figs. 1 and 2 that for the 99·9% material the rapid change in both the susceptibility and the intensity of magnetization occurs in the same temperature interval. This is consistent with measurements on single crystals (Néel and Pauthenet 1952). The specimen to which 0·98% Ti had been added, showed similar transitions in both susceptibility and magnetic moment. Differences in measuring procedure cannot therefore account for Morin's failure to find a transition in his Ti doped specimens.

Fig. 3

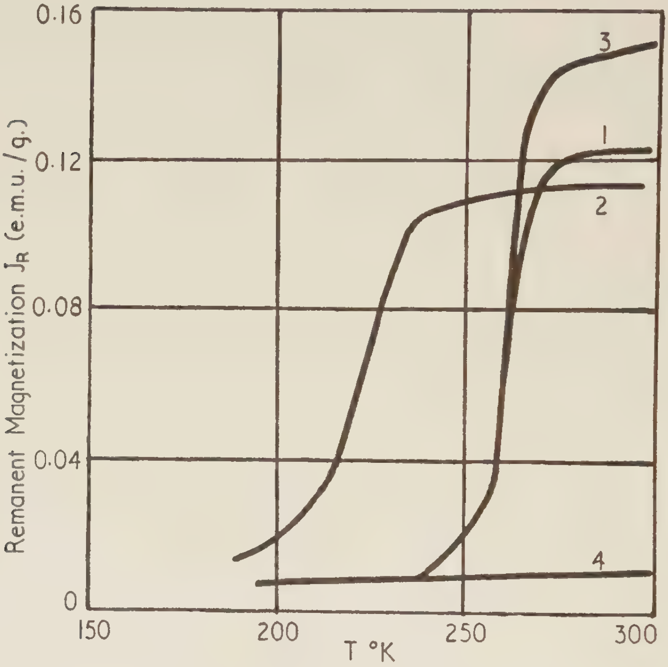

Variation of J_R with temperature for α Fe_2O_3 (from Haigh).

Curve 1. Pure powder (99·9% after heating for 16 hrs in oxygen).
Curve 2. Powder containing 0·98% Ti.
Curve 3. High purity (99·99% after heating for 16 hrs in oxygen).
Curve 4. Commercially produced α Fe_2O_3.

It will be noted that the σ curve for the commercially produced Fe_2O_3 differs from the other specimens in increasing at low temperatures. This type of behaviour has been found in other specimens containing large amounts of impurity (Ishikawa and Akimoto 1957).

It is of some interest to compare the above data, and particularly the σ results, with the values of the room temperature remanent magnetization (J_R) at different temperatures as obtained by Haigh (1957) for the same materials. To facilitate comparison, Haigh's data have been redrawn in fig. 3.

It can be seen that for all materials, with the exception of the commercially produced Fe_2O_3, the general shape of the J_R and σ curves are similar, although there are differences, not only in σ, but also in the shape of the hysteresis loop even for the two pure materials. For the commercial material, however, there is no indication of a transition from the J_R curve, though this certainly takes place, as can be seen from both the χ and σ curves.

ACKNOWLEDGMENTS

We should like to thank Professor Blackett, F.R.S. and Dr. Haigh for supplying the samples.

REFERENCES

HAIGH, G., 1957, *Phil. Mag.*, **2,** 505.
ISHIKAWA, Y., and AKIMOTO, S., 1957, *J. phys. Soc., Japan*, **12,** 1083.
MORIN, J., 1950, *Phys. Rev.*, **78,** 819.
NÉEL L., and PAUTHENET, R., 1952, *Compt. rend.*, **234,** 2172.

Soft X-ray Emission Spectra from Lithium and Lithium–Magnesium Alloys

By J. A. Catterall and J. Trotter
Communication from the National Physical Laboratory

[Received June 30, 1959]

Abstract

An examination of the emission spectra from lithium and lithium–magnesium alloys has indicated that in the alloys electron transfer takes place from magnesium to lithium. The shape of the high-energy edge of the lithium K emission spectrum could be explained by broadening of the 1*s* ionic level in the crystal.

§ 1. Introduction

Recent calculations of the band structure of lithium by Parmenter (1952), Schiff (1954), and Glasser and Callaway (1958), which indicated a predominance of *p* states at the Fermi surface, were at variance with the observed K emission spectrum (Skinner 1946) which showed a maximum before the high-energy end of the band was reached. More recent experimental work on the K emission spectrum (Bedo and Tomboulian 1958) was in general agreement with the earlier results, so that the discrepancy between theory and experiment remained unresolved. Jones and Schiff (1954) suggested that this difference could arise because emission takes place in the neighbourhood of an excited atom, the wave functions and transition probability consequently being altered. From an examination of satellite spectra Catterall and Trotter (1958) considered this suggestion unlikely.

The K emission spectrum of lithium falls in intensity from a maximum to zero over a range of an electron volt or so at the high-energy end. A broad fall of this nature is characteristic of filled energy bands and chemical compounds, and it was considered possible that with the experimental techniques of previous work where relatively high powers and long exposure times were required, a surface film of contaminated lithium might have formed on the x-ray target, giving rise to a false spectrum. Such a film would probably be lithium oxide or nitride, formed by reaction with the residual air in the target chamber. It was hoped that the use of an electron multiplier instead of a photographic plate (Catterall *et al.* 1958) would enable an emission spectrum to be obtained before any film of appreciable thickness could build up on the target face.

§ 2. K Emission Spectrum of Pure Lithium

The lithium was evaporated onto the target from a tantalum cup. Ten separate experiments were performed, the average time required to obtain an emission band being some 5 min. The band was traversed from the high to the low-energy end so that the most important feature, namely the high-energy fall, was obtained within the first 2 min. The target power required was about 5 w which, according to the experiments of Bedo and Tomboulian, would put the temperature of the target surface around 50°c. The emission curve obtained by smoothing the ten separate curves is shown in fig. 1. The intensity is accurate to ±5% and the resolution 0·2 ev. The broad fall is still present, the curve dropping smoothly from the peak to zero, and agreeing very well with Bedo and Tomboulian. Skinner's curve obtained with liquid oxygen in the target, drops somewhat more sharply in the final stages suggesting the presence of an emission *edge* of the kind found in other metals, lying beyond the peak in the emission curve and becoming more diffuse at higher temperatures. No such edge, however, is indicated in either the curves of Bedo and Tomboulian or ourselves at room temperature.

We shall refer later to the curve shown in fig. 4, but in order to avoid confusion we shall henceforth call HJK the ‘high-energy fall’ and JK the ‘high-energy edge’.

Fig. 1

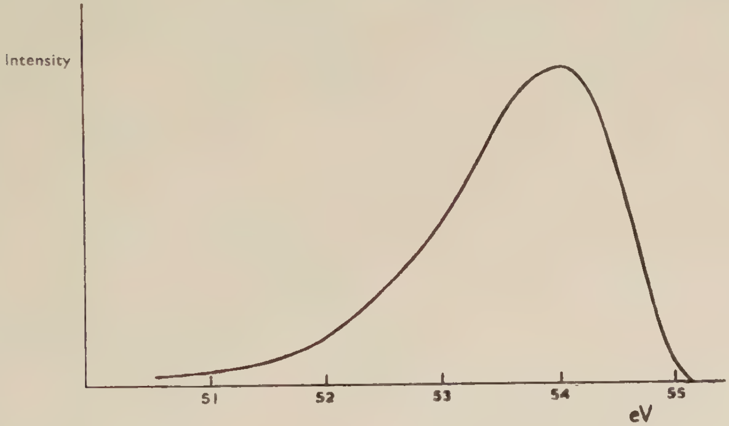

In order to compare the spectrum of lithium oxide with that from pure lithium, lithium oxide was deposited on the target. When the oxide was subjected to electron bombardment a black metallic film immediately formed under the electron beam, and an emission curve was obtained which closely resembled fig. 1. This was interpreted as decomposition of the oxide into metallic lithium and oxygen. Lithium nitride was not investigated, but since it has a lower heat of formation than the oxide it is presumably less stable. The high energy shape of the curve consequently appears to be characteristic of the pure metal.

An interesting suggestion, reported by Tomboulian (1957), is that the broad fall may be due to the presence in evaporated lithium of both the body-centred cubic and the face-centred cubic modifications. An approximate idea of the difference in the bandwidths of these two structures may be obtained from the calculated 'free electron' values, using the known lattice parameters. The difference is less than 0·1 ev, so that this is unlikely to explain the observed effect.

In order to obtain further information about the electron energy distribution a series of alloys of lithium with magnesium was examined. Lithium can dissolve some 70 at % of magnesium. Adopting a simple two-band picture of the alloying process (cf. Varley 1954) transfer of electrons might be expected to take place from magnesium to lithium, which would increase the bandwidth of lithium and yield information about its upper energy limit. Accordingly, three alloys containing 54·7, 30·5 and 20·9 at % lithium were prepared in the form of annealed strip, and soldered onto the target. The first two alloys consisted of the body-centred cubic solid solution based on lithium, and the third a mixture of this phase with the magnesium-rich solid solution. Before examination the surfaces were scraped clean in the target-chamber vacuum.

§ 3. K EMISSION OF LITHIUM FROM THE ALLOYS

The three curves obtained from the three alloys are shown in fig. 2, scaled to match at the peak intensities and superimposed on pure lithium for comparison. The curves for the 54·7, 30·5 and 20·9 at % alloys were obtained by smoothing the curves from nine, six and seven experiments respectively.

Fig. 2

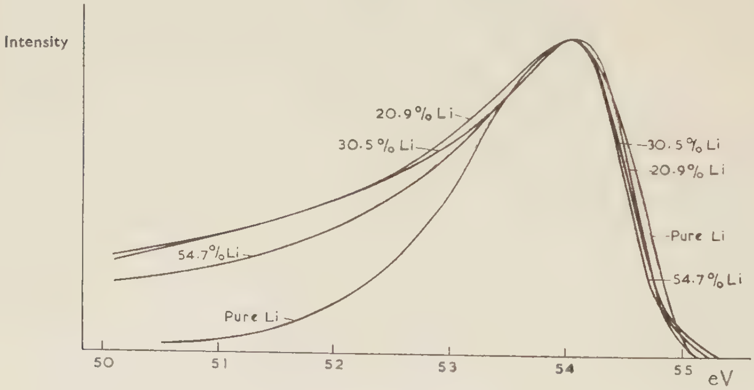

§ 4. L_{23} EMISSION OF MAGNESIUM FROM THE ALLOYS

The curves obtained from the three alloys are shown in fig. 3, scaled to match at the peak intensities and superimposed on pure magnesium for comparison. The curves for the 54·7, 30·5 and 20·9 at % alloys were obtained by smoothing the curves from eleven, four, and nine experiments respectively.

Fig. 3

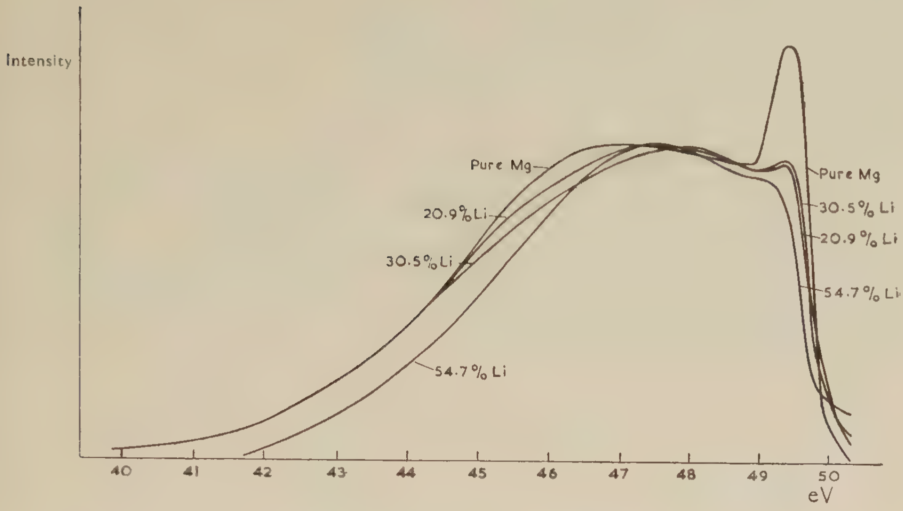

§ 5. Discussion of Results

The most significant features of the emission bands from the alloys are as follows:

(*a*) Except for the disappearance of the high-energy peak in magnesium, the shapes of the emission bands generally resemble those of the pure metals and not those of each other.

(*b*) The position of the high-energy ends of both the magnesium and lithium bands in the alloys is practically the same on the wavelength scale as in the pure metals, so that changes in the widths are visible only by alteration of the positions of the low-energy ends.

(*c*) The lithium bandwidth increases progressively with increase in the percentage of magnesium, but the width and shape of the high-energy fall remains practically unaltered.

(*d*) The magnesium bandwidth decreases progressively with increase in the percentage of lithium, and in particular the high-energy 'spike' disappears.

Point (*a*) above raises the whole question of the correct model for the electronic structure of a concentrated alloy. It is not intended to discuss this point here, except to note that in order to explain the x-ray data, some type of two-band model based on the suggestions of Varley (1954) appears to be required. Varley's model may be used (Varley 1956) to explain (*b*) above: the change in screening of the ionic levels caused by electron transfer offsets the alteration of the upper energy limits of the bands arising from the same process. We are concerned in particular, however, with points (*c*) and (*d*). The changes in widths of the bands suggest that electron transfer from magnesium to lithium is taking place in this alloy system, and the disappearance in the alloys of the 'spike' associated with the zone overlap in pure magnesium is especially noteworthy. Such changes due to electron transfer have previously been observed in Mg–Al alloys by Das Gupta and Wood (1955) and by Gale and Trotter (1956). This simple picture is supported by the fact that there are no humps which could be attributed to bound states appearing on any of the curves. Consequently the high-energy limit of the lithium spectrum in the alloys is of considerable interest.

Cohen and Heine (1958) and Garcia-Moliner (1958), from a review of the physical properties, conclude that lithium has the most anisotropic Fermi surface of all the alkali metals. The former workers also believe that this anisotropy causes the anomalous shape of the emission spectrum. This would lead to expectation of an emission curve of the type shown in fig. 4, in which there is a high energy edge JK lying beyond the peak H, and which resembles the spectrum obtained by Skinner.

Fig. 4

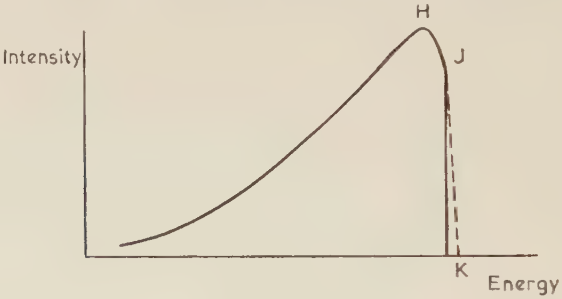

Cohen and Heine have related the distortion of the Fermi surface in the monovalent metals to the parameter

$$d=\frac{\frac{1}{2}(E_S-E_P)}{\frac{1}{2}(E_S+E_P)-E_F}$$

where E_S and E_P are the energy of s and p states at the centre of the nearest zone face, and E_F is the energy at the Fermi level. The quantity E_S-E_P is obtained from Δsp (the excitation energy $s \rightarrow p$ in the free atom), $(BC)_S$ (the s-state boundary correction on forming the metal), and k_F (the wave-number at the Fermi level). The change of the band structure in the α-phase alloys of the noble metals is shown to depend upon the Δsp of the solute atom. For example, in copper where $E_P<E_S$, the addition of a solute with a larger Δsp makes the band structure more nearly spherical. If we adopt this model for the alloying addition of magnesium to lithium, and neglect the remarks we have made above concerning point (*a*), we are unable to explain the shape of the lithium emission curve from the alloys. In lithium $E_P<E_S$ and Δsp is 1·85 ev. In magnesium Δsp is either 2·71 ev or 4·35 ev, depending upon whether the 3*s* and 3*p* electron spins are parallel or anti-parallel. In either case magnesium raises the average Δsp of the alloy, and, as for copper, should make the Fermi surface more

spherical. The alloy containing 54·7 at % lithium has an electron : atom ratio of 1·45, and we conclude that the Fermi surface should be considerably more spherical than in pure lithium and that it may be just in contact with the zone faces or may have detached itself altogether. This last deduction is supported by the fact that the solid solubility boundary extends to an electron : atom ratio of 1·70, so from energy considerations the Fermi level for a ratio of 1·45 is very unlikely to be much beyond the maximum in the density of states curve. Accordingly we expect that the high-energy fall of the emission curve from the lithium in this alloy will be narrower than in pure lithium. The alloying process often broadens high energy *edges*, and widths of up to 0·8 ev are recorded (Das Gupta and Wood 1955). This may partially offset any narrowing of the *fall* expected from the above argument, but should not completely obscure it since the fall occurs over a range of 1·2 ev.

The alternative alloy model of rigid bands implies that an increase in the electron to atom ratio should cause a shift in the edge JK to higher energies relative to H. At an e/a value of 1·45 the change in the free-electron band-widths is 1·34 ev, so that JK should shift relative to H by an amount which should at least be visible in the spectrum. This is contrary to observation, both in the present case and other cases.

Robertson (1958, private communication) has suggested that the explanation of the high-energy fall in lithium may lie in a broadening of the 1*s* ionic level in the metal. The emission intensity $I(E)$ is proportional to

$$\int_{-\infty}^{+\infty} n_1(E') \,.\, n_2(E'') \,.\, p(E', E'') \,.\, dE'$$

where n_1, n_2 are the densities of states in the 1*s* and valence levels respectively, $p(E', E'')$ is the transition probability and $E = E' - E''$. Preliminary calculations of this expression by Robertson using assumed values of n_1 and n_2 based on tight-binding and free-electron distributions respectively, give excellent agreement with our observed pure lithium spectrum. A broadening of the 1*s* level could certainly account also for the high energy fall occurring in the alloys. On the other hand, ionic levels 55 ev below the valence band are normally little affected in the solid, and give emission spectra with narrow high-energy edges. In addition the absorption spectrum of pure lithium obtained by Skinner and Johnston (1937) shows a pronounced, but broad, rise in the absorption at the edge.

Further attempts at an interpretation of the spectra must await a theoretical calculation of the 1*s* level in metallic lithium, and this is at present being carried out by Robertson using the LCAO method.

ACKNOWLEDGMENTS

The work described above has been carried out as part of the General Research Programme of the National Physical Laboratory, and this paper is published by permission of the Director of the Laboratory.

REFERENCES

BEDO, D. E., and TOMBOULIAN, D. H., 1958, *Phys. Rev.*, **109,** 35.
CATTERALL, J. A., and TROTTER, J., 1958 *Phil. Mag.*, **3,** 1424.
CATTERALL, J. A., WILSON, L. F., and TROTTER, J., 1958, *J. sci. Instrum.*, **35,** 393.
COHEN, M. H., and HEINE, V., 1958, *Advanc. Phys.*, **7,** 395.
DAS GUPTA, K., and WOOD, E., 1955, *Phil. Mag.*, **46,** 77.
GALE, B., and TROTTER, J., 1956, *Phil. Mag.*, **1,** 759.
GARCIA-MOLINER, F., 1958, *Proc. phys. Soc. Lond.*, **72,** 996.
GLASSER, M. L., and CALLAWAY, J., 1958, *Phys. Rev.*, **109,** 1541.
JONES, H., and SCHIFF, B., 1954, *Proc. phys. Soc. Lond.* A, **67,** 217.
PARMENTER, R. H., 1952, *Phys. Rev.*, **86,** 552.
SCHIFF, B., 1954, *Proc. phys. Soc. Lond.* A, **67,** 2.
SKINNER, H. W. B., 1946, *Phil. Trans. roy. Soc.* A, **239,** 95.
SKINNER, H. W. B., and JOHNSTON, J. E., 1937, *Proc. roy. Soc.* A, **161,** 420.
TOMBOULIAN, D. H., 1957, *Handb. Phys.*, **30,** 246 (Berlin: Springer).
VARLEY, J. H. O., 1954, *Phil. Mag.*, **45,** 887; 1956, *Nature, Lond.*, **178,** 939

The Statistical Thermodynamics of a Gas with Long and Short-range Forces†

By S. F. Edwards
Theoretical Physics Department, University of Manchester

[Received June 30, 1959]

Abstract

If a gas has long-range Coulomb interactions and short-range interaction, e.g. hard core repulsions, three lengths enter the problem: the radius of the repulsive core, d, the mean interparticle distance, r_0, and λ_D the Debye–Huckel radius, $(8\pi Ne^2/VkT)^{-1/2}$. This paper presents a method of obtaining the equation of state when, in the first instance $\lambda_D \gg r_0 \gg d$, which enables one to obtain higher-order terms in a simple way, and these are calculated. In order to relax the condition $\lambda_D \gg r_0$, a variational method is employed which shows that the usual Debye–Huckel theory makes the grand thermodynamic potential an extremum, the exact result lying between the perfect gas and the Debye–Huckel gas. The results enable one to estimate the contributions to the virial expansion of collective oscillations and of shielded particle encounters, whilst avoiding difficulties such as are associated with redundant coordinates. The extension of the results to the quantum mechanical case are briefly commented upon.

§ 1. Introduction

The problem of obtaining the thermodynamic properties of gas with long-range interactions appears in several places in physics, e.g. in plasmas and in electrolyte theory. Such forces cannot be treated in the same way as short-range forces, since a straightforward calculation of the virial coefficients leads to a divergent answer, so that either the divergent virial series has to be manipulated into a finite answer, or a different approach used, as in the Debye–Huckel electrolyte theory. These methods are increasingly difficult to work if one requires accuracy greater than the first approximation, and it is therefore of interest to invent a method which gives the higher-order corrections in a simple way, and also presents the possibility of investigating these systems when the density is not low. A system with purely long-range forces has both mathematical and physical drawbacks since mathematically the grand thermodynamic potential will have an essential singularity when considered as a function of the interaction constant, or of the temperature, and will only exist at all in the absence of attractive forces; and physically in say an electrolyte, the forces change their nature at short distances. Since in this paper no particular physical system is investigated in detail, the simplest form of the short-range force. an identical repulsive core around every particle is employed. The methods of the paper can be readily extended to other kinds of short-range repulsion, and to different forces acting on different types of particles. For N positive particles and N negative particles interacting with the Coulomb potential and a repulsive core of radius d, and an interparticle distance r_0, $r_0^3N=V$, the equation of state is

---

† Communicated by the Author.

$$PV=2N\kappa T\left[1+\frac{1}{24\pi}\left(\frac{r_0}{d}\right)^3-\frac{64\pi}{3}\left(\frac{d}{r_0}\right)^3\right.$$
$$\left.-\frac{1}{128}\left(\frac{r_0}{\lambda_{\mathrm{D}}}\right)^6+\frac{1}{8\pi}\left(\frac{r_0}{\lambda_{\mathrm{D}}}\right)^3\left(\frac{d}{\lambda_{\mathrm{D}}}\right)^2-8\left(\frac{d}{\lambda_{\mathrm{D}}}\right)^3\right],$$

where λ_{D} is the Debye-Huckel radius $\lambda_{\mathrm{D}}^2=V\kappa T/8\eta Ne^2$.

Analogous results can be obtained in the quantum mechanical case, and the analogous functional formulae are written down, but without detailed calculations.

Use will be made of the extension of certain well-known integrals over a finite number of variables, to the case of an infinite number of variables, and though such forms are familiar in statistical mechanics, for example in the theory of the equilibrium distribution of radiation, they will be briefly reviewed here to familiarize the reader with the notation and concepts. The gaussian integral when written for n variables is

$$\int_{-\infty}^{\infty}\exp\left[-\sum_1^n\xi_\alpha^2a_\alpha\right]\Pi\,d\xi_\alpha=(\pi)^{n/2}\Pi a_\alpha^{-1/2} \quad . \quad . \quad (1.1)$$

$$=(L)^{-1}\quad\text{say.} \quad . \quad . \quad (1.2)$$

Then it is easily seen that

$$L\int_{-\infty}^{\infty}\exp\left[-\sum_1^n\xi_\alpha^2a_\alpha-\sum_1^n\xi_\alpha b_\alpha\right]\Pi d\xi_\alpha=\exp\left[-\tfrac{1}{4}\sum_1^n b_\alpha^2a_\alpha^{-1}\right] \qquad (1.3)$$

and

$$L\int_{-\infty}^{\infty}\exp\left[-\sum_1^n\xi_\alpha^2a_\alpha-\sum_1^n\xi_\alpha^2c_\alpha\right]\Pi d\xi_\alpha=\exp\left[-\tfrac{1}{2}\sum_1^n\log\left(1+\frac{c_\alpha}{a_\alpha}\right)\right]. \quad (1.4)$$

These formulae can also be written for matrices, and if $\sum\xi_\alpha^2a_\alpha$, $\sum\xi_\alpha^2c_\alpha$ are replaced by $\sum\xi_\alpha A_{\alpha\beta}\xi_\beta$ and $\sum\xi_\alpha C_{\alpha\beta}\xi_\beta$, the right-hand sides of (1.3) and (1.4) become

$$\exp\left[-\tfrac{1}{4}\sum b_\alpha(A_{\alpha\beta})^{-1}b_\beta\right]. \quad . \quad . \quad . \quad . \quad . \quad . \quad (1.5)$$

$$\exp\left[-\tfrac{1}{2}\operatorname{Tr}\log\left(1+CA^{-1}\right)\right], \quad . \quad . \quad . \quad . \quad . \quad (1.6)$$

where A^{-1} is the inverse of A. Formula (1.6) can be evaluated in practice by expanding the logarithm, or by the principal axes transformation which reduces it back to (1.4).

Now these formulae can be extended back into the continuum so that (1.5), if the symbol $\delta\xi$ is used for the differentials, becomes

$$L\int_{-\infty}^{\infty}\exp\left[-\int d\alpha\,d\beta\,\xi(\alpha)A(\alpha,\beta)\xi(\beta)-\int d\alpha\xi(\alpha)b(\beta)\right]\delta\xi$$
$$=\exp\left[-\tfrac{1}{4}\int b(\alpha)A^{-1}(\alpha,\beta)b(\beta)d\alpha\,d\beta\right]. \quad . \quad . \quad . \quad (1.7)$$

Similarly, (1.6), in the case of which C, A are diagonal, becomes

$$\exp\left[-\tfrac{1}{2}\int d\gamma \log\left(1+C(\gamma)/A(\gamma)\right)\right]. \qquad (1.8)$$

For the continuous case A^{-1} is defined by

$$\int A^{-1}(\alpha, \beta)A(\beta, \gamma)d\beta=\delta(\alpha-\gamma). \qquad (1.9)$$

so that for example if A is $(4\pi|\boldsymbol{\alpha}-\boldsymbol{\beta}|)^{-1}$, then A^{-1} is $-\delta(\boldsymbol{\alpha}-\boldsymbol{\beta})\nabla_{\alpha}^{2}$ and (1.9) is $-\nabla^{2}|\boldsymbol{\alpha}-\boldsymbol{\beta}|^{-1}=4\pi\delta(\boldsymbol{\alpha}-\boldsymbol{\beta})$.

§ 2. FORMULATION OF THE PROBLEM

The problem of the thermodynamic behaviour of a gas of n positively charged particles and n negatively charged particles, with short-range repulsive interactions, requires the evaluation of the grand partition function Ξ defined by

$$\Xi=\sum_{0}^{\infty}\exp\left(n\mu/\kappa T\right)Z_{n}/n!, \qquad (2.1)$$

where μ is the chemical potential to be fixed by (2.7) below and Z_n is the partition function of the n positive charges labelled with greek indices, and n negative particles labelled with roman indices:

$$Z_{n}=\int\int \Pi d^{3}v_{\alpha}d^{3}v_{i}d^{3}r_{\alpha}d^{3}r_{i}\exp\left[-H_{n}/\kappa T\right]. \qquad (2.2)$$

The Hamiltonian H_n is

$$H_{n}=\sum\tfrac{1}{2}m_{+}v_{\alpha}^{2}+\sum\tfrac{1}{2}m_{-}v_{i}^{2}+e^{2}\sum_{\substack{i>j\\ \alpha>\beta}}\left(\theta r_{ij}^{-1}+\theta r_{\alpha\beta}^{-1}-\theta r_{\alpha i}^{-1}\right)$$

$$+\sum_{\substack{i>j\\ \alpha>\beta}}\left(\psi_{ij}+\psi_{\alpha\beta}+\psi_{i\alpha}\right) \qquad (2.3)$$

where

$$\begin{aligned}\theta(r)&=0 \qquad r<d\\ &=1 \qquad r>d\end{aligned} \qquad (2.4)$$

and

$$\begin{aligned}\psi(r)&=\infty \qquad r<d\\ &=0 \qquad r>d.\end{aligned} \qquad (2.5)$$

In terms of Ξ the equation of state is obtained from

$$PV=\kappa T\log\Xi, \qquad (2.6)$$

$$2N=\partial\Xi/\partial\mu. \qquad (2.7)$$

The factor of 2 in (2.7) arises since we are considering the gas made up of pairs of particles and summing over the pairs in (2.1), a procedure which is most suitable for the present problem.

Now as far as ψ is concerned, the partition function can be expanded in the usual way (absorbing the κT into ψ for convenience since this is a singular function)

$$\exp[-\sum\psi]=\Pi\exp[-\psi] \quad (2.8)$$

$$=\Pi(1+[\exp(-\psi)-1]) \quad (2.9)$$

$$=1+\sum_{\substack{a>b\\ \alpha>\beta}}(\exp(-\psi_{ab})-1)$$

$$+\sum_{\substack{a>b\\ a>c}}\sum_{c>d}(\exp[-\psi_{ab}]-1)(\exp[-\psi_{cd}]-1)+\dots \quad (2.10)$$

This cluster expansion gives a series of terms which are non-zero only when the particles in the cluster are close together. The long-range potential cannot be treated in this way, so that Ξ will be expanded into a series, each term of which contains unexpanded long-range potentials and one of the short-range expansion terms of (2.10). The long-range potentials are treated by representing them as functional integrals, as in (1.7):

$$\exp[-(e^2/\kappa T)\sum(\theta r_{ij}{}^{-1}+\theta r_{\alpha\beta}{}^{-1}-\theta r_{\alpha i}{}^{-1})]$$

$$\equiv L\int\delta\phi\exp\Big[(e'/\kappa T)(\sum\phi(r_i)-\sum\phi(r_\alpha))$$

$$-(8\pi\kappa T)^{-1}\int\phi(r)Q(r,s)\phi(s)d^3rd^3s\Big] \quad (2.11)$$

where $e'=ie$ and Q is the operator which has the property that

$$\int Q(\mathbf{r},\mathbf{s}')\theta(\mathbf{s}'-\mathbf{s})|\mathbf{s}'-\mathbf{s}|^{-1}d^3s'=4\pi\delta(\mathbf{r}-\mathbf{s}), \quad (2.12)$$

i.e. the Fourier transform of $Q(\mathbf{r}-\mathbf{s})$ is $k^2\sec kd$. The explicit displacement that obtains (2.11) is

$$\phi(\mathbf{r})=\phi'(\mathbf{r})+e'\Big(\sum_i\theta|\mathbf{r}-\mathbf{r}|^{-1}-\sum_\alpha\theta|\mathbf{r}-\mathbf{r}_\alpha|^{-1}\Big). \quad (2.13)$$

A slightly simpler case is if $d=0$ when

$$Q(\mathbf{r},\mathbf{s})=-\delta(\mathbf{r}-\mathbf{s})\nabla^2 \quad (2.14)$$

so that

$$\int\phi Q\phi d^3r\,d^3s=\int(\nabla\phi).(\nabla\phi)d^3r. \quad (2.15)$$

If ϕ is regarded as a potential, this is the electrostatic energy; however, one has to use ie rather than e in (2.11). This is a similar situation to the rôle of the longitudinal photon in field theory where devices like an indefinite metric are employed to obtain well-defined results. As far as this work is concerned it causes no difficulties and any way (2.11) can always be regarded simply as a mathematical identity. Taking the first term of the series (2.10) one is left with the integration over coordinates in Z_n of

$$\int \exp\,[-(e^2/\kappa T)(\sum \theta r_{ij}{}^{-1} + \theta r_{\alpha\beta}{}^{-1} - \theta r_{\alpha i}{}^{-1})]\Pi d^3r_i\, d^3r_\alpha$$

$$= L \int \delta\phi \exp\,(-I(\phi)) \left[\int\!\!\int \exp\,[(e'/\kappa T)(\phi(\mathbf{r}_1) - \phi(\mathbf{r}_2))]d^3r_1\, d^3r_2 \right], \qquad (2.16)$$

where

$$8\pi\kappa T I(\phi) = \int \phi Q \phi d^3r\, d^3s. \qquad (2.17)$$

This form results because each of the integrations over r_i, r_α is separable The integration over kinetic energy gives the usual $(2\pi\kappa T/m)^{3n}$ so that the first term of Ξ is

$$L \int \delta\phi e^{-I} \left[\sum_n \frac{1}{n!} \exp\,(n\mu/\kappa T)\; (2\pi\kappa T/m)^3 \Big(\int\!\!\int \exp\,[(e'/\kappa T)\phi(\mathbf{r}_1) - \phi(\mathbf{r}_2)]d^3r_1\, d^3r_2 \Big)^n \right]$$

$$= L \int \delta\phi e^{-I} \exp \Big[(2\pi\kappa T/m)^3 \exp\,(\mu/\kappa T) \times \int\!\!\int \exp\,[(e'/\kappa T)(\phi(\mathbf{r}_1) - \phi(\mathbf{r}_2))d^3r_1\, d^3r_2] \Big]. \qquad (2.18)$$

Now consider the second term which involves a factor $\sum(\exp(-\psi)-1)$ where a, b run over i, j; α, β, i, α. There are $n(n-1)/2$ terms of type α, β and i, j and n^2 of type i, α, but the distinction between n^2 and $n(n-1)$ can be ignored as also ultimately can that between ψ_{ij} and $\psi_{\alpha\beta}$ in this calculation. This leaves

$$\Big(\int\!\!\int \exp\,[(e'/\kappa T)(\phi(\mathbf{r}_1) - \phi(\mathbf{r}_2))]d^3r_1\, d^3r_2 \Big)^{n-2} n(n-1)$$

$$\times \Big\{ \int\!\!\int \exp\,[(e'/\kappa T)(\phi(\mathbf{a}) - \phi(\mathbf{b}))]d^3a\, d^3b \int\!\!\int [\exp\,(-\psi_{cf}) - 1]$$

$$\times \exp\,[(e'/\kappa T)(\phi(\mathbf{c}) - \phi(\mathbf{f}))]\, d^3c\, d^3f + \int\!\!\int \exp\,[(e'/\kappa T)(\phi(\mathbf{a}) + \phi(\mathbf{b}))]d^3a\, d^3b$$

$$\times \int\!\!\int [\exp\,(-\psi_{cf}) - 1] \exp\,[(e'/\kappa T)(\phi(\mathbf{c}) + \phi(\mathbf{f}))]\, d^3c\, d^3f \Big\}. \qquad (2.19)$$

Introduce $z = (2\pi\kappa T/m)^3 \exp\,(\mu/\kappa T)$, then the contribution is got by multiplying (2.19) by $z^n n(n-1)/n!$ $(= z^2 z^{n-2}/(n-2)!)$. If the two terms in the right-hand bracket in (2 19) are called $\zeta_2{}^{(1)}(\phi)$ and $\zeta_2{}^{(2)}(\phi)$ respectively, the sum over n gives

$$L \int \delta\phi e^{-I} \exp \left[z \int\!\!\int d^3r_1\, d^3r_2 \exp\,[(e'/\kappa T)(\phi(\mathbf{r}_1) - \phi(\mathbf{r}_2))] \right]$$

$$\times z^2(\zeta_2{}^{(1)}(\phi) + \zeta_2{}^{(2)}(\phi)). \qquad (2\ 20)$$

In general, defining $\zeta_1 = 1$ and realizing that the first-order term in the cluster expansion appears in the form $z^{2(l-1)} \sum_{j=1}^{l} \zeta_l^{(j)} = z^{2(l-1)} \zeta_l$ say, the final form becomes

$$\Xi = \sum_{l=1}^{\infty} z^{2(l-1)} \Xi_l \quad . \quad . \quad . \quad . \quad . \quad . \quad . \quad (2.21)$$

where

$$\Xi_l = L \int \delta\phi\, e^{\;l} \zeta_l(\phi) \exp \left[z \int\int d^3r_1\, d^3r_2 \exp\,[(e'/\kappa T)(\phi(\mathbf{r}_1) - \phi(\mathbf{r}_2))] \right]. \quad . \quad . \quad . \quad (2.22)$$

This form, expanding clusters of the short-range force while preserving the long-range effects, is now suitable for calculation.

§ 3. EVALUATION IN THE LOW-DENSITY CASE

The parameters governing the evaluation of (2.22) are λ_D, the Debye length, r_0 the mean separation and d the core radius. The quantity d will always be considered small and in this section it will also be assumed that $\lambda_D > r_0$, the low-density condition, so that the thermodynamic potential, $\kappa T \log \Xi$, can be expressed in a series in $r_0 \lambda_D{}^{-1}$, $d\lambda_D{}^{-1}$ and $dr_0{}^{-1}$. This object can be achieved by expanding the exponent in a power series in e':

$$\begin{aligned}
&\int d^3r_1\, d^3r_2 \exp\,[(e'/\kappa T)(\phi(\mathbf{r}_1) - \phi(\mathbf{r}_2))] \\
&= \int d^3r_1\, d^3r_2 \Big\{ 1 + (e'/\kappa T')^3 (\phi^2(\mathbf{r}_1) - \phi(\mathbf{r}_1)\phi(\mathbf{r}_2)) \\
&\quad + \frac{1}{12} (e'/\kappa T)^4 (\phi^4(\mathbf{r}_1) - 4\phi(\mathbf{r}_1)\phi^3(\mathbf{r}_2) + 3\phi^2(\mathbf{r}_1)\phi^2(\mathbf{r}_2)) \Big\} \quad . \quad . \quad . \quad (3.1) \\
&= V^2 - V^2 (e/\kappa T)^2 \int \phi^2(\mathbf{r}) d^3r + (e/\kappa T)^2 \left(\int \phi(\mathbf{r}) d^3r \right)^2 \\
&\quad + \frac{1}{12} V (e/\kappa T)^4 \int \phi^4(\mathbf{r}) d^3r - \frac{1}{3} (e/\kappa T)^4 \int \phi(\mathbf{r}_1) d^3r_1 \int \phi^3(\mathbf{r}_2) d^3r_2 \\
&\quad + \tfrac{1}{4} (e/\kappa T)^4 \left(\int \phi^2(\mathbf{r}) d^3r \right)^2 + 0(e^6) \quad . \quad . \quad . \quad . \quad . \quad . \quad . \quad (3.2)
\end{aligned}$$

where V is the total volume.

The first two terms are the key terms, whilst all the remainder can be expanded further. Retaining the first two terms one has to evaluate

$$L \int \delta\phi \exp \left[zV^2 - (8\pi\kappa T)^{-1} \int \phi [Q + 8\pi z (e^2/\kappa T) V \delta(\mathbf{r}, \mathbf{s})] \phi d^3r\, d^3s \right]. \quad (3.3)$$

Putting

$$\lambda^2 = \kappa T (8\pi z e^2)^{-1} \quad . \quad . \quad . \quad . \quad . \quad . \quad . \quad . \quad (3.4)$$

and

$$\int (Q + \lambda^{-2} \delta(\mathbf{r} - \mathbf{s})) P(\mathbf{s} - \mathbf{r}') d^3s - \delta(\mathbf{r} - \mathbf{r}') \quad . \quad . \quad . \quad . \quad (3.5)$$

this becomes

$$\exp(zV^2) L \int \delta\phi \exp \left[-(8\pi\kappa T)^{-1} \int \phi P^{-1} \phi d^3r\, d^3s \right]. \quad . \quad . \quad (3.6)$$

The quantity λ is not yet the Debye length λ_D as z has yet to be evaluated, but it is in the first approximation. Also if the effect of the core d were ignored, P would satisfy

$$(-\nabla^2+\lambda^{-2})P(\mathbf{r}-\mathbf{r}')=\delta(\mathbf{r}-\mathbf{r}') \quad . \quad . \quad . \quad (3.7)$$

$$P(\mathbf{r})=(4\pi r)^{-1}\exp(-r/\lambda), \quad . \quad . \quad . \quad . \quad . \quad . \quad (3.8)$$

which is the usual shielded potential. The integral (3.3) is brought into the diagonal form (1.8) by changing variables from $\phi(\mathbf{x})$ to its Fourier transform and the formula (1.8) gives its value

$$\exp\left[zV^2-\tfrac{1}{2}(2\pi)^{-3}V\int\log\left[1+(k^2\lambda^2)^{-1}\cos kd\right]d^3k\right]. \quad . \quad . \quad (3.9)$$

The integral

$$J=\int\log\left[1+(k^2\lambda^2)^{-1}\cos kd\right]d^3k \quad . \quad . \quad . \quad . \quad (3.10)$$

can be performed in a series in d/λ by using the fact that

$$(k^2\lambda^2)^{-1}\cos kd\,k^2\,dk=0 \quad . \quad . \quad . \quad (3.11)$$

so that

$$J=\int\log\left[1+(k^2\lambda^2)^{-1}\cos kd\right]d^3k-\int(k^2\lambda^2)^{-1}\cos kd\,d^3k. \qquad (3.12)$$

Writing $\cos kd=1-2\sin^2(kd/2)$, the logarithm can be expanded and gives

$$J=4\pi\int_0^\infty\left[\log(1+(k^2\lambda^2)^{-1})-(k^2\lambda^2)^{-1}\right]k^2\,dk$$

$$-8\pi\lambda^{-3}\int\sin^2(kd/2\lambda)(k^2+1)^{-1}k^2dk \quad . \quad . \quad . \quad . \quad (3.13)$$

$$=\frac{4\pi^2}{3\lambda^3}+\frac{2\pi^2}{\lambda^3}\left[1-\exp(-d/\lambda)\right]+\ \ldots. \quad . \quad . \quad . \quad . \quad (3.14)$$

To order d/λ therefore

$$J=4\pi^2/3\lambda^3+2\pi^2d\lambda^{-4}+0(d^2\lambda^{-5}) \quad . \quad . \quad . \quad . \quad . \quad (3.15)$$

and hence Ξ_1 becomes

$$\exp\left[zV^2-(12\pi\lambda^3)^{-1}V-(8\pi\lambda^4)^{-1}Vd\right]. \quad . \quad . \quad . \quad . \quad (3.16)$$

The first two terms in the exponential are those of the Debye–Huckel approximation. The remaining terms in the expansion of the $e\phi$ series (3.2) can easily be integrated; the third and fifth terms give a small contribution being down by a factor λ^3/V from the leading terms which are $\int\phi^4$ and $\int\phi^2\int\phi^2$. These give together $V(128\pi^2\lambda^3)^{-1}(r_0{}^3\lambda^{-1}\lambda_D{}^{-2})$. Since this is still a small term it can be written in the exponent to give the first approximation to Ξ:

$$\Xi_1=\exp\{zV^2-(12\pi\lambda^3)^{-1}V-(8\pi\lambda^3)^{-1}V(d\lambda^{-1})$$

$$+(128\pi^2\lambda^3)^{-1}V(r_0{}^3\lambda^{-1}\lambda_D{}^{-2})\}. \quad . \quad . \quad . \quad (3.17)$$

The next term in (2.22) is the ζ_2 term which in the absence of long-range forces would give the second virial coefficient. The calculation is quite straightforward and will not be reproduced in detail.
The result is that

$$\Xi_2 = -\frac{64}{3}\pi d^3 V z^2 (1 - r_0{}^3(4\pi\lambda_D{}^2\lambda)^{-1})\Xi. \qquad (3.18)$$

These being small terms, Ξ evaluated to this order becomes

$$\begin{aligned} V^{-1}\log\Xi = {} & zV - (12\pi\lambda^3)^{-1} - (8\pi\lambda^3)^{-1}(d\lambda^{-1}) \\ & + (128\pi^3\lambda^3)^{-1}(r_0{}^3\lambda^{-1}\lambda_D{}^{-2}) - \frac{64}{3}\pi d^3(Vz)^2 \\ & + \frac{16}{3} d^3(VZ)^2(r_0{}^3\lambda_D{}^{-2}\lambda^{-1}). \qquad (3.19) \end{aligned}$$

Recalling that $\lambda = \lambda_D z^{-1/2}\,(NV^{-2})^{1/2}$ and

$$N = (\partial/\partial z)\log\Xi \qquad (3.20)$$

one has

$$\begin{aligned} N = {} & zV^2 - (8\pi)^{-1}(r_0{}^3\lambda_D{}^{-1})^3(zV^2N^{-1})^{3/2} \\ & - (4\pi)^{-1}N(ZV^2N^{-1})^2(dr_0{}^{-1})(r_0\lambda_D{}^{-1})^3 \\ & + (64\pi)^{-1}N(r_0\lambda_D{}^{-1})(zV^2N^{-1}) - 128(3\pi)^{-1}(dr_0{}^{-1})^3N(zV^2N^{-1})^2 \\ & + (16/3)(dr_0{}^{-1})^3(zV^2N^{-1})^{5/2}(r_0\lambda_D{}^{-1})^3. \qquad (3.21) \end{aligned}$$

This can now be solved to give z and the corrected shielding radius. It clearly will give a large number of terms and the relative magnitudes of these will depend on r_0, λ_D and d. In order to be definite, keep the leading term of each type as in (3.19), i.e. solve (3.21) by putting $zV^2 = N$ in the terms on right in (3.21). This then gives

$$\begin{aligned} PV = 2N\kappa T[& 1 + (24\pi)^{-1}(r_0\lambda_D{}^{-1})^3 + \tfrac{1}{3}(64\pi)(dr_0{}^{-1})^3 \\ & - 128\pi(r_0\lambda_D{}^{-1})^3 + (8\pi)^{-1}(r_0\lambda_D{}^{-1})^3(d\lambda_D{}^{-1}) \\ & - 8(d\lambda_D{}^{-1})^3]. \qquad (3.22) \end{aligned}$$

The terms in the bracket on the right-hand side can be analysed in this way in the order in which they come:

(1) Perfect gas of $2N$ particles.

(2) Long-range interaction in the first approximation, which is the Debye–Huckel result, see e.g. Landau and Lifshitz (1958).

(3) First approximation to the hard sphere gas, i.e. the familiar second virial coefficient without long-range interaction.

(4) The second approximation to the purely long-range effects, which is rather difficult to obtain by other methods.

(5) The effect of (3) upon (2).

(6) The effect of (2) upon (3).

It may be emphasized that though only the leading terms have been kept in this analysis there was no difficulty in proceeding further, except that the number of terms of course becomes very large. The series is asymptotic in d, which roughly speaking stemmed from integrals like

$$\int_d^\lambda \exp(-e^2/r\kappa T)d^3r,$$

which cannot be analytic in d however small e is.

§ 4. THE PHYSICAL INTERPRETATION OF THE THERMODYNAMIC POTENTIAL

It is interesting to compare the above results with the approach of the theory of plasma oscillations. If the Fourier components of the densities of positive and negative particles are

$$\rho_{\mathbf{k}} = \sum_{j=1}^{N} \exp[2\pi i(\mathbf{k}\,.\,\mathbf{r}_j)V^{-1/3}], \quad . \quad . \quad . \quad . \quad . \quad . \quad (4.1)$$

$$\sigma_{\mathbf{k}} = \sum_{\alpha=1}^{N} \exp[2\pi i(\mathbf{k}\,.\,\mathbf{r}_\alpha)V^{-1/3}], \quad . \quad . \quad . \quad . \quad . \quad . \quad (4.2)$$

and these are taken as coordinates instead of the r_i's and r_α's, then one has the difficulty that only a finite number of **k** values can be used. However if one does so, the first approximation to the Jacobian is given by

$$\Pi d^3r \rightarrow \Pi d\rho_{\mathbf{k}} d\sigma_{\mathbf{k}} \exp\left[-\sum_{\mathbf{k}}\sigma_{\mathbf{k}}\sigma_{\mathbf{k}}{}^*/N - \sum_{\mathbf{k}}\rho_{\mathbf{k}}\rho_{\mathbf{k}}{}^*/N\right] \quad . \quad . \quad . \quad (4.3)$$

(see for example Bohm and Pines (1952), Edwards (1958)). This can be written in terms of $\rho + \sigma$ and $\rho - \sigma$, as can the part of the potential energy which can be expressed by the limited set of **k**'s available

$$(e^2/\kappa T)\sum(r_{ij}{}^{-1} + r_{\alpha\beta}{}^{-1} - r_{i\alpha}{}^{-1}) = \sum_{\mathbf{k}}(\rho_{\mathbf{k}} - \sigma_{\mathbf{k}})(\rho_{\mathbf{k}}{}^* - \sigma_{\mathbf{k}}{}^*)r_0{}^2k^{-2}\lambda_{\mathrm{D}}{}^{-2}N^{-1} + \text{remainder.} \quad . \quad . \quad . \quad (4.4)$$

The remainder can be treated by expanding it in cluster terms as was done to the hard core above. It is easy to correlate these points of view, for the integral (3.12) with $d \sim 0$:

$$\int k^2\, dk \log(1 + (k^2\lambda_{\mathrm{D}}{}^2)^{-1}) - \int dk \lambda_{\mathrm{D}}{}^{-2}$$

can be split at the value $k = \lambda_{\mathrm{D}}{}^{-1}$ into two parts. The integral from 0 to $\lambda_{\mathrm{D}}{}^{-1}$ is precisely that obtained by using (4.3) and (4.4) and the first $Nr_0{}^3\lambda_{\mathrm{D}}{}^{-3}$ values of k^1. The integral from $\lambda_{\mathrm{D}}{}^{-1}$ to infinity is precisely that obtained by a cluster expansion of the remainder, which if the first $Nr_0{}^3\lambda_{\mathrm{D}}{}^{-3}$ values of k are subtracted from the potential energy, is just the shielded potential $(r)^{-1}\exp(-r/\lambda_{\mathrm{D}})$. The exact point at which one separates the potential into two parts and just how it is done is a difficulty in attempting to treat the problem this way, but taking the first $Nr_0{}^3\lambda_{\mathrm{D}}{}^{-3}$ values of **k**, the contribution to Ξ is equal from the small and from the large **k** values, so that physically one can say that the deviations from the perfect gas behaviour due to the collisions of particles interacting on an average with the shielded potential and the contribution coming from the potential energy part of plasma oscillations of the charge separation are roughly equal and proportional to $(r_0^3\lambda_D^{-3})$ and that this is a very small quantity in an ionized gas under normal conditions. To do the calculation entirely using the ρ's is very awkward due to their failure to handle the short range effects, and so though the use of the ϕ is very close to this treatment, $\phi(k)$ being roughly just $(\rho_{\mathbf{k}}-\sigma_{\mathbf{k}})/k^2$, the present treatment completely avoids the redundant coordinate problem.

§ 5. THE VARIATIONAL APPROACH

The method of evaluating Ξ seems to have advantages over 'summation of diagram methods', but these methods can nevertheless reproduce the results if applied to a sufficiently high order of accuracy. It is interesting therefore to look at a form like Ξ_1 and see if it suggests methods of approach which are obscured by other methods. In particular if one wishes to relax the condition $\lambda_D > r_0$, a variational approach suggests itself. None of the remaining discussion will involve d, so it will be assumed that $\lambda_D, r_0 \gg d$, and d will not be further mentioned. A variational principle for functional integrals of the type Ξ_1 has been used by Feynman (1955) in the polaron problem, and a similar approach has been used by Lieb (1957) in the theory of a nucleus with non-linear mesonic forces. The argument runs as follows: if one needs to evaluate an integral

$$X=\int \exp\left(K(\phi)+J(\phi)\right)\delta\phi \qquad (5.1)$$

and K can be approximated by K_0, so that if

$$J'=J+K_0, \qquad (5.2)$$

$$X=\int \exp\left[(K-K_0)+J'\right]\delta\phi. \qquad (5.3)$$

This may be regarded as the expectation value of the quantity $\exp(K-K_0)$ and Feynman suggests that, since for any positive weight,

$$\langle e^A\rangle > e^{\langle A\rangle} \qquad (5.4)$$

X be calculated via

$$X=\int \exp\left[\langle K-K_0\rangle+J'\right]\delta\phi \qquad (5.5)$$

and K_0 chosen so as to maximize this expression. In our situation

$K(\phi)$ is $z\int\int \exp\left[(e'/\kappa T)(\phi(\mathbf{r})\phi(\mathbf{s}))\right]d^3r\,d^3s$ and J is $(8\pi\kappa T)^{-1}\int(\nabla\phi)^2 d^3r$.

The simplest trial function to take is

$$K_0=zV^2+l^{-2}\int \phi^2(r)d^3r, \qquad (5.6)$$

l is then an effective Debye-radius and implies that $\exp(-r/l)/r$ is the effective potential arising from a charged particle. With this trial function the necessary integrals are easily performed and the logarithm of X is

$$-(12\pi l)^{-3}V+[\tfrac{3}{2}(V/12l^3\pi)-zV^2\exp(r_0{}^3/8\pi\lambda_{\mathrm{D}}{}^2l)]. \quad . \quad . \quad (5.7)$$

Varying l one has

$$Vl^{-2}=zV^2r_0{}^3\lambda_{\mathrm{D}}{}^{-2}\exp(r_0{}^3/\lambda_{\mathrm{D}}{}^2l8\pi), \quad . \quad . \quad . \quad . \quad . \quad (5.8)$$

i.e.

$$\left(\frac{\lambda_{\mathrm{D}}}{l}\right)^2=\left(\frac{zV^2}{N}\right)\exp(r_0{}^3/\lambda_{\mathrm{D}}{}^2l8\pi). \quad . \quad . \quad . \quad . \quad . \quad (5.9)$$

Here z has of course been regarded as a fixed parameter through this calculation, but now is eliminated via (2.7). This gives

$$z=NV^{-2}\exp(-r_0{}^3/8\pi\lambda_{\mathrm{D}}{}^2l) \quad . \quad . \quad . \quad (5.10)$$

and gives precisely $\lambda_{\mathrm{D}}=l$. Thus the variational principle has with this trial function reproduced the Debye–Huckel answer, and proved that the latter is an extremum. A somewhat more general trial function is $\int\phi(\mathbf{r})p(\mathbf{r}-\mathbf{s})\phi(\mathbf{s})d^3r\,d^3s$ which requires the variation of the function $p(\mathbf{r}-\mathbf{s})$. It turns out however that $p(\mathbf{r}-\mathbf{s})$ is just $\lambda_{\mathrm{D}}{}^{-2}\delta(\mathbf{r}-\mathbf{s})$ and again the same results obtain.

That the Debye–Huckel solution is an extremum can be seen in a rather simpler way by observing that the first n terms of the expansion of $\cos\theta$ are either everywhere greater or everywhere less than $\cos\theta$ according to whether n is odd or even. Thus

$$\begin{aligned}&\exp\left[z\int\cos(e/\kappa T[\phi(r)-\phi(s)])d^3r\,d^3s\right]\\&<\exp zV^2\\&>\exp\left[zV^2-(e/\kappa T)^2\int(\phi(\mathbf{r})-\phi(\mathbf{s}))^2d^3r\,d^3s\right] \quad . \quad . \quad (5.11)\end{aligned}$$

and so on for even numbers of terms. It is also true for odd numbers but all except the first are divergent and so trivially greater than the true value. It follows therefore that as a function of z the thermodynamic potential $\Omega=-\kappa T\log\Xi=-PV$ satisfies

$$\Omega_{\text{Debye}}>\Omega_{\text{true}}>\Omega_{\text{perfect gas}}. \quad . \quad . \quad . \quad . \quad . \quad (5.12)$$

§6. QUANTUM MECHANICAL CASE

Using the formalism of second quantization the quantum mechanical system of N electrons is very analogous to the above work and if the Green functions of the quantum gas are evaluated and the time replaced by $-ih/\kappa T$, it is a straightforward matter to show that the statistical partition functions are obtained. There are several accounts of this in the literature (e.g. Bloch and De Dominicis (1958), Montroll and Ward (1958), Abrikosov *et al.* (1959)). It is worth noting that this problem can also be written in functional form, but requires an auxiliary $\phi(\mathbf{x}, t)$ which is time dependent. If $G(\mathbf{x}, \mathbf{x}'; \ t, t'; \ [\phi])$ is the Green function of the Schrödinger equation

$$\left(\frac{\hbar^2}{2m}\nabla^2 + i\hbar\frac{\partial}{\partial t} - i\mu + e\phi(\mathbf{x}, t)\right) G(\mathbf{x}, \mathbf{x}'; \ t, t'; \ [\phi]) = \delta(\mathbf{x}-\mathbf{x}')\delta(t-t'). \quad (6.1)$$

Then

$$\Xi = L\int \delta\phi \exp\left[\frac{i}{8\pi\hbar}\int (\nabla\phi(x, t))^2 d^3x\, dt \pm \operatorname{Tr}\log(1+G(\phi))\right] \quad (6.2)$$

where Tr stands for the three dimensional trace of the function $\log(1 \pm G(\phi))$, ± for fermions or bosons, the latter being understood in the 'matrix' sense, i.e.

$$\operatorname{Tr}\log(1 \pm G(\phi)) = \int d^3x G(\mathbf{x}, \mathbf{x}; \ t, t'[\phi]) + \int d^3x\, d^3x' G(\mathbf{x}, \mathbf{x}'; \ t, t'[\phi]) G(\mathbf{x}', \mathbf{x}; \ t, t'; \ [\phi]) + \ldots. \quad (6.3)$$

When $h \to 0$, or $T \to \infty$, the classical formulae appear very simply as the limit, only the first term of the logarithm surviving and being just the exponential of ϕ times the kinetic energy term; the $I(\phi)$ also checks with the classical form, ϕ becoming independent of $t-t'$, i.e. of T. The other extreme is the low temperature case when the analogue of the expansion (3.1) keeping only the term in ϕ^2 yields the high density limit, which has been observed in terms of the summation of diagrams by Montroll and Ward (1958). The functional form however opens the possibility of more exact treatments of this problem, by for example variational techniques.

ACKNOWLEDGMENTS

The author would like to thank Mr. J. J. Sanderson for checking the calculation in this paper and Professor B. H. Flowers for useful discussions of this work.

REFERENCES

ABRIKOSOV, A. A., GOR'KOV, L. P., and DEYALOSHINSKII, I. E., 1959, *J. exp. theor. Phys.*, **36**, 900.
BLOCH, C., and DE DOMINICIS, C., 1958, *Nucl. Phys.*, **7**, 451.
BOHM, D., and PINES, D., 1953, *Phys. Rev.*, **92**, 22.
EDWARDS, S. F., 1958, *Phil. Mag.*, **3**, 119.
FEYNMAN, R. P., 1955, *Phys. Rev.*, **97**, 660.
LANDAU. L., and LIFSHITZ, E. M., 1958, *Statistical Physics* (Pergamon Press).
LIEB, E. H., 1957, *Proc. roy. Soc.* A, **241**, 339.
MONTROLL, E., and WARD, J., 1958, *Phys. Fluids*, **1**, 55.

The Thermal Conductivity of Water
An Investigation of a Reported Anomaly

By R. W. Powell and A. R. Challoner
Communication from the National Physical Laboratory

[Received July 9, 1959]

Abstract

Thermal conductivity determinations made on water in a guarded hot-plate apparatus over the range 24° to 48°c for two sample thicknesses are in agreement with earlier work. They fail to confirm the departure from the smooth curve, reported by Frontas 'ev as occurring at about 35°c.

The writers have devoted considerable attention to the thermal conductivity of water. Careful experimental determinations have been made (Challoner and Powell 1956) using a guarded hot-plate apparatus and a critical review of known data has recently been published (Powell 1958). The experimentally determined values were believed to be accurate to $\pm 1\%$, and in the review paper what appeared to be the most likely values for the thermal conductivity of water were included as ' proposed values '. Over the temperature range 20°c to 80°c these proposed values were from $\frac{2}{3}\%$ to $\frac{1}{2}\%$ lower than our own experimental values and the values of several other workers were also in close agreement. The conclusion reached was that the proposed values could be recommended for use over this range of temperature but that more work was desirable at temperatures below 20°c.

This further paper stems from some observations by Frontas 'ev (1956) on the thermal conductivity of water which should have been included in the above review but which have only recently been noticed, and a later paper by the same author (Frontas 'ev 1958). Frontas 'ev claims to have established that the variation of thermal conductivity of water with temperature undergoes a small anomalous change between 35° and 45°c and thus parallels previously recorded changes in other properties of water. Frontas 'ev was rather critical of the reliability of earlier thermal conductivity work and adopted a method of the flat-plate type which was distinctive and novel in that the quantity of heat flowing across the liquid film was determined calorimetrically and the temperature gradient established in the liquid layer was determined by an optical method. One merit claimed was that by confining these measurements to the liquid layer there could be no possibility of any temperature discontinuities at the bounding solid surfaces being included as part of the temperature drop across the liquid. Another was that by restricting this temperature drop to only 1° to 1·5°C any non-linear changes in the thermal conductivity with temperature could be more readily detected.

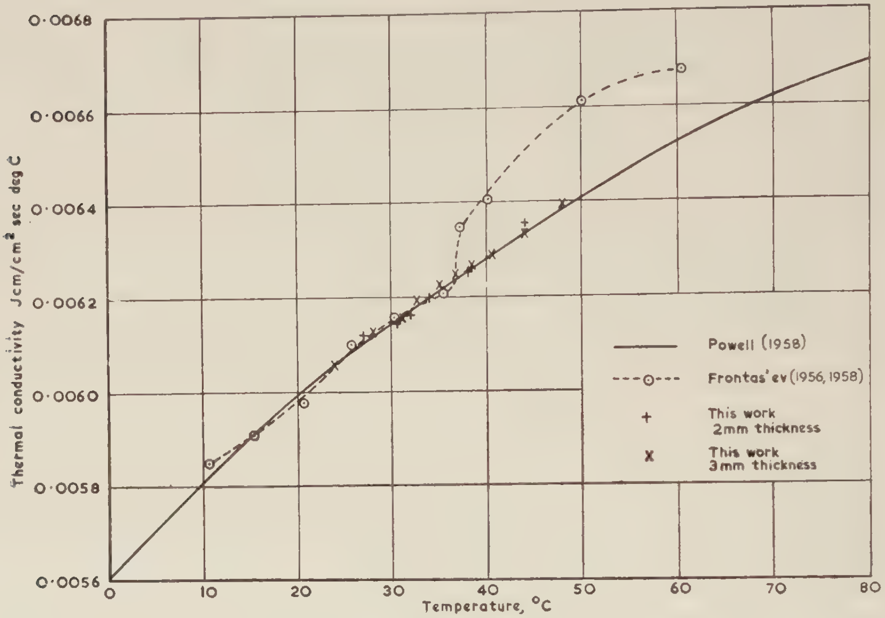

Variation of thermal conductivity of water with temperature.

The experimental results as tabulated by Frontas’ev are plotted in the figure, together with a curve based on the above-mentioned ‘proposed values’. From 10° to 35°C the values obtained by Frontas’ev agree well with this curve, but just beyond 35°C the marked increase in temperature coefficient occurs, to which he directs attention, and this leads to an increasing difference which reaches a maximum a little over 3% at about 50°C. A definite difference is therefore to be noted between the results of Frontas’ev and those of other workers, not only in the region of 35° to 40°C on which he comments but at still higher temperatures. He claims an accuracy of ± 0·5% for his own values and includes in his papers a table to show the close agreement of his values at 20°, 40° and 60°C with some theoretical values as calculated by Eigen (1952). At 20°C both gave 0·00143 cal/cm sec deg C, at 40°C the values were 0·00153 (Frontas’ev), 0·00152 (Eigen) and at 60°C, 0·00160 (Frontas’ev) and 0·00161 (Eigen) which certainly appeared satisfactory.

Whilst the observations in fig. 3 of the paper by Challoner and Powell clearly did not support the pronounced bulge in the region of 50°C, they could provide no check on the suggested anomaly in the region of 35°C, since it chanced that only one experimental point had been included in the range 30° to 43°c.

In view of the possible theoretical interest likely to be aroused by the results of Frontas 'ev and the sparcity of our own data in part of the region concerned some further measurements have been carried out and these are described below.

The additional measurements were undertaken in the guarded hot-plate apparatus previously described, a small change had however been made in that the surfaces of the hot and cold plates had been nickel plated and re-lapped.

The apparatus was charged in the usual way with distilled water which had been de-aerated by heating under a reduced pressure. Two series of steady-state measurements of thermal conductivity were made at small mean temperature intervals. The first covered the temperature range 24° to 48°c and used a horizontal water film 0·3 cm in thickness, and the second a temperature range 27° to 44°c using a different sample in a film 0·2 cm in thickness. The differences in temperature between the hot and cold plates were about 2·7 and 2·4°c in the two instances.

The results of these two experiments are plotted in the figure. Their mutual consistency is seen to be very good and the results show that our earlier conclusion, that no serious thermal resistance can occur at the liquid to metal interfaces, also holds good in the temperature region to which Frontas 'ev has directed attention. The other factor is the close agreement of these latest values with the proposed values for water, each of the present points lying within $\frac{1}{3}\%$ of the proposed curve.

The present work is believed to have met the general criticisms made by Frontas 'ev and clearly does not support his experimental values at temperatures above 32·5°c. It would seem that above this temperature some conditions particular to his experiments have led to rather higher values being obtained and that these values are not supported by the results of careful experiments made by conventional methods.

In the course of the recent measurements with this apparatus, a further check test has been included which arises from some entirely different considerations. Allen (1959) has questioned the reliability of such steady state methods when used for electrically non-conducting fluids, on the grounds that the existence of electrical potentials might affect the results. The precaution has accordingly been taken of making some independent tests with the hot and cold plates connected electrically. After making the measurements at 44°c for the 0·2 cm film, one wire of a thermocouple attached to the cold plate was twisted to one of the thermocouple wires fixed to the hot plate and the readings repeated after the lapse of 30 min. No change was observed, either in the hot and cold-plate temperatures nor in the energy supplied to the hot plate. This served to check that the difference between the present results and those of Frontas 'ev was not associated with any spurious effect in our work of the type suggested by Allen.

ACKNOWLEDGMENT

The work described above has been carried out as part of the research programme of the National Physical Laboratory, and this paper is published by permission of the Director of the Laboratory.

REFERENCES

ALLEN, P. G. H., 1959, *Thermodynamic and Transport Properties of Gases, Liquids and Solids* (The American Society of Mechanical Engineers), p. 350.
CHALLONER, A. R., and POWELL, R. W., 1956, *Proc. roy. Soc.* A, **238,** 90.
EIGEN, M., 1952, *Z. Elektrochem.*, **56,** 176.
FRONTAS 'EV, V. P., 1956, *Doklady Akad. Nauk. S.S.S.R.*, **111,** 1014; 1958, *J. tech. Phys.*, Moscow, **28,** 1839 (for translation see *Soviet Phys., Tech. Phys.*, 1959, **3,** 1696).
POWELL, R. W., 1958, *Advanc. Phys.*, **7,** 276.

The Effect of Quenching on the Formation of G.P. Zones and θ′ in Al Cu-Alloys†

By J. M. Silcock‡
Liverpool University

[Received 8 July, 1959]

Abstract

X-ray methods have been used to estimate the quantities of G.P. zones and θ' formed in Al–4% Cu and Al–4% Cu 0·05% In alloys after various heat treatments.

The rate of formation of G.P. zones decreases not only on slower quenching but also on lowering the reversion treatment temperature. The addition of a trace of indium (Cd, Sn) is known to decrease the rate of zone formation which is then negligible except after very fast quenching.

The rate of formation of the metastable precipitate θ' is dependent on dislocations present in the alloy rather than an excess mobile vacancy concentration. Traces of indium (or cadmium) form even more efficient nuclei for θ' than dislocations but the effect of the indium (or cadmium) is destroyed by fast quenching or cold work. It appears that there is a strong indium-vacancy association which prevents excess vacancies from accelerating the diffusion rate of the copper. When sufficient dislocations are present the indium atoms are trapped and no longer nucleate θ'.

§ 1. Introduction

It is well known that the rate of formation of G.P. zones in Al–Cu alloys is markedly dependent on the method of quenching and is much slower after a reversion treatment (Guinier 1952) (i.e. a short anneal at about 200°c). This has recently been attributed to variations in the concentration of quenched-in vacancies (Federighi 1958, Seitz 1952, de Sorbo *et al.* 1958).

Results have now been obtained showing slower rates of zone formation the lower the reversion treatment temperature and the effect on subsequent θ' formation is discussed. Recently Graf (1958) has found a similar effect in Al–10% Zn and obtains an activation energy for the formation of zones that is the same as that obtained by Bradshaw and Pearson (1957) for the formation of vacancies in pure aluminium.

§ 2. Methods

The quenching rate is very sensitive to specimen thickness, and in this work single crystals in the form of sheets about 0·3 cm^2 in area and 0·05 cm thick were used. The time for cooling from 525°c to 20°c is approximately 0·1 sec on water quenching and about 1 sec on acetone quenching. Unless otherwise stated, the low-temperature treatment was given immediately after quenching from the solution treatment temperature of 525°c. The intensity of streaks or spots on MoKα oscillation photographs were compared. These were obtained with the crystal at room temperature except for ageing times of less than two hours at 30°c, when the crystal was held at −195°c by a stream of liquid nitrogen. For G.P. zone [1] streaks the intensities have a relative accuracy of only about ± 10% and are less accurate at higher zone concentrations. There is an additional complication that the streaks formed after a low temperature treatment are more diffuse, due to a slightly smaller average zone size. For the range of sizes obtained in these experiments, the intensity at a given diffraction angle may vary by ± 10%. The comparative intensities have not been corrected for zone size.

---

† Communicated by the Author.

‡ Late: Metallurgist, Fulmer Research Institute.

§ 3. The Formation of G.P. Zones [1]

3.1. *Al–4% Cu Alloy*

The results shown in fig. 1 clearly indicate a decrease in the rate of zone formation at 30°c in the order—water quenched, acetone quenched, and then water quenched from the re-heating temperature of 300, 260, 240, 200 and 130°c.

It can be seen that after water quenching from the solution treatment temperature, the formation of zones at 30°c is already apparent after 3 min; the intensity of the streaks is then about 6% of the maximum intensity, i.e. about 3% of the copper in the alloy has already formed zones. Zone formation after water quenching is complete in two hours whereas after a 200°c treatment, less than one-third of the total possible quantity of zones have formed after ten days.

Fig. 1

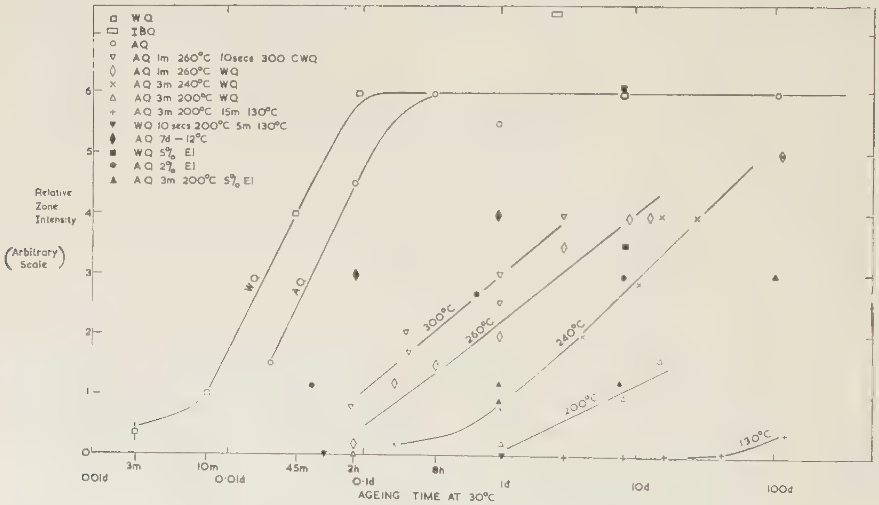

Intensity of streaks from Al–4% Cu crystals after ageing at 30°c.

The displacement of the curves in fig. 1 can be attributed to a decrease in the effective diffusion coefficient as a result of prior heat treatment. The order of magnitude of the experimental diffusion coefficients D_{exp} has been obtained from the ageing curves using the equation (Darken and Gurry 1953, Turnbull 1954) $D = x^2/t$ where x is the average distance travelled by a copper atom (i.e. one quarter of the average zone spacing), and t is the time for half completion of zone formation. The average distance between zones at the end of ageing was taken to be 80 Å.

We wish to compare these experimental values with calculations of the diffusion coefficient due to the presence of excess vacancies. The coefficient of diffusion of copper in aluminium at 30°C, $D_{\mathrm{Cu}\,30}$, obtained by extrapolating high temperature data, gives a value of 5×10^{-25} cm^2/sec. The apparent diffusion coefficient due to the presence of excess vacancies can be obtained by multiplying $D_{\mathrm{Cu}\,30}$ by the excess concentration of vacancies (Federighi 1958). These values are given in table 1. Bradshaw and Pearson's (1957) values have been assumed to hold at temperatures lower than their lowest experimental limit (360°C) and the concentration retained on quenching is assumed equal to the equilibrium value at the quenching temperature. It can be seen that this calculation gives values showing reasonable agreement with the experimental values. Since the specimen will continually lose vacancies, the experimental values would be expected to be lower than the calculated values. It might have been expected that the annealing time at 300°C was insufficient for the vacancy concentration to reach the equilibrium value at this temperature. However this result gives better agreement than the value obtained after the 200°C anneal. The 130°C value is uncertain but a low value would be expected since these specimens were air cooled. It may be remarked that

Table 1. Comparison of Experimental and Theoretical Diffusion Coefficients

Quench		t days	Log D_{expt} cm^2/sec	Log D from excess vacancy theory $\frac{C_{VT}}{C_{V30}} \times D_{\mathrm{Cu}30}$‡
Final Temp. °C	Medium †			
525	W	0·02	−16·6	−16·1
525	A	0·04	−16·9	
200	W	0·9	−18·3	−18·1
260	W	2·4	−18·7	−18·5
240	W	9·0	−19·3	−19·0
200	W	444·0	−21·0	−19·4
130	Air	8×10^5 ?	−24.2	−20·4

† W = water quench. A = acetone quench.

‡ = Using Bradshaw and Pearson's values for C_V and $D_{\mathrm{Cu}30} = 5 \times 10^{-25}$ cm^2/sec.

the value obtained is comparable with the extrapolated value of −24·3 assuming no excess vacancies.

We may conclude that it is possible for the excess vacancy concentration to explain the enhanced rate of G.P. zone formation but more numerical details are required for an exact comparison.

3.2. *Al–4% Cu–0·05% In Crystals*

In Al-Cu alloys containing a trace of cadmium (0·1 wt %) indium or tin (0·05 wt %) the rate of zone formation after normal quenching is very slow (Hardy 1951/2) but a considerable variation in zone formation rate has since been observed in small crystals. Figure 2 shows some results for 0·020 in. thick crystals and it can be seen that although the rate of zone formation is very low after acetone quenching, it is much faster after water quenching. If, however, a fast quenched crystal is held at a low temperature at which zone formation is suppressed but vacancies can still move (in this case −12°c) then on subsequent ageing at 30°c the crystal will behave as a slow quenched crystal. In the binary Al–4% Cu alloy the effect of low-temperature treatment is similar in that the subsequent zone formation rate is decreased by holding at −12°c but the effect is not as pronounced as in the cadmium-containing crystals.

Fig. 2

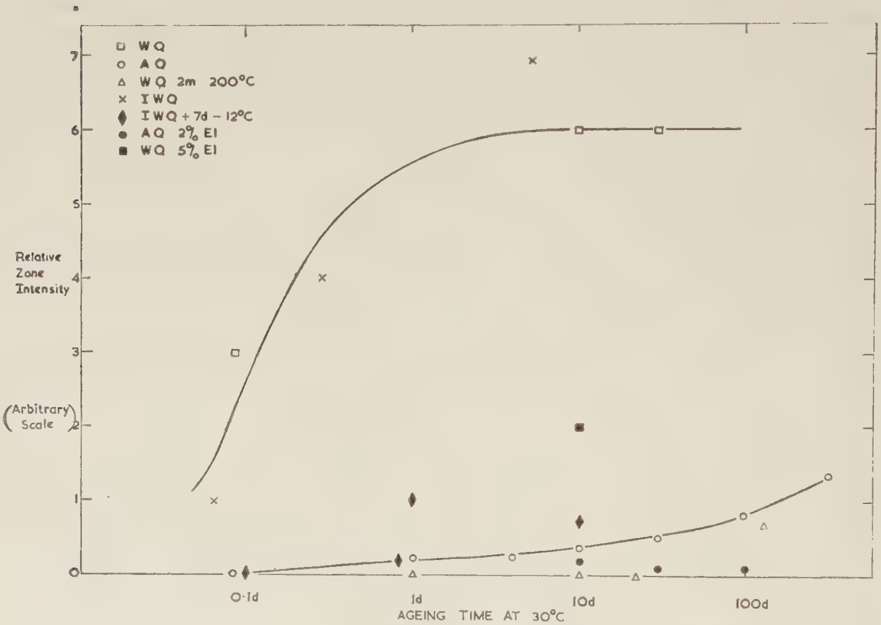

Intensity of streaks from Al–4% Cu–0·05% In crystals after ageing at 30°c.

These results support the hypothesis that cadmium, indium or tin can immobilize the vacancies. These atoms are evidently not associated with vacancies at the solution treatment temperature since G.P. zone formation can occur after very fast quenching rates. The effect of holding at −12°c is more pronounced in indium-containing alloys than the binary alloys and it appears that the number of jumps a vacancy can make before immobilization is low in the presence of cadmium, indium or tin.

The addition of 0·09% Mg to Al–4% Cu or Al–4% Cu 0·1% Cd did not appreciably alter the rate of formation of G.P. zones in acetone quenched crystals of either alloy. Also G.P. zones [1] formed fairly rapidly at 20°c in Al–3·5% Cu–0·5% Mg. It has recently been stated that Mg probably associates with vacancies (Panseri *et al.* 1958), but in the presence of copper this association cannot be as restricting to copper diffusion as the cadmium-vacancy association.

3.3. *The Effect of Strain at Room Temperature*

It can be seen from figs. 1 and 2 that the effect of strain immediately after quenching and before ageing is generally to reduce the rate of formation of zones. (There is one exception in the Al–4% Cu alloy quenched from 200°c and strained.) Presumably the increased number of sinks for vacancies restricts the number of jumps before annihilation. When the concentration of vacancies is low (e.g. after a 200°c re-heat) it appears that the deformation at room temperature can increase this concentration in Al–Cu alloys but not in the Al–Cu–In alloy.

§ 4. THE EFFECT OF QUENCHING ON θ' FORMATION

4.1. *Binary Al–4% Cu Alloys*

It is known that both cold work and rapid quenching accelerate the rate of formation of θ', and that room temperature ageing appears to reduce the effect of cold work (Silcock *et al.* 1955/6).

Table 2 gives some measurements of θ' and G.P. [2] quantities obtained after ageing for one day at 190°c expressed as a percentage of the maximum

Table 2. Quantities of θ' and G.P. [2] in Al–4% Cu Aged One Day at 190°c

Quench	Pre-ageing treatment	θ'%	G.P.[2]%
W	—	64	14
W	1 min, 200°c W.Q.	28	1
W	10 sec, 200°c, 5 min, 130°c	32	5
A	—	17	40
A	3 min, 240°c W.Q.	17	0
A	1 and 3 min, 200°c W.Q.	10	44
A	5 min, 130°c W.Q.	14	60
A	8 days, 110°c	10	20
A	12 wks, 20°c	10	40
A	2% El.	42	<10

quantity possible in this alloy. The quantity of θ' is much greater after water than acetone quenching and is not reduced as drastically by low temperature anneals as is the formation of G.P. [1]. Nucleation of θ' is therefore not by the same means as acceleration of G.P. [1] formation. In both binary and ternary alloys (see § 4·2), the behaviour of thin crystals (0·004 in.) [in which thermal gradients during quenching must be small] was the same on ageing after rapid quenching as the (0·020 in.) thick crystals. In water-quenched crystals as well as cold-worked crystals, the formation of G.P. zones [2] and θ' is not always in equal quantities in the three possible orientations. The full implications of this observation will be discussed in a later paper; however, it obviously suggests nucleation by dislocations in both cases. Hirsch *et al.* (1958) have recently observed dislocation rings in thin water-quenched aluminium sheet, which supports the assumption that there are two differences between fast and slow quenched alloys. The fast-quenched alloys have an excess of mobile vacancies and also a greater number of dislocations. The latter are presumably due to condensation of some of the vacancies but, from the work on G.P. [1] formation it appears that an excess of mobile vacancies remains which can however be removed by low temperature annealing.

4.2. *Ternary Al–4% Cu–0·05% in alloy*

A modified θ' is nucleated very rapidly in these ternary alloys but is hindered by cold work and also by fast quenching, table 3. Although holding a rapidly quenched ternary specimen at −12°c for ten days will lower the rate of G.P. zone [1] formation at 30°c, there is no difference in

Table 3. Alloys Aged Four Hours at 190°c

Alloy	Prior treatment†	Approximate quantity of Precipitate			Remarks
		θ'%	G.P.[2]%	In′%	
Al–4% Cu	I.W.Q.	5	3	—	θ' and G.P.[2] spots slightly broadened
Al–4% Cu–0·05% In	A.Q.	30	None	None	θ' spots very broad with superstructure
,,	A.Q. 5% El.	35	0·8 ?	V. little	θ' spots fairly sharp
,,	I.W.Q.	45	6	V. little (20 ?)	θ' spots sharp
,,	I.W.Q. + 10d, −12°c	45	6	,,	θ' spots sharp
,,	Direct quench to 190°c bath	90	None	Little (30 ?)	θ' spots broad with superstructure

† I.W.Q. = iced water quench (0°c). A.Q. = acetone quench.

the formation of θ' on ageing at 190°c. This again indicates that the formation of G.P. zone [1] is not accelerated by the same mechanism as that which accelerates θ' formation and that the behaviour of fast-quenched crystals is similar to that of deformed crystals as regards θ' formation.

The modified θ' structure is obtained on ageing at 190°c by direct quenching to 190°c as well as after slow cooling to room temperature. Thus the nuclei are able to form at 190°c and are not dependent on lower temperature annealing.

In the binary Al–(Cd, In, Sn) alloys the element Cd In or Sn precipitates from solid solution extremely rapidly (Silcock 1955/56) (about 15 min at 190°c). These elements do not precipitate in slow quenched ternary alloys until after peak hardness (about five hours at 190°c). Deformation, fast quenching and direct quenching increase the rate of precipitation of Cd, In, or Sn as compared with the slow quenched crystals but the rate is still much slower than in binary crystals. Modified θ' forms after direct quenching (table 3). The rate of precipitation of the ternary element as Cd, In, or Sn, is not sufficient to explain the decreased rate of precipitation of θ' and decreased proportion of modified θ' as due to removal of the ternary element by prior precipitation. Some other factor must be retarding the normal nucleating action of the ternary addition.

It is thought that the modification of θ' is a superstructure involving the ternary addition and that the normal action in slow cooled crystals is a reduction of the critical nucleus size by a reduction of surface energy. The ternary addition must, however, be able to get to the 'correct' position with respect to the copper atoms. It is suggested that either cadmium (indium or tin) can be released from associated *vacancies* at temperatures at which this modified θ' structure forms (110°c is the lowest *known* temperature) or that cadmium plus a single vacancy can move fairly freely so that in slow quenched alloys the cadmium (indium or tin) is free to reach the correct position However, if the cadmium (indium or tin) atoms are trapped by dislocations they cannot be released at 190°c and presumably the position in the dislocation is not correct for nucleation by the ternary element. Since the ternary addition is presumed to become attached to vacancies they are likely to frequent the dislocation rings in fast quenched alloys, and in cold worked alloys they are presumably trapped by moving dislocations. This will explain why the modified θ' structure does not form after fast quenching or cold working.

§ 5. Conclusions

It is not possible to explain the variations of the rates of G.P. zone [1] and θ' formation by the same mechanism. A supersaturation of mobile vacancies appears to explain the acceleration of G.P. zone [1] formation. The acceleration of θ' formation in fast quenched crystals is analogous to that in cold worked crystals and is due to dislocations formed on quenching as observed by Hirsch and Smallman in fast quenched aluminium.

Since this paper was originally written a number of papers have appeared on similar subjects. Boltax (1958) has suggested that the sessile rings found after quenching from a high temperature can act as nucleation sites for precipitation. Thomas and Whelan (1959) have been able to show helical dislocations in thin foils of Al–4% Cu which vary in pitch with quenching temperature. They also suggest that copper is likely to segregate to relieve the stress field around edge components of the dislocation and hence that dislocations can act as nuclei for θ' formation.

In the ternary alloys the mechanism by which cadmium (indium or tin) prevent G.P. zone formation is not the same as the mechanism by which they nucleate a modified θ'. It is suggested that cadmium atoms are efficient vacancy trappers and so readily slow down G.P. zone formation. It is also considered that the atoms are in turn readily trapped by dislocations and that they are not freed from dislocations at 190°c. Only those atoms that can move fairly freely can nucleate the modified θ' by a lowering of the interfacial energy of θ'.

ACKNOWLEDGMENTS

The author wishes to thank her former colleagues of Fulmer Research Institute, particularly Dr. E. A. Calnan and Dr. B. S. Berry, for helpful discussion, and many others who helped with the experimental work.

REFERENCES

BOLTAX, A., 1958, *Acta Met.*, **6,** 721.
BRADSHAW, F. J., and PEARSON, S., 1957, *Phil. Mag.*, **2,** 570.
DARKEN, S., and GURRY, R. W., 1953, *Physical Chemistry of Metals* (New York: McGraw-Hill).
FEDERIGHI, T., 1958, *Acta Met.*, **6,** 379.
GRAF, R., 1958, *Comptes Rendus*, **246,** 1544.
GUINIER, A., 1952, *Z. Elektrochem*, **56,** 468.
HARDY, H. K., 1951/2, *J. Inst. Met.*, **80,** 483.
HIRSCH, P. B., SILCOX, J., SMALLMAN, R. C., and WESTMACOTT, K. H., 1958, *Phil. Mag.*, **3,** 897.
PANSERI, C., GATES, F., and FEDERIGHI, T., 1958, *Acta Met.*, **6,** 198.
SEITZ, F., 1952, *L'Etat Solide* (Solvay: Institute International de Physique). p. 401.
SILCOCK, J. M., 1955/6, *J. Inst. Met.*, **84,** 19.
SILCOCK, J. M., HEAL, T. J., and HARDY, H. K., 1955/6, *J. Inst. Met.*, **84,** 23.
SORBO, W. DE, TREAFTIS, H. N., and TURNBULL, D., 1958, *Acta Met.*, **6,** 401.
THOMAS, G., and WHELAN, M. J., 1959, *Phil. Mag.*, **4,** 511.
TURNBULL, D., 1954, *Defect in Crystalline Solids*, *Bristol*, p. 210.

REVIEWS OF BOOKS

Analytical and Canonical Formalism in Physics. By ANDRE MERCIER. (Amsterdam: North Holland Publishing Company, 1959.) [Pp. 222.] 40*s*.

UNTIL Quantum Theory gave it new life, classical analytical mechanics was becoming somewhat boring. It was not sufficiently abstract to interest pure mathematicians, yet too far from material things to be useful to physicists. Now we see more clearly its elegance and power, and why no theoretical physicist should be without it. Even unsophisticated experiments have to operate with Hamiltonians sometimes. This book deals with the Lagrangian and Hamiltonian theories for classical particles and fields, with due attention to general relativistic invariance, spinors, electrodynamics, transformation theories, and CPT symmetry. It would scarcely qualify as an introduction to the subject, being too dry, and abstract in tone, but it will be useful to research workers in classical and quantal field theory for its wide range of general theorems and principles and their careful proofs. Unfortunately, it is not free from misprints, nor from misuse of English idiom. J. M. Z.

Matrix Calculus. By E. BODEWIG. (Second Revised and Enlarged Edition.) (Amsterdam: North-Holland Publishing Company, 1959.) [Pp. 452.] 65*s*.

THE first edition of this book is well known among mathematicians interested in those branches of numerical analysis which deal with linear equations and matrices. In this revised edition some of the errors of the previous edition have been eliminated and new sections have been added. Among the new methods described are Lanczos' *pq*-algorithm and the LR method of Rutishauser. There is also a section on the procedures used by Wilkinson for obtaining real latent roots and vectors, and described by him in 1955.

The author is not afraid to express views about the utility of the practical procedures he describes, particularly in relation to their suitability for use with automatic machines. It is not always clear, however, whether he has in mind fast electronic computers of the modern type, or punched card equipment such as was widely used for mathematical computation a few years ago. The lumping together in the index of digital computers and punched cards strengthens the suspicion that there is some confusion; this suspicion may, however, be unfounded, since the author's English, while vigorous, is not idiomatic, and it is necessary to read him carefully in order to get his meaning.

Although no one could say that this is a perfect book, it covers recent development in a way not found in other books, and many numerical analysts will like to have their personal copies. M. V. W.

Sulphur in Proteins. Proceedings of a Symposium held at Falmouth, Massachusetts, May 1958. Organized and Edited by R. BENESCH, R. E. BENESCH, P. D. BOYER, I. M. KLOTZ, W. R. MIDDLEBROOK, A. G. SZENT-GYÖRGYI, D. R. SCHWARZ. (New York and London: Academic Press, 1959.) [Pp. 469.] $14.00.

SULPHUR is not one of the more abundant elements in proteins, but its unique and important influence upon the properties and reactions of many proteins makes it a suitable topic for a symposium. This book contains the twenty-eight reports presented at the symposium as well as the discussion following each paper. Although sulphur in the form of methionine occurs in most proteins, this amino acid is hardly mentioned, and the reports are concerned chiefly with the function, reactions and methods of measurement of sulphydryl and disulphide groups in proteins. Among the topics included, in which sulphydryl groups or disulphide bonds appear to be of importance, are: structure of wool and of hair, clotting of blood plasma, oxygenation of haemoglobin, storage of iron in ferritin, enzymic catalysis, muscle contraction, structure of viruses and bacteriophage, and cell division. In general, disulphide groups are necessary for maintaining structure in a number of proteins: i.e. wool, hair, certain enzymes, plasma clots and the mitotic apparatus of dividing cells. There is good evidence that sulphydryl groups are necessary in many enzymes for binding substrate or coenzyme to the protein. An interesting paper is presented on the role of the thioether bridges linking the haeme moiety to two cysteine residues in the protein portion of cytochrome *c*. Studies comparing the amino acid sequence around the haeme in this protein from mammals, fish, birds, insects and yeast are included. Also of interest is a discussion of the enormous laevorotatory contribution of cystine to the optical rotation of proteins. Discussions of the pitfalls encountered in measuring the number of sulphydryl groups in proteins form an especially useful feature of this book which can be warmly recommended to protein chemists.

A. S.

Introduction to the Theory of Quantized Fields. By N. N. Bogoliubov and D. V. Shirkov. Translated by G. M. Volkoff. (Interscience Publishers, 1959.) [Pp. 720.] Price 128*s.*

Mathematicians will find this soothing reading. Its authors have done all in their very considerable power to discuss the foundations of quantum field theory and the renormalization programme with due regard to mathematical respectability. The exposition is clear and detailed and makes smooth reading in Volkoff's admirable translation. The approach employed is often unusual. Thus quantization is introduced through postulating properties of the infinitesimal generators of the Lorentz group rather than through the canonical formalism. The S matrix is built up in the manner of Stueckelberg from the requirements of unitarity and causality rather than appearing as a limit of improper transformation operators.

The first five hundred pages, therefore, form an introduction to quantum field theory that usefully complements the treatments available elsewhere. For good measure we are also given a chapter on the renormalization group together with a hundred and fifty pages of dispersion relations of which the greater part is concerned with Bogoliubov's celebrated proof of the relations for non-vanishing momentum transfer. By this stage we are long past an introduction and well in the thick of it.

J. C. P.

[*The Editors do not hold themselves responsible for the views expressed by their correspondents.*]

Fig. 1

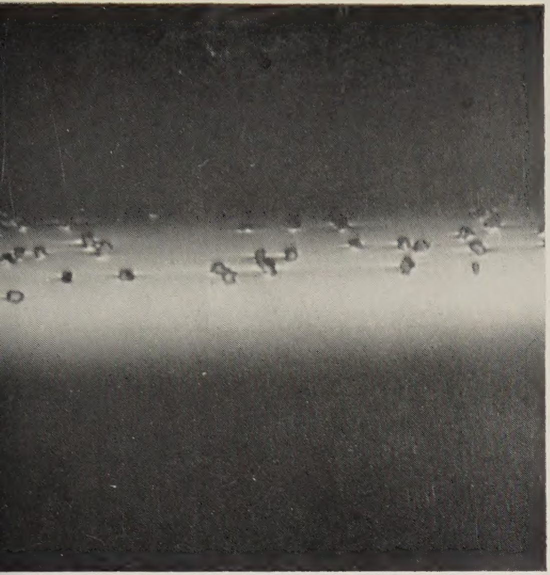

fects on the surface of a fibre of Pyrex glass drawn from rod at approximately 920°c (× 175).

Fig. 2

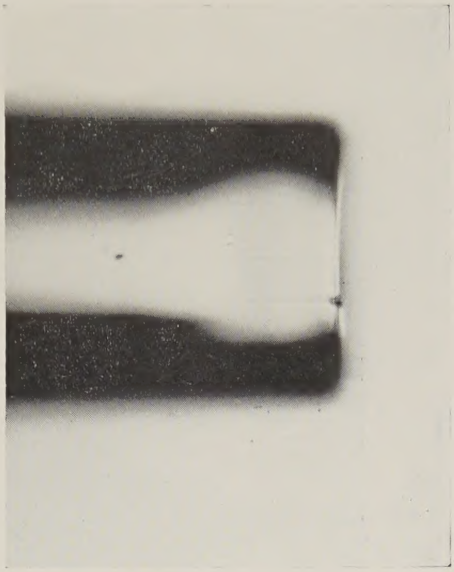

Defect at the edge of the fracture surface on a fibre of Pyrex glass (× 150).

Fig. 3

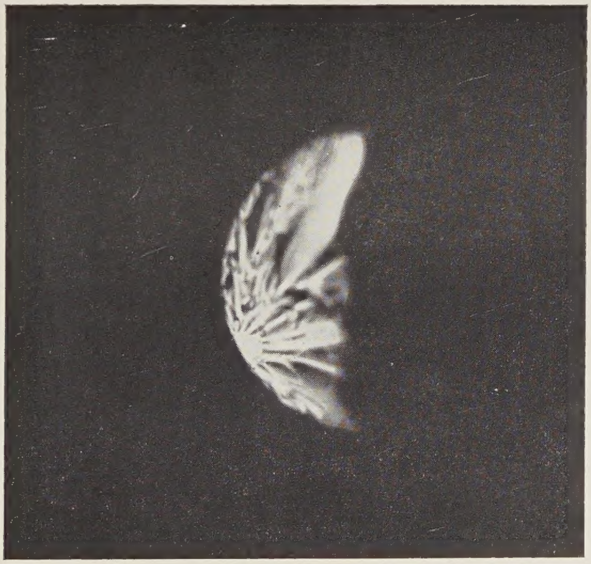

Fracture surface of a fibre of Pyrex glass. (The smooth ‘ mirror ’ region which occurs around the point of origin of fracture is often larger than in this example) (× 150).

Fig. 3

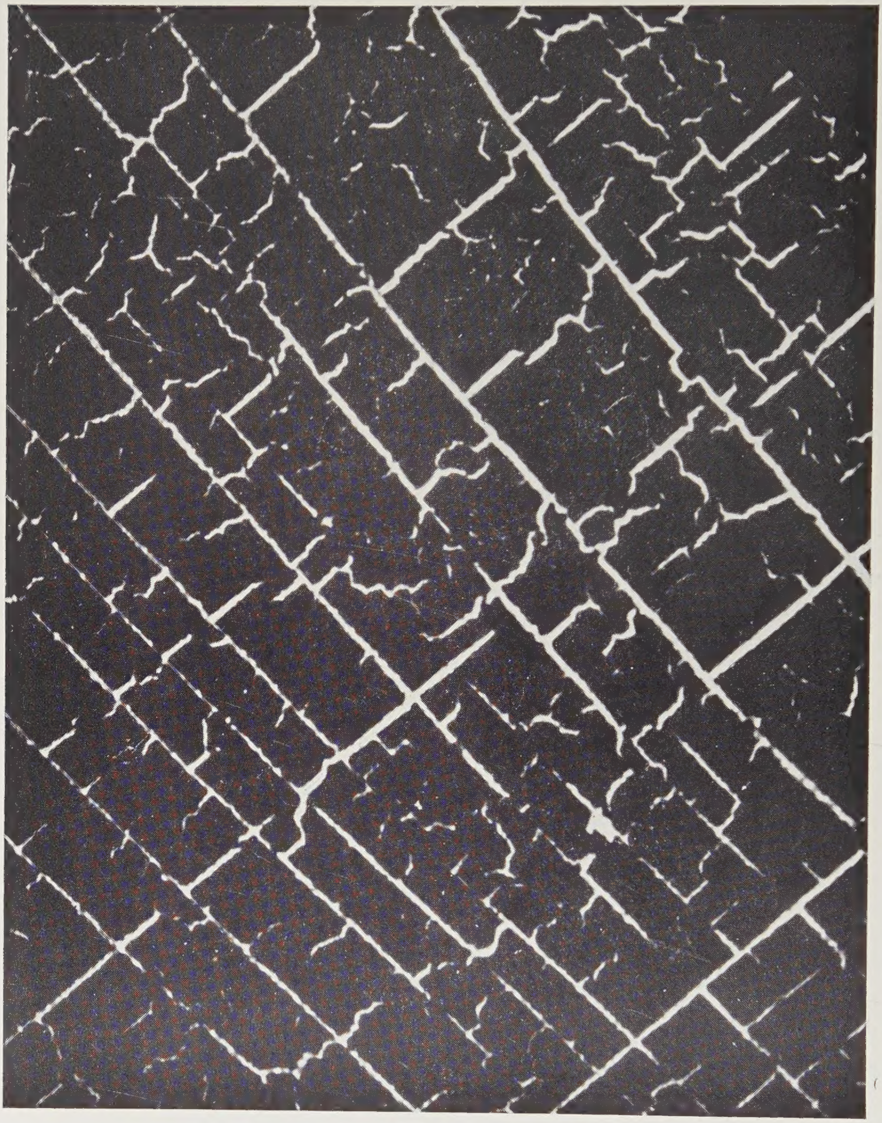

Evaporated film pattern of untreated crystal (200 ×).

Fig. 4

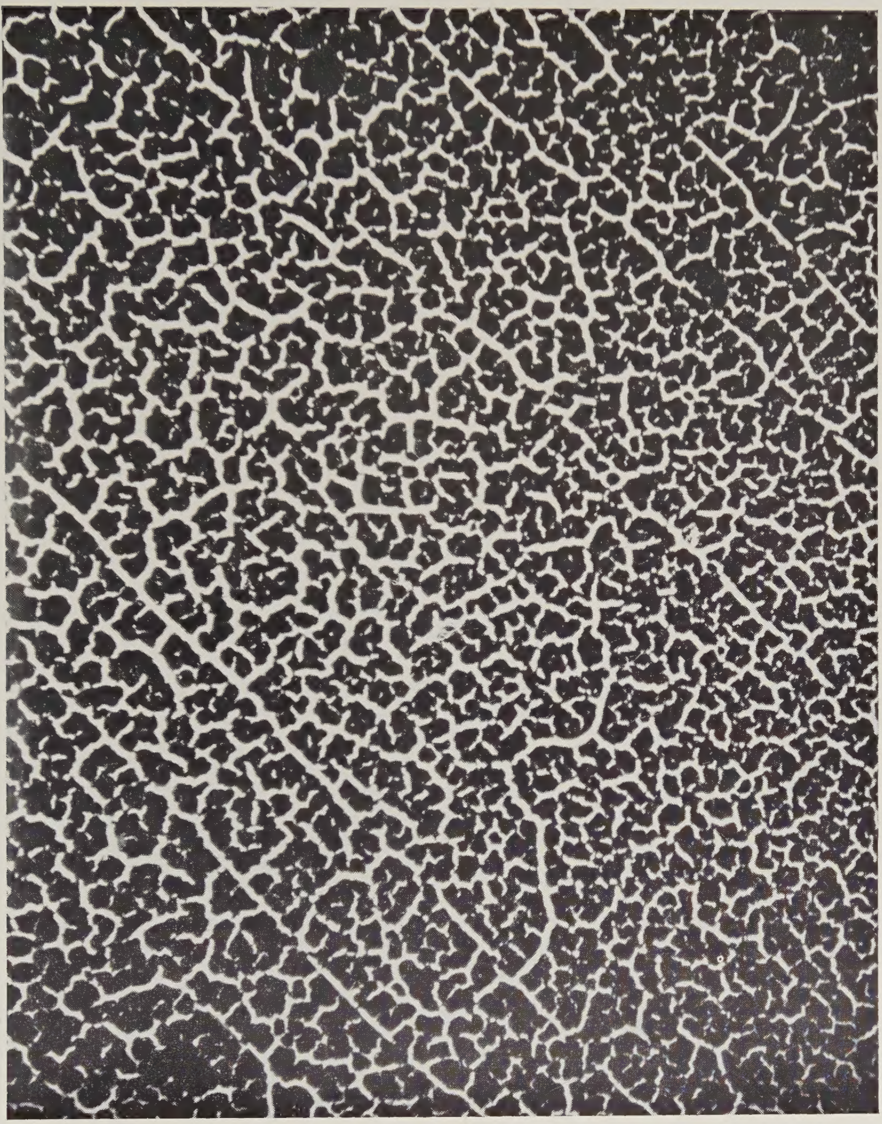

Evaporated film pattern after crystal had been chilled in liquid nitrogen (200 ×).

Fig. 1

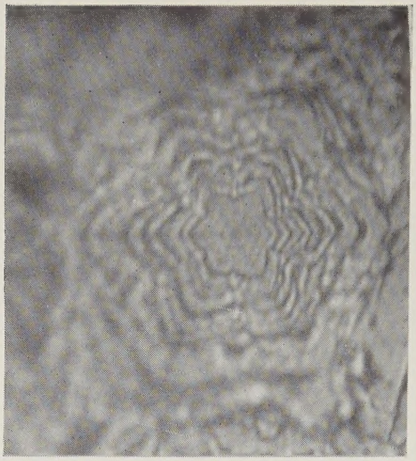

×1230

Fig. 2

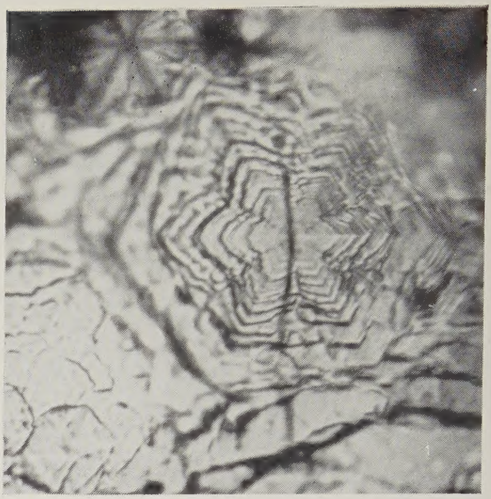

×1230

Fig. 3

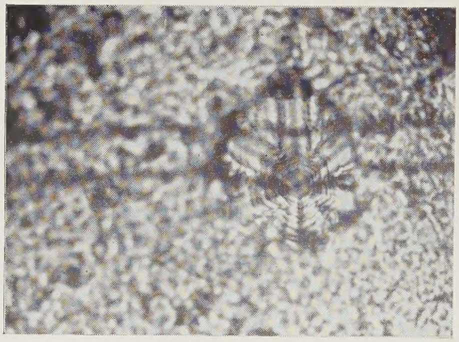

×570

Fig. 5

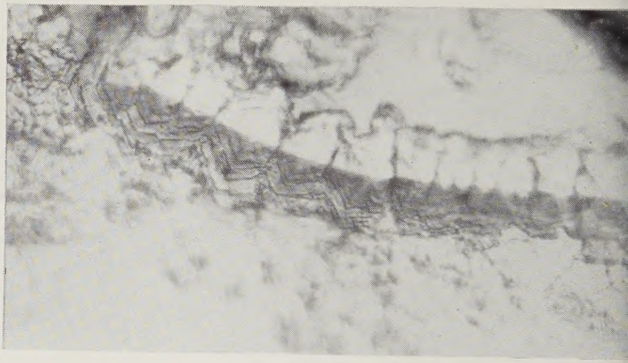

×570

Fig. 4

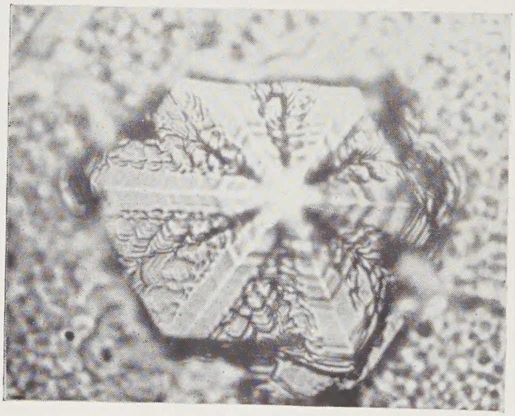

×1230

Fig. 6

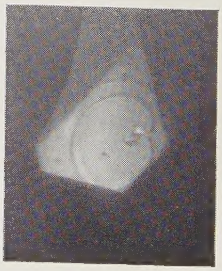

×570